Translational profiling of stress-induced small proteins uncovers an unexpected connection among distinct signaling systems

Sangeevan Vellappan[1,2,3], Junhong Sun[1], John Favate [2,3], Pranavi Jagadeesan[1], Debbie Cerda[1,2], Premal Shah [2,3], Srujana S. Yadavalli[1,2]*

[1]Waksman Institute of Microbiology, Rutgers University, Piscataway, NJ USA

[2]Department of Genetics, School of Arts and Sciences, Rutgers University, Piscataway, NJ USA

[3]Human Genetics Institute of New Jersey, Rutgers University, Piscataway, New Jersey, USA

*Corresponding author

Waksman Institute of Microbiology

Rutgers University

190 Frelinghuysen Rd

Piscataway NJ 08854

Phone: 848-445-0251

Email: sam.yadavalli@rutgers.edu

Highlights

- Ribo-RET identifies 17 small proteins induced under low Mg^{2+} stress in *E. coli*
- Many of these proteins are transcriptionally activated by PhoQP signaling system
- Half of the stress-induced small proteins localize to the membrane
- Deletion or overexpression of specific small proteins affects growth under stress
- Small protein YoaI connects PhoR-PhoB and EnvZ-OmpR signaling networks

Summary

Signaling networks in bacteria enable sensing and adaptation to challenging environments by activating specific genes that help counteract stressors. Small proteins (≤ 50 amino acids long) are a rising class of bacterial stress response regulators. *Escherichia coli* encodes over 150 small proteins, most of which lack known phenotypes and their biological roles remain elusive. Using magnesium limitation as a stressor, we investigate small proteins induced in response to stress using ribosome profiling, RNA sequencing, and transcriptional reporter assays. We uncover 17 small proteins with increased translation initiation, a majority of which are transcriptionally upregulated by the PhoQ-PhoP two-component signaling system, crucial for magnesium homeostasis. Next, we describe small protein-specific deletion and overexpression phenotypes, which underscore the physiological significance of their expression in low magnesium stress. Most remarkably, our study reveals that a small membrane protein YoaI is an unusual connector of the major signaling networks – PhoR-PhoB and EnvZ-OmpR in *E. coli*, advancing our understanding of small protein regulators of cellular signaling.

Graphical abstract

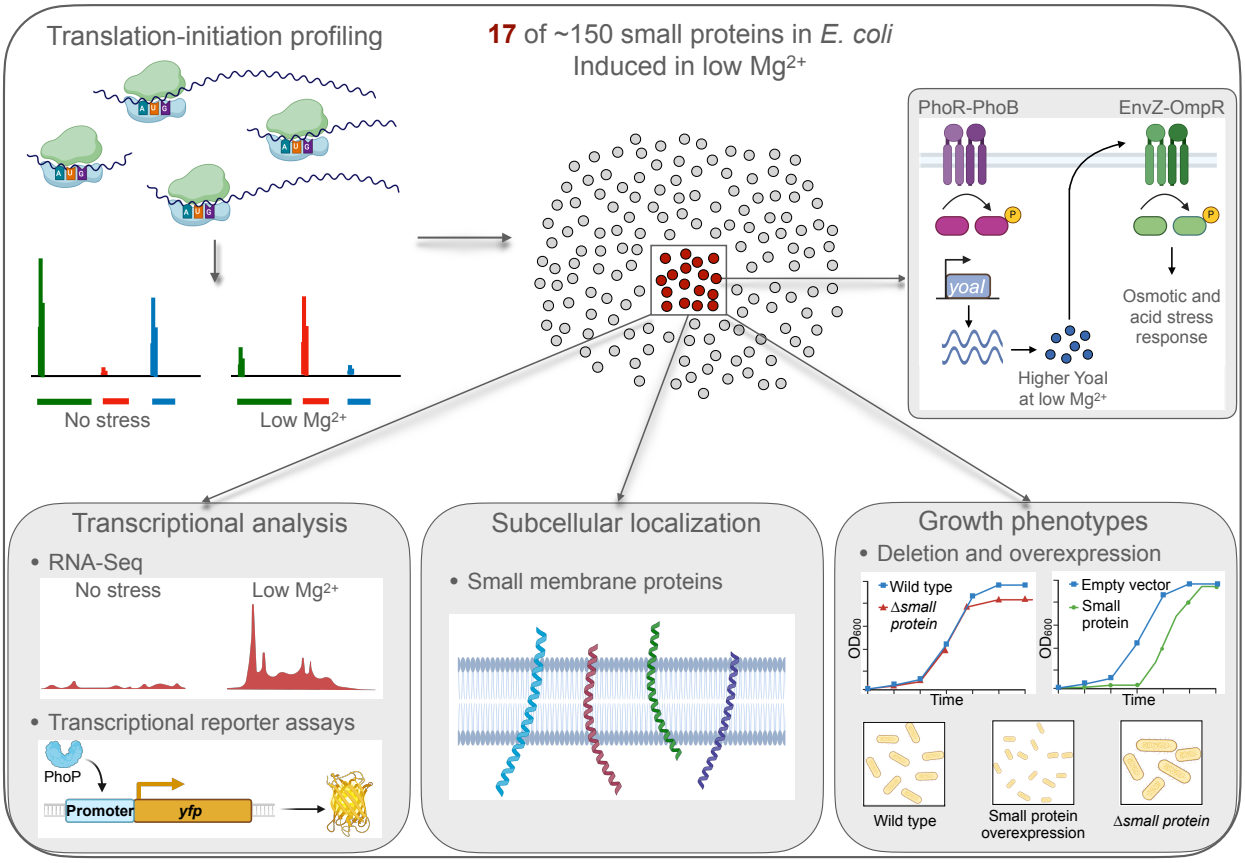

Keywords

Bacterial stress response, translation-profiling, small proteins, magnesium starvation, two-component signaling, PhoQ-PhoP, fluorescent reporters

Introduction

Living organisms sense and respond to environmental stressors through a wide variety of gene regulatory mechanisms [1]. In bacteria, signal transduction is primarily carried out by two-component signaling systems [2–4]. Gene expression regulation can occur at various stages including transcription, post-transcription, translation, and post-translation [5–8]. While some of these mechanisms involving regulators such as transcription factors and small RNAs have been extensively studied [9–11], other regulatory pathways essential for stress adaptation remain less well understood. Small proteins (≤50 amino acids in prokaryotes and ≤100 amino acids in eukaryotes), encoded by authentic small open reading frames, are emerging as key regulators of stress response [12–14], highlighting a need for further investigation into their roles and mechanisms of action.

Advances in bioinformatics, gene expression studies, and ribosome profiling have identified hundreds of previously unannotated small proteins in all kingdoms of life including humans [13,15–20]. In *Escherichia coli,* more than 150 small proteins have been documented [13,15]. While there has been significant progress in identifying small proteins, a major gap in our knowledge is the lack of understanding of the functions of most of these proteins [12,15]. Small proteins are typically non-essential, at least under standard growth conditions used in the labs, and their requirement is likely conditional when the activity of a larger target needs fine-tuning. In support of this idea, it was previously observed that some small proteins accumulate at higher levels in a specific growth phase, medium, or stress condition [21,22]. Magnesium (Mg^{2+}) is an important cofactor affecting the catalysis and stability of numerous proteins and RNAs involved in vital cellular processes, including translation [23]. Given the central role of Mg^{2+}, its deprivation poses a major stress to the cells. The signal transduction and physiological response to low Mg^{2+} is fairly well understood, which involves the activation of the master regulator, PhoQP two-component signaling system in gammaproteobacteria [23–25].

So far, three small proteins are known to mediate stress response to magnesium limitation in bacteria. Firstly, MgrB, a 48-aa transmembrane protein negatively regulates the sensor kinase PhoQ of the PhoQP signaling system [26,27]. During magnesium starvation, the absence of MgrB leads to hyperactivation of the PhoQP pathway, resulting in cell division inhibition and filamentation in *E. coli* [28]. In addition to its role in Mg^{2+} stress, loss of MgrB in *E. coli* increases tolerance to trimethoprim, an antibiotic commonly used to treat bacterial infections [29]. In clinical isolates of *Klebsiella pneumoniae*, disruption of MgrB-mediated inhibition of PhoQ also leads to acquired colistin resistance [30]. A second small membrane protein, MgtS is also induced under low Mg^{2+} stress and is important for magnesium homeostasis [31,32]. MgtS protects the magnesium transporter, MgtA, from degradation when Mg^{2+} is limited [31]. PmrR is the third small membrane protein shown to be expressed under low Mg^{2+} stress in *Salmonella enterica* [33,34]. PmrR is activated by the PmrAB two-component system [33,35,36] in a PhoP-dependent manner and inhibits the lipopolysaccharide modification enzyme, LpxT.

Here we ask, what subset of the ~150 small proteins in *E. coli* are induced under magnesium limitation? We hypothesized that, like MgrB, MgtS, and PmrR, many other small proteins with potential regulatory roles are yet to be identified as part of this stress response. We leveraged the translation-initiation profiling method, Ribo-RET [37,38] to identify small proteins induced by low magnesium stress, revealing a set of 17 proteins representing a substantial proportion (~11%) of the documented small proteins in *E. coli*. To investigate the transcriptional regulation of the stress-induced small proteins, we utilized RNA-Seq and transcriptional reporter assays, we investigated the transcriptional regulation of these stress-induced small proteins, shedding light on the genomic regions responsible for their expression and discerning any regulatory influence from the PhoQP system. Additionally, using epitope tagging, microscopy, and biochemical analysis, we meticulously examined the localization, overexpression, and loss-of-function phenotypes of these small proteins. Through these experiments, we unexpectedly uncovered how the small membrane protein YoaI, transcriptionally controlled by the PhoRB signaling pathway [39], displays increased protein levels under magnesium stress and activates another well-studied two-component system EnvZ-OmpR [40] in *E. coli*.

Results

Identification of low magnesium stress-induced small proteins in *E. coli* using translation-initiation profiling.

To identify small proteins that accumulate under low magnesium stress, we adapted the translation initiation profiling method called Ribo-RET (Figure 1A) – a modified ribosome profiling approach utilizing translation initiation inhibitors for the identification of small proteins in bacteria [41]. Retapamulin (RET) is an antimicrobial compound that can stall ribosomes at the translation start sites to help identify previously unannotated open reading frames [37,38]. In this study, we prepared Ribo-RET libraries of wild-type *E. coli* cells grown in media with or without magnesium to examine small proteins expressed in response to magnesium starvation.

In our Ribo-RET data, we observe an increase in reads mapping to a specific distance of the ribosomal P-site codon from the 3' end of the reads in our libraries, ~6-10 nucleotides (nt) downstream of the expected start codon (Figure S1), similar to the pattern observed in previous translation initiation profiling studies [38]. We calculated ribosome density at annotated translation initiation sites using reads mapped from 4 to 20 nt downstream of the first nucleotide in the start codon, using a broad window of 16 nt to capture all relevant footprint sizes. In our analysis, the ribosome footprint sizes range from 16-24 nt, as illustrated in Figure S1, as anticipated for the bacterial systems [42].

The PhoQP signaling system is upregulated under Mg^{2+} limitation [43] (Figures S2A-B). As expected, the read counts at the translation start site for PhoP and PhoQ were more than 4-fold and 10-fold higher, respectively, under stress conditions compared to no stress. Three small proteins known to be induced under low Mg^{2+} stress – MgrB, MgtS, and PmrR, show a 9-fold, 5-fold, and 5-fold increase in the reads mapping to the translation start sites, respectively, under stress vs. no stress (Figures 1B-C, S2C). Overall, in our Ribo-RET data, we see a moderate correlation between the reads mapping to the start sites of all proteins expressed under these two conditions (Figure 1C), which is indicative of the anticipated changes in the translation initiation of proteins during stress response.

We detected 379 proteins with ≥3-fold increase in read counts under stress, several among these are small proteins <50 aa in length (Table S4). We narrowed down a set of 17 small proteins namely MgtS, MgrB, PmrR, MgtT, YmiC, YmiA, YoaI, YobF, YddY, YriB, YadX, YkgS, YriA, YdgU, YqhI, YadW and DinQ for further analysis (Table 1). Ribosome footprints at the start site of an open reading frame are a good proxy for the expression of the corresponding protein. However, it is critical to establish whether a given small open reading frame (sORF) results in a protein product of that specific size. All but one protein YoaI were previously validated for expression via genomic epitope-tagging (Table S5). In the case of YoaI, the protein could not be detected in rich media or specific growth conditions, including envelope stress, acid stress, and heat shock [21,22]. Given the strong signal for expression of YoaI in our Ribo-RET data (~12-fold increase in RPM for stress vs. no stress) (Figure S4A), we wondered if YoaI is conditionally expressed during magnesium limitation. To examine the expression of YoaI, we utilized a strain carrying chromosomally-encoded fusion protein YoaI-SPA [21,22]. We grew cells in

media containing different levels of Mg^{2+}, prepared membrane and cytoplasmic fractions, and performed western blot analysis. Consistent with our hypothesis, we detected expression of YoaI in a magnesium-dependent manner, where the protein level is highest at the lowest concentration of magnesium (Figure S4B). In addition, this result also confirms that YoaI is predominantly associated with the membranes, consistent with the bioinformatic prediction that it is a membrane protein (Table S6).

14 of the 17 shortlisted small proteins were not previously associated with expression under low magnesium stress. Small proteins YobF [22,44] and DinQ [45] have been linked to other stress responses in *E. coli*, here we find the expression of these two proteins in low magnesium stress as well. Many of these small proteins have not been characterized biochemically and have no documented function yet. In the following sections, we systematically study these low-Mg^{2+}-induced small proteins by investigating their transcriptional regulation and cellular localization and characterizing their overexpression and deletion phenotypes.

Transcriptional regulation of low magnesium stress-induced small proteins.

To determine changes in the levels of transcripts encoding stress-induced small proteins, we performed RNA-Seq using cells grown to early exponential phase in high and low Mg^{2+} conditions. It is well-established that in cells depleted for Mg^{2+}, the PhoQP signaling system is stimulated, leading to PhoP-mediated transcriptional activation of hundreds of genes necessary for the stress response [24]. Not surprisingly, we see an increase in the mRNA abundances for *phoQ* and *phoP* (Figure S3). Differential expression analysis of our RNA-seq data revealed significant upregulation (fold change threshold of >2 and a p-value threshold of <0.05) in transcription under low Mg^{2+} stress for at least 10 of the 17 small proteins shortlisted, including MgtS, MgtT, and MgrB (Figure 2). It is worth noting that YadX also showed a small increase (1.7-fold) although it falls below the >2-fold threshold we applied in our data analysis. Intriguingly, YriA, whose open reading frame overlaps with YriB by ~60% did not show an increase in the transcript levels. In addition, we did not see a significant change in the mRNA levels corresponding to YoaI, YobF, YkgS, and DinQ. In these cases, it is possible that the change in transcript abundances is generally low and therefore fell below the significance threshold. Alternatively, gene expression might be regulated at a post-transcriptional or translational level under low magnesium stress. Indeed, *yobF* expression is induced post-transcriptionally during heat shock response [22]. The expression of *yobF* under magnesium limitation may be controlled via a similar post-transcriptional regulatory mechanism.

To delve deeper into the transcriptional control mechanism of the small proteins we sought to: 1) identify the regulatory regions upstream of each sORF, and 2) determine if the expression is PhoQ-dependent. To identify the regions containing the putative promoters of low Mg^{2+}-induced small proteins, we carefully selected ~200 to 500 base pairs upstream of each sORF (Table 2). In general, we did not include any annotated full-length ORFs or non-coding RNAs occurring within the regulatory region being tested, to avoid interference from the ectopic expression of the corresponding product. In cases where a sORF appeared to be in the middle of an operon, we selected two regions to test: one upstream of the entire operon and another immediately upstream of the sORF of interest. We designed transcriptional reporter constructs to measure

the activity of each putative regulatory region, as shown in the schematic (Figure 3A). To analyze which of these sORFs are regulated by the PhoQP two-component system, we measured the transcriptional reporter activities in a *phoQ* deletion strain and compared them to that of the wild type (Figure 3B).

Consistent with our RNA-seq data, we saw an increase in the transcriptional activity for regulatory regions corresponding to 11 sORFs with this upregulation under low Mg^{2+} condition being PhoQ-dependent (Figure 3B). Two sets of overlapping (out-of-frame) sORFs including *mgtS-mgtT* and *yriA-yriB*, strongly suggest their association within the same operon. Three other genes, *yadW, ymiC,* and *ydgU* are likely regulated as part of the operons, *yadX-clcA-yadW*, *ymiA-yciX-ymiC*, and *asr-ydgU*, respectively. For all the sORFs occurring within an established or putative operon, the region upstream of the operon showed a higher transcriptional reporter activity in response to stress, while a second region immediately upstream of the given sORF had negligible activity (Table 2, Figure 3B). Based on the reporter assay, the transcriptional activity for the 11 sORFs (*mgrB*, *mgtS*, *mgtT*, *ymiA*, *ymiC*, *yddY*, *yriA*, *yriB, yadX*, *yadW*, and *ydgU*) peaks at ~6-10 hours. The RNA-Seq data represent transcriptomic abundances at a given time point of growth (early exponential phase). This transcriptional reporter assay captures temporal changes in the reporter activity and serves as a complementary approach to RNA-Seq, where changes in low-abundance transcripts would be missed. For instance, we did not observe a significant upregulation of *yadX* and *yadW* in the RNA-Seq data, but we see a PhoQ-dependent increase in the reporter activity for the putative regulatory region $P_{yadX\text{-}clcA\text{-}yadW}$ region under low magnesium stress. Conversely, for *pmrR* and *yqhI*, while the RNA-Seq data suggested upregulation, we did not detect a significant increase in the transcriptional reporter activity under stress suggesting that there may be distal or additional regulatory factors, outside of our reporter construct, involved in controlling their transcription. Indeed, *pmrR* is shown to be transcriptionally activated by the PmrA-PmrB signaling system during magnesium limitation through the PhoQP-regulated connector protein PmrD in *Salmonella enterica* [33] . This connection between the PhoQ-PhoP and PmrA-PmrB signaling pathways is also active in *E. coli* under specific conditions including high stimulation of the PhoQ-PhoP system [35,46]. We did not observe a reporter activity for *dinQ, ykgS, yobF*, and *yoaI* in either the wild-type or *ΔphoQ* cells, consistent with the results from the RNA-Seq.

In summary, our RNA-Seq and transcriptional reporter assays reveal transcriptional upregulation of 13 of the 17 small proteins, of which PhoQ regulates at least 11 under magnesium starvation.

Regulation of small membrane protein YoaI under Mg^{2+} stress.

YoaI is known to be regulated by the PhoRB two-component system [47–49], which responds to phosphate starvation [39]. PhoRB signaling is also activated under low magnesium stress due to the slowdown of protein synthesis and reduction of cytoplasmic phosphate levels [50]. Consistently, we noticed a 10-fold increase in reads mapping to the PhoB translation start site under magnesium stress (Figure S2D). We then tested our transcriptional reporter for *yoaI* (P_{yoaI}-YFP) in a low-phosphate medium and saw increased transcriptional activity for P_{yoaI} when compared to no-stress condition, in a PhoB-dependent manner (Figure 4A). This transcriptional

activation is PhoQ-independent as we see an amplification of P_{yoaI} reporter in Δ*phoQ* cells as well (Figure 4B). Taken together, these results show that *yoaI* transcription is controlled by PhoB, and there is no significant effect of low magnesium stress on *yoaI* transcription based on RNA-Seq and transcriptional reporter data (Figures 2, 3B). Yet YoaI protein levels increase under low magnesium conditions, and we wondered if PhoQ controls YoaI abundance. To test this possibility, we examined YoaI protein expression in wild-type and Δ*phoQ* cells in high and low magnesium conditions by western blotting. Our results demonstrate that YoaI's expression remains magnesium-dependent in a Δ*phoQ* strain, mirroring the pattern seen in the wild type (Figure 4C), suggesting that PhoQ does not affect YoaI levels. Therefore, YoaI expression is induced in a PhoQ-independent manner under magnesium limitation potentially via a post-transcriptional regulatory mechanism that enhances translation initiation.

About half of the low Mg^{2+} stress-induced small proteins localize to the membrane.

As a first step to classifying the 17 stress-induced small proteins, we checked if a given small protein is likely associated with the membrane or cytoplasm. Most of these proteins have limited or no documented information, so their cellular localization can provide insights into their potential mechanisms of action and interactions within the cell. Using bioinformatic tools TMHMM [51], TMPred [52], and Phobius [53] to predict membrane helices, we find that at least 9 of our candidates are putative membrane proteins. Three of them, MgrB, MgtS, and DinQ, were previously shown to localize to the membrane in *E. coli* [21,45]. Additionally, PmrR from *S. enterica* was shown to be membrane-bound [33]. Our bioinformatic analyses predict that small proteins YdgU, YmiA, YmiC, YoaI, and YobF also localize to the membrane (Table S6).

Next, to confirm the membrane association and visualize the small protein localization we used epitope-tagging with GFP. Taking into account the predicted orientation of the putative transmembrane protein, we created either an N- or C-terminal fusion of GFP by tagging the end that is expected to face the cytoplasm (Figure S5A, Table S6) to ensure proper folding of GFP [54]. Accordingly, YdgU, YmiA, and YmiC were tagged at the N-terminus, and YoaI was tagged at the C-terminus. Upon observation by fluorescence microscopy, cells expressing GFP-tagged YdgU, YmiA, YmiC, and YoaI revealed bright fluorescence at the cell periphery indicative of membrane localization, similar to the known membrane protein, MgrB (Figure S5B). As a control, cells expressing GFP alone showed uniform fluorescence indicative of cytoplasmic localization.

For PmrR, we constructed an N-terminal fusion with GFP, where the tag was expected to localize to the cytoplasm. However, we did not observe membrane localization (Figure S5B). Considering the predicted membrane helices, this suggests that the tag interferes with PmrR localization. Alternately, we tagged the C-terminus of *E. coli* PmrR with a hexahistidine (6XHis) tag (Figure S5C) and performed western blotting using membrane and cytoplasmic fractions. PmrR-6XHis strongly associated with the membrane fraction (Figure S5D), consistent with the bioinformatic prediction and data from *S. enterica* PmrR. As in the case of PmrR, YobF-GFP localized to the cytoplasm, which was inconsistent with its predicted membrane localization (Table S6). Therefore, we used a 6XHis-tagged version of YobF, which showed a greater

association with the membranes than the cytoplasmic fraction (Figure S5D). Overall, among the 17 small proteins induced under low Mg^{2+}, we find that 9 of them are membrane proteins.

Three small proteins exhibit stress-specific growth defects upon gene deletion.

To identify potential defects in growth and cellular morphology caused by the absence of each small protein in the cell, we utilized single gene deletions of *mgtS*, *mgtT*, *pmrR*, *yadW*, *yadX*, *yddY*, *ykgS*, *ymiC*, *yqhI*, *yobF, dinQ*, *ydgU*, *ymiA*, and *yoaI* in the *E. coli* genome. *mgtT* lies in an operon with *mgtS* [38], with an out-of-frame overlap between the stop codon of MgtS and the start codon of MgtT. Therefore, we carefully generated an *mgtS* deletion without affecting the start codon of MgtT, and similarly, an *mgtT* deletion while keeping the stop codon for MgtS intact (for details see materials and methods, Table SI). In the case of *yriAB*, the two small proteins YriA and YriB have overlapping open reading frames, where ~80% of the *yriB* gene overlaps with that of *yriA* (Figure 6C, schematic), so, we first deleted the combined *yriAB* ORF to see if there is a phenotype. 12 out of the 17 small proteins displayed no discernible growth defects upon deletion relative to the wild-type strain when grown under magnesium limitation. However, four mutants – namely *ΔpmrR, ΔyobF, ΔyqhI,* and *ΔyriAB* – exhibit reduced growth yields when grown over 24 hours (Figure 5). The cells carrying these deletions entered the stationary phase earlier than the wild type. Notably, PmrR and YobF are membrane-bound proteins, while YqhI, YriA, and YriB are putative soluble proteins (Figure S5D, Table S6).

To determine whether these growth defects are specifically related to the loss of these small proteins, we complemented the deletion strains with plasmids encoding the corresponding small proteins and induced with IPTG. Successful rescue of growth is observed for *ΔpmrR*, and *ΔyobF* (Figure 6A, B; top panel). To confirm that this complementation is specific to the small protein and not due to a cryptic ORF or regulatory element present within the small protein coding region, we prepared plasmids carrying *pmrR* and *yobF* where their start codons are mutated to stop codons. When tested for complementation in *ΔpmrR* and *ΔyobF*, respectively, the start codon mutants retained the growth defect similar to that observed for the empty vector (Figure 6A, B; top panel), reinforcing that the growth phenotype is specific to the small proteins themselves. In addition, we investigated whether the growth defect observed with *pmrR* and *yobF* deletions is specific to low magnesium stress. Our results indicate that deletions of *pmrR* and *yobF* do not cause growth defects in the absence of stress (Figure 6A, B; bottom panel), and the phenotype is specific to magnesium-limited conditions. Intriguingly, expression of plasmid-encoded PmrR in the absence of stress resulted in a growth defect (Figure 6A, bottom panel), suggesting that increased expression of PmrR under no-stress conditions may be detrimental.

Given the growth phenotype observed for Δ*yriAB*, we performed complementation with either plasmid-encoded YriA and/or YriB to establish if the loss of either protein is responsible for the growth defect. Intriguingly, complementation with either YriA or YriB alone failed to restore growth but a plasmid expressing the region from *yriB* to *yriA,* mimicking the native genomic arrangement (*yriAB*), partially rescued the growth defect (Figure 6C, top panel). In our plasmid construct encoding YriB and YriAB, there is a possibility of a spurious small protein produced due to the intact, out-of-frame YriA start codon within the *yriB* ORF (Figure 6C, schematic) that potentially interferes with the complementation. To address this issue, we created a modified *yriB* construct

where YriA start codon ATG is mutated to TAA, this substitution changes codons 4 (Asp) and 5 (Val) in YriB to 4 (Ile) and 5 (Ile). This variant of YriB confers full complementation (Figure 6C, top panel), indicating that loss of YriB contributes to the growth phenotype, at least in part. In addition, we see that the growth defect associated with *yriAB* deletion is specific to low magnesium stress condition (Figure 6C, bottom panel).

Finally, the growth defect observed in *ΔyqhI* is not complemented with a plasmid encoding YqhI (Figure 6D), which suggests that this phenotype is not directly related to the YqhI protein itself. Intriguingly, we did not see a growth defect in *ΔmgtS* strain when grown in a low magnesium medium (Figure 5), contrasting with the previous report [31]. This discrepancy might be due to differences in strain construction and/or growth media. Together, our results underscore the complexities in studying overlapping small ORFs and their phenotypes.

Seven small proteins affect growth and cell morphology upon overexpression.

As a parallel approach to analyzing loss-of-function phenotypes, we explored the phenotypes associated with the overexpression of small proteins. We cloned the genes corresponding to the untagged small proteins into either an IPTG-inducible (all except DinQ as we were unable to generate a DinQ clone in the IPTG-inducible pEB52 background) or arabinose-inducible (DinQ) vector. Upon induction, slow growth or a prolonged lag phase is observed for 7 out of the 17 small proteins tested: MgtS, MgrB, PmrR, YmiA, YoaI, YkgS, and DinQ (Figure 7). Notably, six of these proteins are membrane-bound (MgtS, MgrB, PmrR, YmiA, YoaI, and DinQ). In the case of MgtS, MgrB, PmrR, YmiA, and YoaI, induction of expression with IPTG leads to an extended lag phase lasting for ~8-10 hours, after which the cells grow exponentially at growth rates similar to that of control cells carrying empty vector, eventually reaching saturation at comparable levels. Interestingly, cells expressing small proteins YkgS and DinQ did not display a long lag phase but grew at a slower rate, eventually catching up to the same growth yield as the control cells. The growth defect due to DinQ overexpression aligns with previous studies indicating that its overexpression disrupts membrane potential and depletes intracellular ATP levels [45]. It is worth noting that overexpression of the other 10 small proteins, including 3 membrane proteins YdgU, YmiC, and YobF had a negligible impact on cell growth under the same condition, suggesting that cells may tolerate high amounts of these proteins (Figure 7). More importantly, the lack of a phenotype for most of these small proteins indicates that the growth defects observed here are not due to a generic burden on the cell from plasmid-driven protein overexpression.

To be cautious in interpreting the overexpression data, we considered the possibility that the observed growth defects might be attributed to a cryptic small open reading frame or regulatory element within the small ORF being overexpressed. To check if the growth defects are indeed small protein-dependent, we prepared plasmid constructs containing variants of the small protein where the start codon (ATG) is substituted with a stop codon (TAA). For all 7 small proteins displaying overexpression phenotypes, we repeated the growth assay with the start codon mutants of each small protein. Expression of the mutant small proteins rescued the growth defect with the cells exhibiting similar growth patterns to those carrying the empty vector (Figure 8A), reinforcing that the observed growth defects are specific to the overexpression of these small proteins.

In addition to the impact on growth, we explored whether overexpression of these 7 small proteins (MgtS, MgrB, PmrR, YmiA, YoaI, YkgS, and DinQ) influences cell size and morphology, especially given the delayed growth (Figures 7, 8A). We hypothesized that cells overexpressing these small proteins may undergo morphological changes as part of adaptation during the extended lag and log phases of growth. Using phase contrast microscopy, we imaged cells induced for expression of the small proteins during the lag and exponential growth phases. As controls, we used wild-type cells carrying either an empty vector or a plasmid containing a variant of the small ORF where its start codon (ATG) is mutated to a stop (TAA). The control cells exhibited a roughly uniform cell size with volumes around 1.1-1.3 fL and 1.2-1.4 fL in lag and log phases, respectively. Intriguingly, overexpression of small proteins MgtS, MgrB, PmrR, YkgS, YoaI, and YmiA causes distinct changes in cell size (Figures 8B, S6). Specifically, overexpression of MgtS results in smaller cell size (Figure 8B), with a reduction in cellular volume to ~30-36% of the control cells carrying either empty vector or start codon mutants in both lag and log phases (Figure S6). Similarly, overexpression of PmrR and YoaI leads to a ~29% decrease in cell size and volume during the lag phase, however, the cell size reverts to that of control cells during the exponential phase (Figures 8B, S6). In contrast, overexpression of MgrB leads to an increase in cell size, with an average volume of 2.2 fL, ~1.6-fold larger than the controls in the lag phase (Figures 8B, S6), akin to the Δ*phoQ* cells grown in low magnesium conditions (Figure S7). This finding is remarkable because MgrB is known to inhibit PhoQ [26,27], consistently, plasmid overexpression of MgrB likely leads to strong inhibition of PhoQ, resulting in a cellular morphology similar to that of Δ*phoQ*. These cells eventually return to normal size (cell volume of 1.2 fL) in the exponential phase. Overexpression of YkgS and YmiA causes varying extents of cell elongation affecting cell size and volume (Figures 8B, S6). Cells overexpressing DinQ did not show a significant change in cell size.

Overall, the slow or delayed growth observed here along with the diverse morphological phenotypes at distinct growth stages reflects how cells adapt in response to the overexpression of small proteins mentioned above.

Small protein YoaI connects distinct signaling systems – PhoQ-PhoP, PhoR-PhoB, and EnvZ-OmpR.

We wondered whether the growth delay observed upon overexpression of the 7 small proteins described above is PhoQ-dependent, given the pivotal role of PhoQ in low magnesium stress. To explore this, we evaluated the effects of overexpressing these proteins in a Δ*phoQ* strain under magnesium limitation. Notably, the growth phenotype associated with protein overexpression is retained in the Δ*phoQ* cells, similar to those observed in the wild-type strain for 6 out of 7 candidates – MgrB, MgtS, PmrR, YmiA, YkgS, and DinQ (Figures 8C), indicating that these effects are PhoQ-independent. Interestingly, in the case of YoaI overexpression, the extended lag phase observed in wild-type cells is completely abolished in the Δ*phoQ* cells, suggesting a direct or indirect link between PhoQ and YoaI where PhoQ functions upstream of YoaI in this regulatory pathway.

To check if YoaI and PhoQ physically interact with each other, we employed a bacterial two-hybrid (BACTH) assay based on reconstituting split adenylyl cyclase (CyaA) [55,56]. In this system, CyaA activity is restored when the two fragments T18 and T25 come close leading to an increase in cyclic AMP (cAMP) levels and subsequent expression of β-galactosidase (β-gal) from the *lac* promoter. We fused the T18 fragment to YoaI and tested it against T25-PhoQ. We included the T18-MgrB and T25-PhoQ pair as a positive control and two other histidine kinases, PhoR and EnvZ, each fused to the T25 fragment as additional controls. In this experiment, YoaI did not show an interaction with either PhoQ or PhoR, however, to our surprise there was a strong signal between YoaI and EnvZ that is comparable to the positive control (Figure 9A). EnvZ is primarily known to be an osmosensor, integral to the EnvZ-OmpR two-component system, which regulates porins in response to changes in osmolarity, pH, temperature, and growth phase [40]. Several small membrane proteins are known to modulate the activities of sensor kinases [14]. A 127-amino acid protein, MzrA regulates EnvZ resulting in higher levels of phosphorylated OmpR [57]. Based on the BACTH interaction between YoaI and EnvZ, we suspected YoaI might influence the activity of the EnvZ-OmpR signaling system. To address this possibility, we utilized an EnvZ-OmpR-regulated transcriptional reporter strain with chromosomal fusion of mScarlet to P_{omrB} [58] and measured *omrB* promoter activity in cells grown in low magnesium vs. no-stress media. Interestingly, we observe an increase of 2.5-fold in EnvZ-regulated transcription under stress in wild-type cells (Figure 9B). The significantly high activity of *omrB* reporter in low Mg^{2+} conditions suggests that upregulation of YoaI protein levels may mediate this effect (Figures 4C, S4). Upon deletion of *yoaI*, the *omrB* transcription reduced by ~1.4-1.5-fold in both low and high Mg^{2+} media, indicating that YoaI affects EnvZ-OmpR activity regardless of stress. Together with our observation that YoaI-SPA levels increase under low Mg^{2+} stress (Figures 4C, S4B), the higher transcriptional activity of the EnvZ-regulated promoter can be attributed to the positive interaction of YoaI with EnvZ. To further support the idea that an increase in YoaI levels is responsible for modulating the activity of the EnvZ-OmpR system, we examined *omrB* transcription upon plasmid overexpression of YoaI in wild-type *E. coli* cells. We observed a greater than 6-fold increase in P_{omrB}-*lacZ* reporter activity in cells expressing YoaI on a plasmid (Figure S8A) relative to the control cells carrying an empty vector. We also tested two other reporters to genes *ompF*, P_{ompF}-YFP and *ompC*, P_{ompC}-CFP [59], and found a ~2-fold change in their transcriptional activities (Figures S8B, C), consistent with the activation of EnvZ [40,60,61]. In summary, these findings suggest that YoaI interacts with and stimulates EnvZ activity, potentially enhancing OmpR-P levels.

Discussion

In this study, we identified 17 small proteins (≤50 amino acids) induced by low magnesium stress from approximately 150 documented small proteins in *E. coli*, using Ribo-RET [37,38]. Only 3 of these proteins, MgrB, MgtS, and PmrR were previously studied in the context of magnesium starvation [27,31,33]. For all the stress-induced small proteins except one (YoaI), expression from the genomic locus was verified *in vivo* (Table S5). In a previous report when cells were grown in a rich medium, expression of YoaI tagged with SPA epitope from a genomic translation fusion was undetected [21]. Interestingly, our observation of cells grown in low Mg^{2+} detected a robust expression of YoaI expression using the same construct, highlighting the condition-specific expression of this protein (Figures 4C, S4B). Using RNA-Seq, we found that

many of these stress-induced proteins are transcriptionally activated in low magnesium media. Further, we identified the regions upstream of these small ORFs responsible for transcriptional regulation using operon fusions and reporter assays. Few hits, including YoaI and YobF, do not show a change in transcription levels under low Mg^{2+}, suggesting that they are regulated post-transcriptionally.

Lacking any functional or phenotypic information for most of these stress-induced proteins, we began their characterization by predicting their subcellular localization using bioinformatic tools (Tables 1, S6). By epitope tagging and imaging or western blotting, we empirically determined that 9 of the 17 shortlisted stress-induced small proteins localize to the membrane (Figure S5). These membrane-bound small proteins may interact with, stabilize, or fine-tune the activities of large transmembrane proteins, such as sensor kinases, channel proteins, and drug efflux pumps, thereby mediating cellular adaptation and stress responses [14]. Among the 9 candidates, three proteins – MgrB, MgtS, and PmrR are shown to have specific membrane protein targets, as described earlier. To further investigate their biological roles, we performed targeted deletion and protein overexpression analysis.

Loss-of-function analysis of small proteins can be a useful approach to understanding their physiological roles. For example, deleting *mgrB* causes hyperactivation of the PhoQP two-component system, leading to cell division inhibition and filamentation of cells grown under low magnesium stress [28]. In clinical isolates of *Klebsiella pneumoniae,* the absence of MgrB-mediated PhoQ inhibition has been linked to acquired colistin resistance [30,62]. In the current work, we found deletion phenotypes associated with the following small proteins—PmrR, YobF, YriA/B, and YqhI—leading to an early entry into the stationary phase and reduced yield at saturation under magnesium limitation. Based on plasmid complementation, growth defects caused by PmrR and YobF are specific to the respective small proteins. The overlapping ORFs of YriA and YriB present a unique challenge in interpreting the Δ*yriAB* growth phenotype observed under low magnesium stress. While expressing the native *yriAB* region partially rescues the defect, individual expression of YriA or YriB fails to do so; however, modifying YriB by mutating the out-of-frame YriA start codon fully restores growth, emphasizing that the loss of YriB is a critical factor in the observed phenotype. In the case of YqhI, the deletion phenotype could not be fully complemented by plasmid-encoded small protein, pointing to putative cryptic ORF or regulatory factors within the small ORF that warrant further investigation.

We also analyzed overexpression phenotypes associated with each of the stress-induced small proteins to gain insights into cellular pathways or components functionally linked to these proteins. For instance, overexpression of MgtS is shown to activate the PhoRB two-component system by regulating the phosphate transporter, PitA [32]. Similarly, DinQ overexpression disrupts membrane potential and depletes intracellular ATP levels [45]. We observed overexpression phenotypes for 7 of the 17 small proteins induced under magnesium stress—MgtS, MgrB, PmrR, YmiA, YoaI, YkgS, and DinQ—resulting in either a long lag phase or slow growth (Figure 7). These overexpression phenotypes are specific to each small protein as we see control plasmids carrying a mutated start codon do not cause growth defects (Figure 8A). Analysis of the cell morphology during the lag and exponential phases of growth revealed interesting variations in cell sizes and

volumes that reflect how cells adapt to the overexpression of these small proteins. Remarkably for one of the small proteins, PmrR, both the deletion and overexpression caused growth defects under low magnesium stress. It is unclear how cells balance small protein levels when needed during specific conditions vs. when not needed, say in the absence of stress. In this context, complementation of the *ΔpmrR* strain with plasmid-encoded PmrR restored normal growth under magnesium limitation but caused a growth defect under no-stress condition (Figure 6A). This suggests that PmrR levels may be controlled precisely in cells undergoing stress, as both its absence and its overexpression disrupt the balance necessary for cellular homeostasis.

In *Salmonella enterica,* PmrR has been shown to inhibit the inner membrane protein LpxT, which plays a role in lipopolysaccharide modification [33,34,36]. We explored whether the growth defects associated with PmrR deletion and overexpression in *E. coli* are mediated through its interaction with LpxT. Interestingly, expressing PmrR in a Δ*lpxT* background did not alleviate the growth defects regardless of stress (Figure S9A). It is possible that higher LpxT levels, resulting from the absence of PmrR, could lead to growth defects. However, both single deletions (*ΔlpxT* and *ΔpmrR*) and the double deletion (*ΔpmrR ΔlpxT*) exhibited growth defects under magnesium stress (Figure S9B). This result suggests that the growth defect upon *pmrR* deletion is independent of PmrR's interaction with LpxT. PmrR may be involved in other pathways or regulatory mechanisms where it has additional interacting partners. It is not uncommon for small proteins to have multiple binding partners, as seen with MgtS, which interacts with both MgtA and PitA [31,32]. Whether PmrR associates with other targets contributing to phenotypes observed here warrants further investigation.

Finally, we would like to discuss the interesting case of the small membrane protein YoaI, whose transcription is controlled by the PhoR-PhoB signaling system [47–49]. YoaI levels are quite low or undetectable when cells are grown in a rich medium or specific stress conditions [21,22]. However, we find that YoaI protein levels strongly increase under magnesium limitation and it becomes detectable (Figure 4C). Overexpression of YoaI leads to a long delay in growth (Figures 7, 8A, S4B). This phenotype is abolished in a *phoQ* mutant (Figure 8C), hinting at an unknown PhoQ-dependent factor that may contribute to the growth defect observed upon YoaI overexpression. Through a bacterial two-hybrid assay, we found a direct interaction of YoaI with the EnvZ sensor kinase (Figure 9A), which controls osmoregulation [40] suggesting that this small protein acts as a connector between the PhoR-PhoB and EnvZ-OmpR signaling networks. Activation of EnvZ by YoaI is supported by the data from our transcriptional reporter analysis of promoters regulated by the EnvZ-OmpR system (Figures 9B, S8). Modulation of sensor kinases via small protein connectors appears to be a general theme that many small membrane proteins of unknown function may fall under [14]. For instance, under acidic conditions, a 65-amino acid protein SafA is activated by the EvgS-EvgA two-component system, which subsequently interacts with and activates the PhoQ-PhoP system [63]. In a second example, an 88-amino acid protein PmrD connects the PmrB-PmrA and PhoQ-PhoP signaling systems in *Salmonella* [64,65]. Another 127-amino acid protein MzrA is known to bind and activate EnvZ, which links the CpxA-CpxR and EnvZ-OmpR pathways in *E. coli* [57]. Taken together, our findings outlining the transcriptional regulation of YoaI by PhoB (Figure 4A), PhoQ-dependent growth phenotype upon YoaI overexpression (Figure 8C), and YoaI's physical interaction with EnvZ and

modulation of EnvZ-regulated promoter activity (Figures 9B, S8) reveal how this 34-amino acid small protein acts as a connector between distinct two-component signaling systems – PhoRB, PhoQP, and EnvZ-OmpR to integrate diverse stress responses (Figure 9C).

Most small proteins (≤50 amino acids in prokaryotes) are of unknown function and little is known about when/if they are expressed in the cell and what their physiological relevance is. Small proteins are thought to fine-tune the activity and/or stability of larger target molecules in the cell, adding a layer of gene regulation. This type of conditional regulation by small proteins may be especially important when cells are grown in non-ideal or stressful environments. Overall, our work describing the identification of condition-specific small proteins and targeted phenotypic characterization provides a deeper understanding of small protein regulation and the physiological consequences of altering their expression levels, laying a foundation for deciphering their functions and regulatory mechanisms under relevant stress conditions.

Materials and methods

Media and growth conditions.

Bacterial cultures were grown in either Luria-Bertani (LB) Miller medium (IBI Scientific) or minimal A medium [66] supplemented with 0.2% glucose, 0.1% casamino acids, and the indicated concentration of $MgSO_4$, with aeration at 37°C, unless otherwise specified. In general, overnight cultures are grown in supplemented minimal A medium containing 1 mM $MgSO_4$ and antibiotic(s) as applicable. Saturated cultures are diluted 1:500 into fresh medium. For low Mg^{2+} stress, no Mg^{2+} was added when overnight cultures were diluted into fresh medium. Media containing 10 mM Mg^{2+} was used as the no-stress condition. For phosphate stress experiments, MOPS minimal medium (Teknova) supplemented with 0.2% glucose, 0.1% casamino acids, and either 1 mM K_2HPO_4 (no-stress) or no K_2HPO_4 (phosphate stress). For routine growth on solid medium, LB containing 1.5% bacteriological-grade agar (VWR Lifesciences) was used. For antibiotic selection, carbenicillin, kanamycin, and chloramphenicol were added at a final concentration of 50-100 μg ml^{-1}, 25- 50 μg ml^{-1}, and 6-25 μg ml^{-1}. b-isopropyl-D-thiogalactoside (IPTG) was used at a final concentration of 500 μM, unless otherwise specified. Arabinose was used at final concentrations of 0.5% and 30 mM for pBAD24-based vectors and pMR120-based vectors, respectively, to induce protein expression when needed.

Strains, plasmids, and cloning.

See supplemental information for details of the strains (Table S1), plasmids (Table S2), and primers (Table S3) used in this study. All the strains used were derived from *Escherichia coli K-12* MG1655. Strain JW2162 was a gift from Dr. Bryce Nickels; plasmids pEB52, pAL38, pAL39, pSMART, pMR120 and strains AML67, MDG147, TIM92, TIM100, and TIM202 were gifts from Dr. Mark Goulian. Strains GSO195, GSO219, GSO225, GSO232, and GSO317 were gifts from Dr. Gisela Storz. Strains JM2110 and JM2113 were kind gifts from Dr. Maude Guillier.

A modified version of the method described by [67] was used to generate in-frame gene deletions corresponding to each small protein. Briefly, the entire small open reading frame (sORF)

(including the stop codon) was deleted from the MG1655 genome and substituted with a kanamycin resistance cassette. While constructing the gene deletions, we avoided deleting any overlapping annotated ORFs, non-coding RNAs, or putative regulatory regions in the vicinity of the target gene. In the case of *yriA-yriB (yriAB),* the two small protein ORFs significantly overlapped; therefore, we deleted the combined *yriAB* ORF. Detailed information on the genomic coordinates of deleted regions can be found in Table S1. Genomic deletions and reporter constructs carrying the kanamycin resistance cassettes were transferred between strains using $P1_{vir}$ transduction [66] and validated by PCR. When necessary, the kanamycin cassette was excised from the chromosome by FLP-mediated recombination using pCP20, as previously described [68]. PCR and loss of antibiotic resistance confirmed the excision of the kanamycin cassette.

Plasmids expressing translational fusions of GFP-A206K to the small open reading frames (sORFs), specifically pPJ1-13 and pSV25, were generated through inverse PCR [69] using pAL39 as a template. Plasmids encoding C-terminally 6XHis-tagged-YobF and -PmrR (sORF-GGSG linker-6XHis) were created using inverse PCR with pEB52 as a template, resulting in pSV14 and pSV26, respectively. Plasmids encoding untagged small proteins (pSV30-pSV37, pSV58, pSV60, and pJS1-pJS7) were also generated by inverse PCR with pEB52 as a template. pSV54 was generated by inverse PCR using pBAD24 as a template. Plasmids pSV38-pSV45, pSV55, pSV59, and pSV61, encoding variants of sORFs with start codon substitutions to stop codons (TAA), were generated by site-directed mutagenesis with inverse PCR using templates pSV35, pSV34, pJS7, pJS4, pSV36, pJS5, pSV54, pSV37, and pSV60 as applicable. For pSV39-pSV42, another in-frame start codon within five amino acids of the annotated start was also substituted to TAA. All constructs were verified by Sanger sequencing. To generate pSV47, *yoaI* was PCR amplified from the MG1655 genome, digested with *XbaI/EcoRI* restriction enzymes, and then cloned into pUT18C at *XbaI/EcoRI* sites.

To examine the transcriptional regulation of the sORFs and identify the putative regulatory regions, ~200-500 bp upstream region of the start codon of each sORF was selected for cloning (see details in Table 2). If a given sORF was suspected to be part of an operon, two putative regions were chosen for analysis, the first directly upstream of the gene and a second region upstream of the entire operon. Each DNA segment was amplified from MG1655 genomic DNA by PCR and inserted upstream of the *yfp* reporter gene in pMR120 into the restriction sites (*XhoI/BamHI* to construct pSV16, while *EcoRI-BamHI* sites were used for the remaining constructs). The pMR120 vector also includes a *cfp* reporter regulated by a constitutive *tetA* promoter, serving as an internal plasmid control. The resulting plasmids (pPJ14, pPJ16-pPJ20, pPJ23, pSV16-21, pSV24, pSV28, pSV29) were confirmed by Sanger sequencing and transformed into MG1655 and TIM202 (*ΔphoQ)*. Note that pSMART (Lucigen), pMR120, and the derivatives are single-copy plasmids when transformed into *E. coli* [70]. *E. cloni* replicator cells (Lucigen) are transformed with these plasmids and cultured with arabinose induction to increase the copy number for plasmid isolation.

Translation initiation profiling (Ribo-RET) and RNA-Seq.

Overnight cultures of wild-type *E. coli* grown in supplemented minimal A medium and 1 mM $MgSO_4$ were diluted 1:500 in 100 ml of fresh medium and the specified concentrations of $MgSO_4$. Once the cultures reached an OD600 of ~0.4, they were split into two 50 ml conical tubes. Cells from one tube were pelleted and submitted to Genewiz for RNA-Seq, while the cells from the second tube were used for Ribo-RET. For Ribo-RET, cells were treated with retapamulin at a final concentration of 100 µg ml^{-1} for 5 minutes at 37°C with continuous shaking. After retapamulin treatment, cells were filtered through a nitrocellulose membrane with a pore size of 0.45 µm, quickly scraped off the surface, and flash-frozen in liquid nitrogen. The resulting samples were processed, and libraries were prepared as described previously [41] with the following modifications. Specifically, RNA fragments of 15-30 nucleotides (nt) in length were isolated by performing a tight gel size selection, and rRNA depletion was performed using the RiboCop for Gram-negative bacteria kit (Lexogen). The resulting RNA fragments were then pooled, and libraries were prepared, with a final library structure consisting of a 5' adapter – 4 random bases – insert – 5 random bases – sample barcode – 3' adapter. The randomized bases serve as Unique Molecular Identifiers (UMIs) for deduplication. The multiplexed library was sequenced on an Illumina HiSeq 4000 with a paired end reading of 150 bases (PE150 runs) at a sequencing depth of 40-60 million raw reads per sample.

Sequencing data analysis.

The raw sequencing data for this project has been deposited in the GEO database with the accession number GSE276379. An R package with codes for data processing and analysis has been made available on GitHub (https://github.com/yadavalli-lab/Small-proteins-induced-under-low-magnesium-stress-in-E.coli). The raw sequencing data was first demultiplexed, and the adaptors were removed using cutadapt [71]. The reads were then depleted of rRNA and tRNA and deduplicated using umi_tools dedup [72]. The Ribo-RET reads were aligned to the *E. coli* MG1655 genome NC_000913.3 (RefSeq assembly accession: GCF_000005845.2) using hisat2 [73], and the ribosome density was assigned to the 3’ end of the reads. Initiation peak density was calculated for the annotated translation start sites by summing up the normalized reads (reads per million, RPM) within 4 to 20 nt downstream of the first nucleotide in the start codon. For transcript quantification of RNA-Seq reads, Kallisto [74] was used. DESeq2 [75] was used for the differential expression analysis of gene expression in the RNA-Seq data. Normalization of the data for differential expression was carried out using the "apeglm" method [76]. Fold-changes were estimated by comparing two replicates of the low Mg^{2+} dataset to two replicates of the no-stress dataset, with filtering criteria set at more than two-fold changes and a p-value below 0.05.

Measurement of growth (optical density) and fluorescence using a microplate reader.

The optical density (OD_{600}) measurements for small protein overexpression and deletion constructs were performed in a clear flat bottom 96-well microplate (Corning) containing 150 µL culture per well using a microplate reader (Agilent BioTek Synergy Neo2S). Fluorescence measurements for transcriptional reporters were carried out similarly, using black-walled, clear-flat bottom 96-well microplates (Corning). Saturated cultures grown in supplemented minimal A or MOPS minimal medium were normalized to the same initial OD_{600} values across all samples and diluted 1:50 in fresh medium containing specified concentrations of $MgSO_4$ or K_2HPO_4, along with appropriate antibiotics and inducers, as indicated. The microplates were incubated at

37 °C with double orbital shaking before the real-time measurements of optical density (at 600 nm), YFP (excitation: 500 nm; emission: 540 nm), or CFP (excitation: 420 nm; emission: 485 nm) were acquired every hour for 20-24 hours.

Microscopy, and image analysis.

For localization of GFP-tagged small proteins, cells were grown to an OD_{600} of ~0.2 (~3 hours) and then rapidly cooled in an ice slurry. Streptomycin was added to a final concentration of 250 μg ml^{-1}. GFP fluorescence was captured with a 475 nm excitation wavelength and a 540 nm emission filter, with an exposure time of 30 ms and 20% intensity. While the exposure times were typically set to these specified values, slight variations were occasionally made to optimize imaging based on the levels of fluorescence expression observed.

For overexpression analysis, overnight cultures were diluted 1:500 into supplemented minimal medium containing no added $MgSO_4$, 50 μg ml^{-1} carbenicillin, and either 500 μM IPTG or 0.5% arabinose, as indicated. Cells were grown to the lag phase (OD_{600} ~0.005), then rapidly cooled in an ice slurry before phase contrast microscopy. For empty vector control and start codon variants, we captured lag phase micrograph images approximately 30-40 minutes post-inoculation and -induction. For MgtS, MgrB, PmrR, YoaI, and YmiA overexpression, lag phase measurements were performed at 2-3 hours, and for YkgS and DinQ, at 1-hour post-inoculation and -induction. To concentrate the cells, 1 mL of the culture was pelleted and resuspended in 30-50 μL minimal A salt solution. For exponential phase analysis (OD_{600} between 0.2-0.4) in cultures carrying empty vector control and start codon variants images were taken at ~3-4 hours. In the case of cells expressing MgtS, MgrB, PmrR, YoaI, and YmiA, images were taken at 16-18 hours, and YkgS and DinQ at 6-8 hours. Microscope slides were prepared using 1% agarose pads as described previously [28], with approximately 5-7 μL of the resuspended cells. A 40 ms exposure time and 20% intensity were applied to capture the phase-contrast images.

For single-cell fluorescence measurements of wild type and Δ*yoaI* cells carrying P_{omrB}-*mScarlet* reporter, overnight cultures were diluted 1:500 into fresh supplemented minimal A medium containing either 10 mM or no added $MgSO_4$. Cells were grown to exponential (OD_{600} ~0.3 for both stress and no stress conditions) and stationary phase (OD_{600} ~1.0 for stress condition and ~3.5 for no stress condition), and then rapidly cooled in an ice slurry. Streptomycin was added to a final concentration of 250 μg ml^{-1}. Fluorescence was measured using the mCherry channel with an excitation wavelength of 570 nm and an emission filter of 645 nm. The exposure time was set to 100 ms, with an intensity of 20%. Background fluorescence was determined by imaging MG1655 cells grown under the same conditions.

For single-cell fluorescence measurements upon YoaI overexpression (to measure reporter activities of P_{ompF}-*yfp* and P_{ompC}-*cfp*), the overnight cultures were diluted 1:500 into fresh supplemented minimal A medium containing 10 mM $MgSO_4$. Cells were grown to exponential phase (OD_{600} between 0.2-0.4), then rapidly cooled in an ice slurry, and streptomycin was added at 250 μg ml^{-1}. YFP fluorescence was measured using a 500 nm excitation wavelength and a 535 nm emission filter. CFP fluorescence was measured using a 435 nm excitation wavelength and a 480 nm emission filter. The exposure time for YFP and CFP measurements was set to 50

ms, respectively, with an intensity of 20%. The background fluorescence was determined by imaging MG1655/pEB52 cells grown under the same conditions.

Image visualization and acquisition were performed using a Nikon Ti-E epifluorescence microscope equipped with a TI2-S-HU attachable mechanical stage. The images were captured with a Prime 95B sCMOS camera from Teledyne Photometrics with 1x1 binning. All image acquisition was managed using Metamorph software (Molecular Devices), version 7.10.3.279. A minimum of 50 cells per replicate were analyzed for cell volume and single-cell fluorescence quantification. The distributions of cellular volume were assumed to follow the sphero-cylindrical shape of *E. coli.* The volume was calculated using the formula $V = \frac{pi}{4} * W^2 * \left(L - \frac{W}{3}\right)$. Images were analyzed, and the cellular length, width, and fluorescence intensity were quantified using ImageJ [77] and MicrobeJ plugin [78].

Preparation of membrane and cytoplasmic fractions.

Membrane and cytoplasmic protein fractions were prepared as described previously [26]. Briefly, saturated cultures of MG1655/pSV14 (PmrR-GGSG-6XHis), MG1655/pSV26 (YobF-GGSG-6XHis), and MG1655/pEB52 (empty vector) were diluted 1:500 in 4 ml of LB media containing 100 µg ml^{-1} carbenicillin and grown at 37 °C. After 4 hours of growth, 0.5 mM IPTG was added to the cultures, and the cells were harvested after 2 hours of induction. Cell pellets were resuspended in 50 µl of cold resuspension buffer containing 20% sucrose, 30 mM Tris pH 8.0, and 1X protease inhibitor cocktail (Sigma, cOmplete, EDTA-free). Then, 50 µl of 10 mg ml^{-1} lysozyme, freshly prepared in 0.1 M EDTA pH 7.0, was added to the cell suspension, and the mixture was incubated on ice for 30 minutes. Next, 1 ml of 3 mM EDTA pH 7.5 was added to each sample, followed by sonication (10s pulse, 10s gap, 6 times) using VCX-130 Vibra-Cell Ultrasonic sonicator (Fisher Scientific). Samples were briefly centrifuged at 6,000 rpm for 10 minutes at 4 °C to remove cellular debris, and the supernatant was collected and spun at 21,000 ×g for 30 minutes at 4 °C. The supernatant from this step is separated and stored as the cytoplasmic fraction. The pellet, representing the membrane fraction, was resuspended in a storage buffer containing 20 mM Tris pH 8.0/20% glycerol. For strains carrying genomic YoaI-SPA translational fusion, cultures were grown to an OD_{600} of ~0.2-0.4 before harvesting, and membrane and cytoplasmic fractions were prepared as mentioned above.

Western blot analysis.

The membrane and cytoplasmic fractions were resuspended in 4X Laemmli sample buffer containing 5% 2-mercaptoethanol and no dyes. The samples were heated at 70 °C for 10 minutes and run on a 12% Bis-Tris gel (NuPage, Invitrogen) using MES running buffer (Invitrogen) at 160V for 80 minutes. After electrophoresis, proteins were transferred to a PVDF membrane (Amersham™ Hybond™) with a 0.2 µm pore size using a semi-dry transfer cell (Bio-Rad Trans-Blot SD). The membranes were blocked with 5% w/v milk in Tris-buffered saline, pH 7.4, with 1% Tween 20 (TBS-T). Primary antibodies – mouse M2 anti-FLAG (Sigma-Aldrich) and rabbit anti-6XHis tag antibody (Rockland) were used at 1:1000 dilution to detect SPA- and 6XHis-tagged constructs, respectively. IRDye 800CW goat anti-mouse and IRDye 680RD donkey anti-rabbit antibodies (LiCOR) were used for secondary detection. SeaBlue™ Plus2 Pre-

stained Protein Standard (Invitrogen) was used as a ladder to visualize lower molecular weight protein bands. The proteins were visualized using a LI-COR Odyssey imager.

Bacterial two-hybrid and β-galactosidase reporter gene assays.

For the bacterial two-hybrid assay, several clones from the transformation plate were picked to reduce heterogeneity [55] and inoculated in LB containing 100 μg ml^{-1} ampicillin and 50 μg ml^{-1} kanamycin. Cultures were grown overnight at 30°C with shaking. The cultures were then diluted 1:1000 into LB supplemented with 500 μM IPTG and grown at 30°C until OD_{600} reached between 0.2-0.4, after which β-galactosidase activities (Miller units) were measured as previously described [79].

For the β-galactosidase reporter gene assay, strains carrying P_{omrB}-*lacZ* with either pSV34 (pYoaI) or pEB52 (empty vector) were grown overnight in LB medium with 100 μg ml^{-1} ampicillin. The next day, the cultures were diluted 1:100 in the same medium and grown at 37 °C. After 3 hours of growth, 0.5 mM IPTG was added to the cultures, and the cells were harvested after 2 hours of induction. For high-throughput measurements in a 96-well format, the protocol was modified as previously described [79].

Resource availability

Lead contact

Further information and requests for resources and reagents should be directed to and will be fulfilled by the lead contact, Srujana S. Yadavalli (sam.yadavalli@rutgers.edu).

Materials availability

Requests for strains and plasmids generated in this study should be directed to and will be fulfilled by the lead contact, Srujana S. Yadavalli (sam.yadavalli@rutgers.edu).

Data and code availability

Next-generation sequencing data generated in this study are deposited at Gene Expression Omnibus (GEO) with accession number GSE276379. All data generated or analyzed during this study are included in the manuscript and its supporting files. Source data files for all figures have been provided. The code used for data processing and analysis is available in a series of R Markdown documents hosted on GitHub (https://github.com/yadavalli-lab/Small-proteins-induced-under-low-magnesium-stress-in-E.coli).

Acknowledgments

The authors would like to thank Drs. Mark Goulian, Bryce Nickels, Gisela Storz, and Maude Guillier for generously sharing strains and plasmids. We thank the past and present members of the Yadavalli, Storz, and Shah Labs for their helpful discussions. We also thank Drs. Gisela Storz and Mark Goulian for critical feedback on the manuscript.
Funding: S.S.Y. is supported by the National Institutes of Health - National Institute of General Medical Sciences (NIH-NIGMS) ESI-MIRA R35 GM147566 and institutional start-up funds from Rutgers. P.S. was supported by NIH/NIGMS grant R35 GM124976 and start-up funds from the Human Genetics Institute of New Jersey at Rutgers University. S.V. is supported by the Waksman Institute Busch Predoctoral fellowship (2022-24). The funders did not play any role in

the study design, data collection and analysis, decision to publish, or preparation of the manuscript.

Author contributions

S.V., P.S., and S.S.Y. conceived the experiments. All authors planned the experiments, designed the methodology, and performed data analysis. S.V., P.S., and S.S.Y. wrote the initial draft of the manuscript, P.S. contributed to revisions and editing, and all authors reviewed the final manuscript.

Declaration of interests

S.S.Y. consults for and collaborates with Designs for Vision, Inc. P.S. a director at an RNA-therapeutics startup, and consults for Designs for Vision, Inc. S.V. declared that no competing interests exist.

References

1. Carlberg, C., and Molnar, F. (2016). Mechanisms of Gene Regulation 2nd ed. (Springer).

2. Goulian, M. (2010). Two-component signaling circuit structure and properties. Curr. Opin. Microbiol. *13*, 184–189.

3. Stock, A.M., Robinson, V.L., and Goudreau, P.N. (2000). Two-component signal transduction. Annu. Rev. Biochem. *69*, 183–215.

4. Laub, M.T. (2014). The role of two-component signal transduction systems in bacterial stress responses. In Bacterial Stress Responses (ASM Press), pp. 45–58.

5. Baumberg, S. ed. (1999). Prokaryotic Gene Expression. Preprint at Oxford University PressOxford, https://doi.org/10.1093/oso/9780199636044.001.0001 https://doi.org/10.1093/oso/9780199636044.001.0001.

6. Banerjee, T. (2022). Regulation of Gene Expression in Prokaryotes. In Genetics Fundamentals Notes (Springer Nature Singapore), pp. 569–596.

7. Tollerson, R., 2nd, and Ibba, M. (2020). Translational regulation of environmental adaptation in bacteria. J. Biol. Chem. *295*, 10434–10445.

8. Cain, J.A., Solis, N., and Cordwell, S.J. (2014). Beyond gene expression: the impact of protein post-translational modifications in bacteria. J. Proteomics *97*, 265–286.

9. Gottesman, S. (2019). Trouble is coming: Signaling pathways that regulate general stress responses in bacteria. J. Biol. Chem. *294*, 11685–11700.

10. Storz, G., Vogel, J., and Wassarman, K.M. (2011). Regulation by small RNAs in bacteria: expanding frontiers. Mol. Cell *43*, 880–891.

11. Seshasayee, A.S.N., Sivaraman, K., and Luscombe, N.M. (2011). An overview of prokaryotic transcription factors : a summary of function and occurrence in bacterial genomes. Subcell. Biochem. *52*, 7–23.

12. Burton, A.T., Zeinert, R., and Storz, G. (2024). Large Roles of Small Proteins. Annu. Rev. Microbiol. https://doi.org/10.1146/annurev-micro-112723-083001.

13. Hemm Matthew R., Weaver Jeremy, Storz Gisela, Lovett Susan T., and Hinton Deborah (2020). Escherichia coli Small Proteome. EcoSal Plus *9*. https://doi.org/10.1128/ecosalplus.ESP-0031-2019.

14. Yadavalli, S.S., and Yuan, J. (2022). Bacterial Small Membrane Proteins: the Swiss Army Knife of Regulators at the Lipid Bilayer. J. Bacteriol. *204*, e0034421.

15. Gray, T., Storz, G., and Papenfort, K. (2022). Small Proteins; Big Questions. J. Bacteriol. *204*, e0034121.

16. Pueyo, J.I., Magny, E.G., and Couso, J.P. (2016). New peptides under the s(ORF)ace of the genome. Trends Biochem. Sci. *41*, 665–678.

17. Patraquim, P., Mumtaz, M.A.S., Pueyo, J.I., Aspden, J.L., and Couso, J.-P. (2020). Developmental regulation of canonical and small ORF translation from mRNAs. Genome Biol. *21*, 128.

18. Sberro, H., Fremin, B.J., Zlitni, S., Edfors, F., Greenfield, N., Snyder, M.P., Pavlopoulos, G.A., Kyrpides, N.C., and Bhatt, A.S. (2019). Large-Scale Analyses of Human Microbiomes Reveal Thousands of Small, Novel Genes. Cell *178*, 1245-1259.e14.

19. Kastenmayer, J.P., Ni, L., Chu, A., Kitchen, L.E., Au, W.-C., Yang, H., Carter, C.D., Wheeler, D., Davis, R.W., Boeke, J.D., et al. (2006). Functional genomics of genes with small open reading frames (sORFs) in S. cerevisiae. Genome Res. *16*, 365–373.

20. Steinberg, R., and Koch, H.-G. (2021). The largely unexplored biology of small proteins in pro- and eukaryotes. FEBS J. *288*, 7002–7024.

21. Hemm, M.R., Paul, B.J., Schneider, T.D., Storz, G., and Rudd, K.E. (2008). Small membrane proteins found by comparative genomics and ribosome binding site models. Mol. Microbiol. *70*, 1487–1501.

22. Hemm, M.R., Paul, B.J., Miranda-Ríos, J., Zhang, A., Soltanzad, N., and Storz, G. (2010). Small stress response proteins in Escherichia coli: proteins missed by classical proteomic studies. J. Bacteriol. *192*, 46–58.

23. Groisman, E.A., and Chan, C. (2021). Cellular Adaptations to Cytoplasmic Mg2+ Limitation. Annu. Rev. Microbiol. *75*, 649–672.

24. Groisman, E.A., Duprey, A., and Choi, J. (2021). How the PhoP/PhoQ System Controls Virulence and Mg2+ Homeostasis: Lessons in Signal Transduction, Pathogenesis, Physiology, and Evolution. Microbiol. Mol. Biol. Rev. *85*, e0017620.

25. Groisman, E.A. (2001). The pleiotropic two-component regulatory system PhoP-PhoQ. J. Bacteriol. *183*, 1835–1842.

26. Yadavalli Srujana S., Goh Ted, Carey Jeffrey N., Malengo Gabriele, Vellappan Sangeevan, Nickels Bryce E., Sourjik Victor, Goulian Mark, Yuan Jing, and Silhavy Thomas J. (2020). Functional Determinants of a Small Protein Controlling a Broadly Conserved Bacterial Sensor Kinase. J. Bacteriol. *202*, e00305-20.

27. Lippa, A.M., and Goulian, M. (2009). Feedback inhibition in the PhoQ/PhoP signaling system by a membrane peptide. PLoS Genet. *5*, e1000788.

28. Yadavalli, S.S., Carey, J.N., Leibman, R.S., Chen, A.I., Stern, A.M., Roggiani, M., Lippa, A.M., and Goulian, M. (2016). Antimicrobial peptides trigger a division block in Escherichia coli through stimulation of a signalling system. Nat. Commun. *7*, 1–10.

29. Patel, V., and Matange, N. (2021). Adaptation and compensation in a bacterial gene regulatory network evolving under antibiotic selection. Elife *10*. https://doi.org/10.7554/eLife.70931.

30. Cannatelli, A., Giani, T., D'Andrea, M.M., Di Pilato, V., Arena, F., Conte, V., Tryfinopoulou, K., Vatopoulos, A., Rossolini, G.M., and COLGRIT Study Group (2014). MgrB inactivation is a common mechanism of colistin resistance in KPC-producing Klebsiella pneumoniae of clinical origin. Antimicrob. Agents Chemother. *58*, 5696–5703.

31. Wang, H., Yin, X., Wu Orr, M., Dambach, M., Curtis, R., and Storz, G. (2017). Increasing intracellular magnesium levels with the 31-amino acid MgtS protein. Proc. Natl. Acad. Sci. U. S. A. *114*, 5689–5694.

32. Yin, X., Wu Orr, M., Wang, H., Hobbs, E.C., Shabalina, S.A., and Storz, G. (2019). The small protein MgtS and small RNA MgrR modulate the PitA phosphate symporter to boost intracellular magnesium levels. Mol. Microbiol. *111*, 131–144.

33. Kato, A., Chen, H.D., Latifi, T., and Groisman, E.A. (2012). Reciprocal control between a bacterium's regulatory system and the modification status of its lipopolysaccharide. Mol. Cell *47*, 897–908.

34. Hong, X., Chen, H.D., and Groisman, E.A. (2018). Gene expression kinetics governs stimulus-specific decoration of the *Salmonella* outer membrane. Sci. Signal. *11*. https://doi.org/10.1126/scisignal.aar7921.

35. Chen, A.I., Albicoro, F.J., Zhu, J., and Goulian, M. (2021). Effects of regulatory network organization and environment on PmrD connector activity and polymyxin resistance in Klebsiella pneumoniae and Escherichia coli. Antimicrob. Agents Chemother. *65*. https://doi.org/10.1128/AAC.00889-20.

36. Tian, X., Manat, G., Gasiorowski, E., Auger, R., Hicham, S., Mengin-Lecreulx, D., Boneca, I.G., and Touzé, T. (2021). LpxT-Dependent Phosphorylation of Lipid A in Escherichia coli Increases Resistance to Deoxycholate and Enhances Gut Colonization. Front. Microbiol. *12*, 676596.

37. Meydan, S., Marks, J., Klepacki, D., Sharma, V., Baranov, P.V., Firth, A.E., Margus, T., Kefi, A., Vázquez-Laslop, N., and Mankin, A.S. (2019). Retapamulin-Assisted Ribosome Profiling Reveals the Alternative Bacterial Proteome. Mol. Cell *74*, 481-493.e6.

38. Weaver, J., Mohammad, F., Buskirk, A.R., and Storz, G. (2019). Identifying Small Proteins by Ribosome Profiling with Stalled Initiation Complexes. MBio *10*. https://doi.org/10.1128/mBio.02819-18.

39. Gardner, S.G., and McCleary, W.R. (2019). Control of the phoBR Regulon in Escherichia coli. EcoSal Plus *8*. https://doi.org/10.1128/ecosalplus.ESP-0006-2019.

40. Kenney, L.J., and Anand, G.S. (2020). EnvZ/OmpR Two-Component Signaling: An Archetype System That Can Function Noncanonically. EcoSal Plus *9*. https://doi.org/10.1128/ecosalplus.ESP-0001-2019.

41. Cope, A.L., Vellappan, S., Favate, J.S., Skalenko, K.S., Yadavalli, S.S., and Shah, P. (2022). Exploring Ribosome-Positioning on Translating Transcripts with Ribosome Profiling. Methods Mol. Biol. *2404*, 83–110.

42. Glaub, A., Huptas, C., Neuhaus, K., and Ardern, Z. (2020). Recommendations for bacterial ribosome profiling experiments based on bioinformatic evaluation of published data. J. Biol. Chem. *295*, 8999–9011.

43. Kato, A., Tanabe, H., and Utsumi, R. (1999). Molecular characterization of the PhoP-PhoQ two-component system in Escherichia coli K-12: identification of extracellular Mg2+-responsive promoters. J. Bacteriol. *181*, 5516–5520.

44. Hobbs, E.C., Astarita, J.L., and Storz, G. (2010). Small RNAs and small proteins involved in resistance to cell envelope stress and acid shock in Escherichia coli: analysis of a bar-coded mutant collection. J. Bacteriol. *192*, 59–67.

45. Weel-Sneve, R., Kristiansen, K.I., Odsbu, I., Dalhus, B., Booth, J., Rognes, T., Skarstad, K., and Bjørås, M. (2013). Single transmembrane peptide DinQ modulates membrane-dependent activities. PLoS Genet. *9*, e1003260.

46. Rubin, E.J., Herrera, C.M., Crofts, A.A., and Trent, M.S. (2015). PmrD is required for modifications to escherichia coli endotoxin that promote antimicrobial resistance. Antimicrob. Agents Chemother. *59*, 2051–2061.

47. Fitzgerald, D.M., Stringer, A.M., Smith, C., Lapierre, P., and Wade, J.T. (2023). Genome-Wide Mapping of the Escherichia coli PhoB Regulon Reveals Many Transcriptionally Inert, Intragenic Binding Sites. MBio *14*, e0253522.

48. Yoshida, Y., Sugiyama, S., Oyamada, T., Yokoyama, K., and Makino, K. (2012). Novel members of the phosphate regulon in Escherichia coli O157:H7 identified using a whole-genome shotgun approach. Gene *502*, 27–35.

49. Chekabab, S.M., Jubelin, G., Dozois, C.M., and Harel, J. (2014). PhoB activates Escherichia coli O157:H7 virulence factors in response to inorganic phosphate limitation. PLoS One *9*, e94285.

50. Pontes, M.H., and Groisman, E.A. (2018). Protein synthesis controls phosphate homeostasis. Genes Dev. *32*, 79–92.

51. Möller, S., Croning, M.D., and Apweiler, R. (2001). Evaluation of methods for the prediction of membrane spanning regions. Bioinformatics *17*, 646–653.

52. Ikeda, M., Arai, M., Okuno, T., and Shimizu, T. (2003). TMPDB: a database of experimentally-characterized transmembrane topologies. Nucleic Acids Res. *31*, 406–409.

53. Käll, L., Krogh, A., and Sonnhammer, E.L.L. (2004). A combined transmembrane topology and signal peptide prediction method. J. Mol. Biol. *338*, 1027–1036.

54. Feilmeier, B.J., Iseminger, G., Schroeder, D., Webber, H., and Phillips, G.J. (2000). Green fluorescent protein functions as a reporter for protein localization in Escherichia coli. J. Bacteriol. *182*, 4068–4076.

55. Battesti, A., and Bouveret, E. (2012). The bacterial two-hybrid system based on adenylate cyclase reconstitution in Escherichia coli. Methods *58*, 325–334.

56. Karimova, G., Pidoux, J., Ullmann, A., and Ladant, D. (1998). A bacterial two-hybrid system based on a reconstituted signal transduction pathway. Proc. Natl. Acad. Sci. U. S. A. *95*, 5752–5756.

57. Gerken, H., Charlson, E.S., Cicirelli, E.M., Kenney, L.J., and Misra, R. (2009). MzrA: a novel modulator of the EnvZ/OmpR two-component regulon. Mol. Microbiol. *72*, 1408–1422.

58. Bastet, L., Korepanov, A.P., Jagodnik, J., Grondin, J.P., Lamontagne, A.-M., Guillier, M., and Lafontaine, D.A. (2024). Riboswitch and small RNAs modulate btuB translation initiation in Escherichia coli and trigger distinct mRNA regulatory mechanisms. Nucleic Acids Res. *52*, 5852–5865.

59. Batchelor, E., Silhavy, T.J., and Goulian, M. (2004). Continuous control in bacterial regulatory circuits. J. Bacteriol. *186*, 7618–7625.

60. Alphen, W.V., and Lugtenberg, B. (1977). Influence of osmolarity of the growth medium on the outer membrane protein pattern of Escherichia coli. J. Bacteriol. *131*, 623–630.

61. Batchelor, E., Walthers, D., Kenney, L.J., and Goulian, M. (2005). The Escherichia coli CpxA-CpxR envelope stress response system regulates expression of the porins ompF and ompC. J. Bacteriol. *187*, 5723–5731.

62. Olaitan, A.O., Morand, S., and Rolain, J.-M. (2014). Mechanisms of polymyxin resistance: acquired and intrinsic resistance in bacteria. Front. Microbiol. *5*, 643.

63. Eguchi, Y., Itou, J., Yamane, M., Demizu, R., Yamato, F., Okada, A., Mori, H., Kato, A., and Utsumi, R. (2007). B1500, a small membrane protein, connects the two-component systems EvgS/EvgA and PhoQ/PhoP in *Escherichia coli*. Proc. Natl. Acad. Sci. U. S. A. *104*, 18712–18717.

64. Kox, L.F., Wösten, M.M., and Groisman, E.A. (2000). A small protein that mediates the activation of a two-component system by another two-component system. EMBO J. *19*, 1861–1872.

65. Kato, A., and Groisman, E.A. (2004). Connecting two-component regulatory systems by a protein that protects a response regulator from dephosphorylation by its cognate sensor. Genes Dev. *18*, 2302–2313.

66. Miller, J.H., and Others (1992). A Short Course in Bacterial Genetics: A Laboratory Manual and Handbook for Escherichia Coli and Related Bacteria (CSHL Press).

67. Datsenko, K.A., and Wanner, B.L. (2000). One-step inactivation of chromosomal genes in Escherichia coli K-12 using PCR products. Proc. Natl. Acad. Sci. U. S. A. *97*, 6640–6645.

68. Cherepanov, P.P., and Wackernagel, W. (1995). Gene disruption in Escherichia coli: TcR and KmR cassettes with the option of Flp-catalyzed excision of the antibiotic-resistance determinant. Gene *158*, 9–14.

69. Ochman, H., Medhora, M.M., Garza, D., and Hartl, D.L. (1990). Amplification of flanking sequences by inverse PCR. PCR protocols: A guide to methods and applications, 219–227.

70. Godiska R, Patterson M, Schoenfeld T, and Mead DA (2005). Beyond pUC: Vectors for Cloning Unstable DNA. In DNA Sequencing: Optimizing the Process and Analysis, J. Kieleczawa, ed. (Jones & Bartlett Learning), pp. 55–76.

71. Martin, M. (2011). Cutadapt removes adapter sequences from high-throughput sequencing reads. EMBnet.journal *17*, 10–12.

72. Smith, T., Heger, A., and Sudbery, I. (2017). UMI-tools: modeling sequencing errors in Unique Molecular Identifiers to improve quantification accuracy. Genome Res. *27*, 491–499.

73. Kim, D., Paggi, J.M., Park, C., Bennett, C., and Salzberg, S.L. (2019). Graph-based genome alignment and genotyping with HISAT2 and HISAT-genotype. Nat. Biotechnol. *37*, 907–915.

74. Bray, N.L., Pimentel, H., Melsted, P., and Pachter, L. (2016). Near-optimal probabilistic RNA-seq quantification. Nat. Biotechnol. *34*, 525–527.

75. Love, M.I., Huber, W., and Anders, S. (2014). Moderated estimation of fold change and dispersion for RNA-seq data with DESeq2. Genome Biol. *15*, 550.

76. Zhu, A., Ibrahim, J.G., and Love, M.I. (2019). Heavy-tailed prior distributions for sequence count data: removing the noise and preserving large differences. Bioinformatics *35*, 2084–2092.

77. Schneider, C.A., Rasband, W.S., and Eliceiri, K.W. (2012). NIH Image to ImageJ: 25 years of image analysis. Nat. Methods *9*, 671–675.

78. Jiang, C., Brown, P.J.B., Ducret, A., and Brun, Y.V. (2014). Sequential evolution of bacterial morphology by co-option of a developmental regulator. Nature *506*, 489–493.

79. Thibodeau, S.A., Fang, R., and Joung, J.K. (2004). High-throughput beta-galactosidase assay for bacterial cell-based reporter systems. Biotechniques *36*, 410–415.

Figures and tables

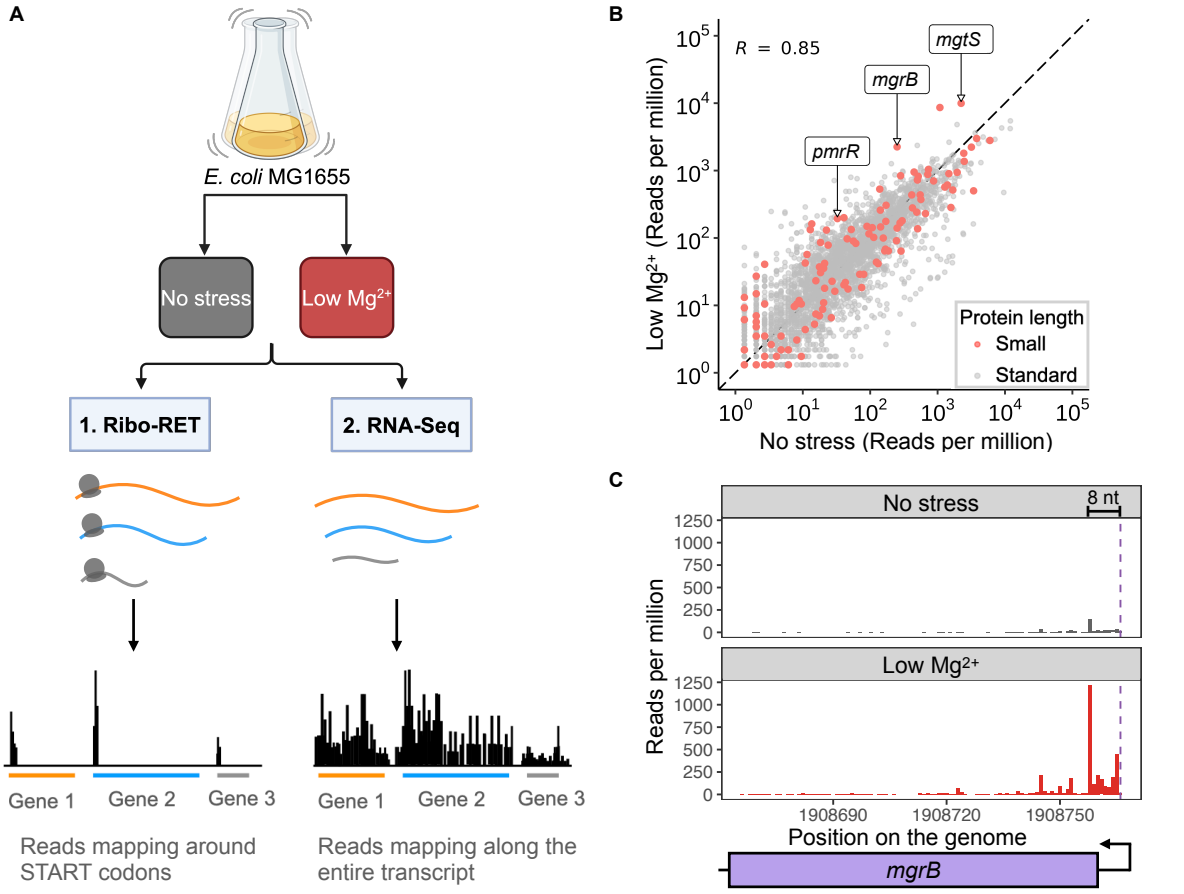

Figure 1. Identification of small proteins induced under low magnesium stress in *E. coli* by translation-initiation profiling (Ribo-RET). (A) Schematic diagram showing the Ribo-RET and RNA-Seq experimental setup used to identify small proteins induced by low magnesium stress. Wild-type *E. coli* K-12 MG1655 cells were grown in supplemented minimal A medium containing $MgSO_4$ at either 10 mM (no stress) or ~1 μM (no added magnesium, low Mg^{2+} stress). (B) Scatterplot showing the correlation between the Ribo-RET reads mapping to the annotated start sites of proteins expressed under low Mg^{2+} stress and no stress. The red dots represent annotated small proteins of ≤ 50 amino acids in length, and the gray dots represent proteins > 50 amino acids long. Small proteins, MgrB, MgtS, and PmrR, known to be induced under magnesium starvation, are highlighted. Pearson's coefficient, r= 0.85. (C) Ribo-RET data for a representative small protein MgrB induced under low Mg^{2+} stress. A purple dashed line indicates the translation start site, and the 8 nucleotide (nt) indicates the distance between the highest ribosome density peak and the first nucleotide of the start codon. (Also see Tables 1, S4, Figures S1 and S2)

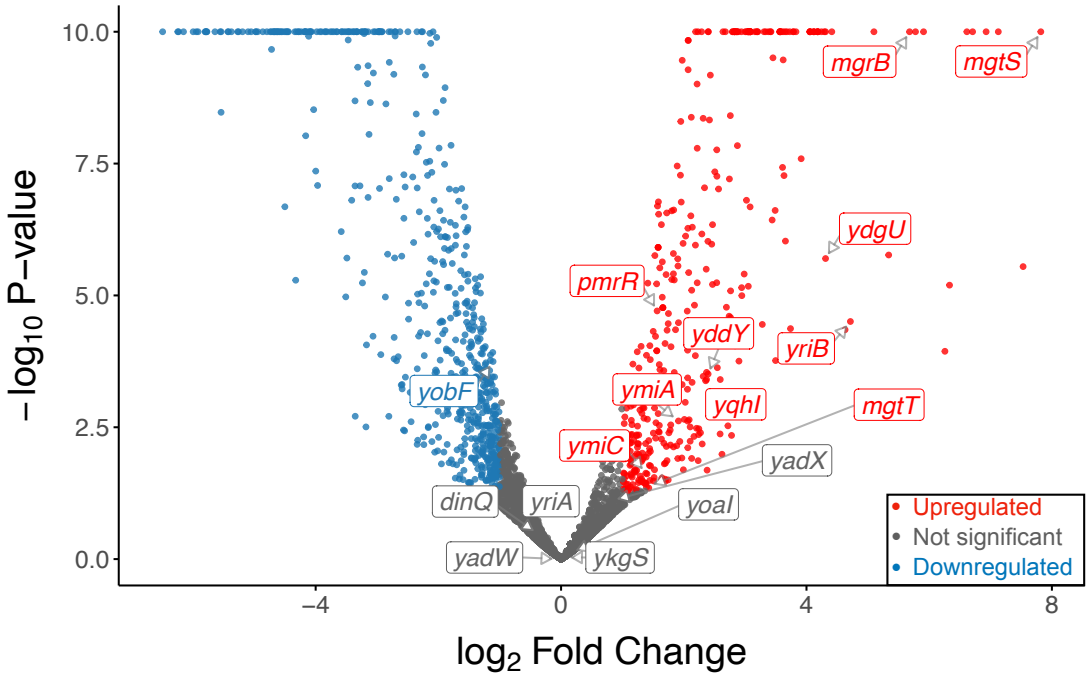

Figure 2. RNA-Seq analysis of transcripts representing small proteins induced under low magnesium stress. Volcano plot illustrating differential expression of small proteins induced under low magnesium stress from RNA-Seq data. Transcripts that are either upregulated or downregulated are highlighted in red or blue, respectively, and those with no significant change are represented in gray. The criteria for significance include a fold change threshold of >2 and a p-value of <0.05. The -$\log_{10}$ P-value of *mgrB* and *mgtS* were 75 and 140 respectively. To prevent distortion from their exceptionally high values dominating the plot, the transformed p-values were capped at 10 to enhance visualization. Data represent differential expression analysis from two independent replicates. (Also see Tables 2, S4, and Figure S3)

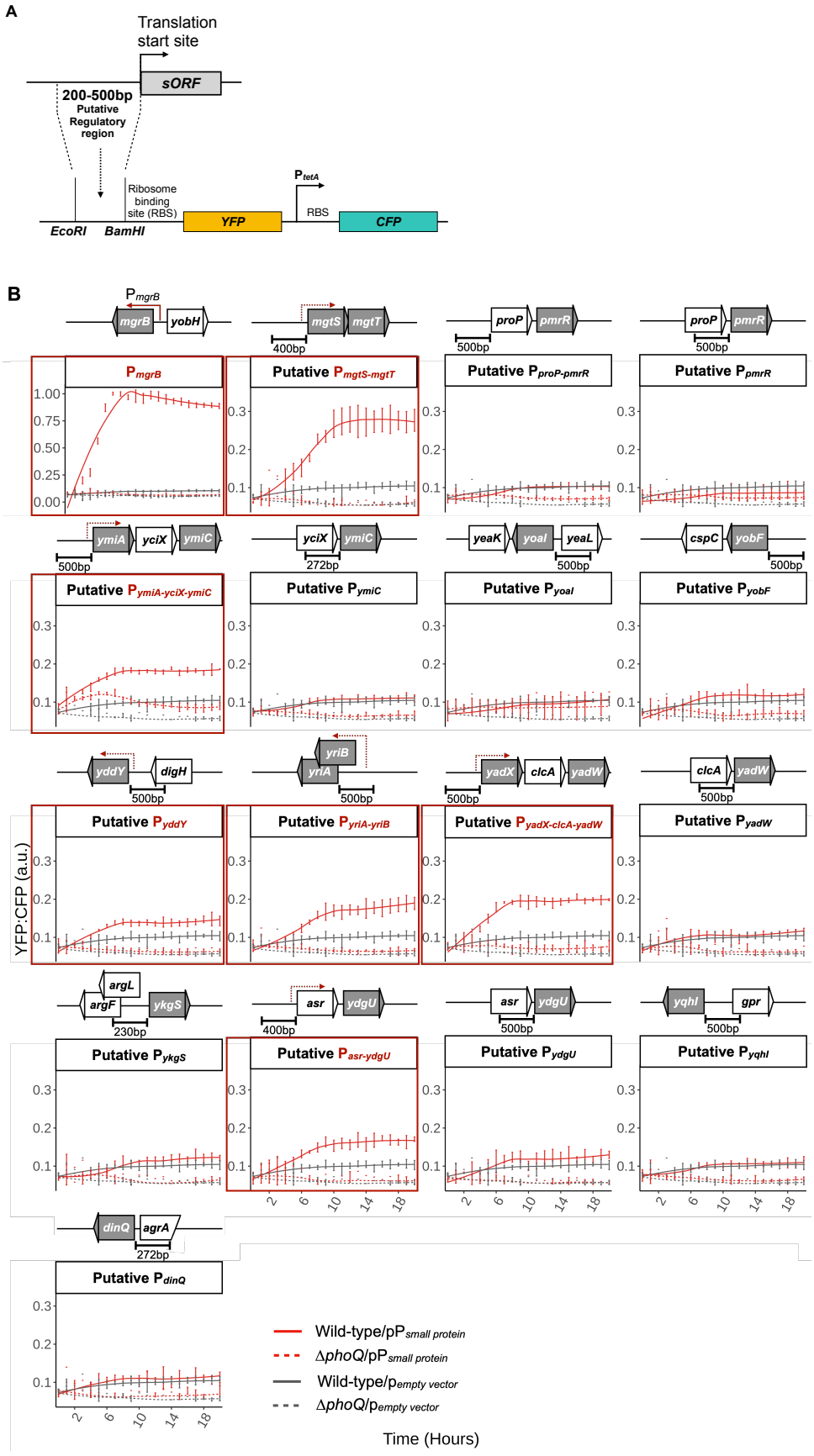

Figure 3. Transcriptional regulation of small proteins under low magnesium stress. (A) Schematic representation of the transcriptional reporter fusion construct. Regions (200-500 bp) upstream of the small open reading frames of interest were amplified from the MG1655 genome and cloned into a YFP-encoding reporter plasmid (pMR120) resulting in plasmids pPJ14, pPJ16-pPJ20, pPJ23, pSV16-pSV21, pSV24, pSV28-pSV29 (See Table 2 for genomic coordinates of the regulatory regions tested here and Table S2 for plasmid details). (B) Measurement of transcriptional reporter activity (YFP:CFP) for the indicated small proteins under low Mg^{2+} (no added magnesium). The solid and dashed lines represent the wild-type *E. coli* MG1655 and Δ*phoQ* cells, respectively, harboring plasmids with either transcriptional fusion for a putative regulatory region of a small protein with *yfp* (red line) or *yfp* only (gray line). The schematic above each plot depicts the arrangement of the small protein-encoding genes (shown in gray), including the putative regulatory regions and operons where applicable. Transcriptional reporters showing an increased activity compared to the empty vector control (pMR120) are highlighted in red. The cultures were grown in a supplemented minimal medium with 6 μg ml^{-1} chloramphenicol. The data represent averages and standard errors of the means for four independent replicates. (Also see Table 2)

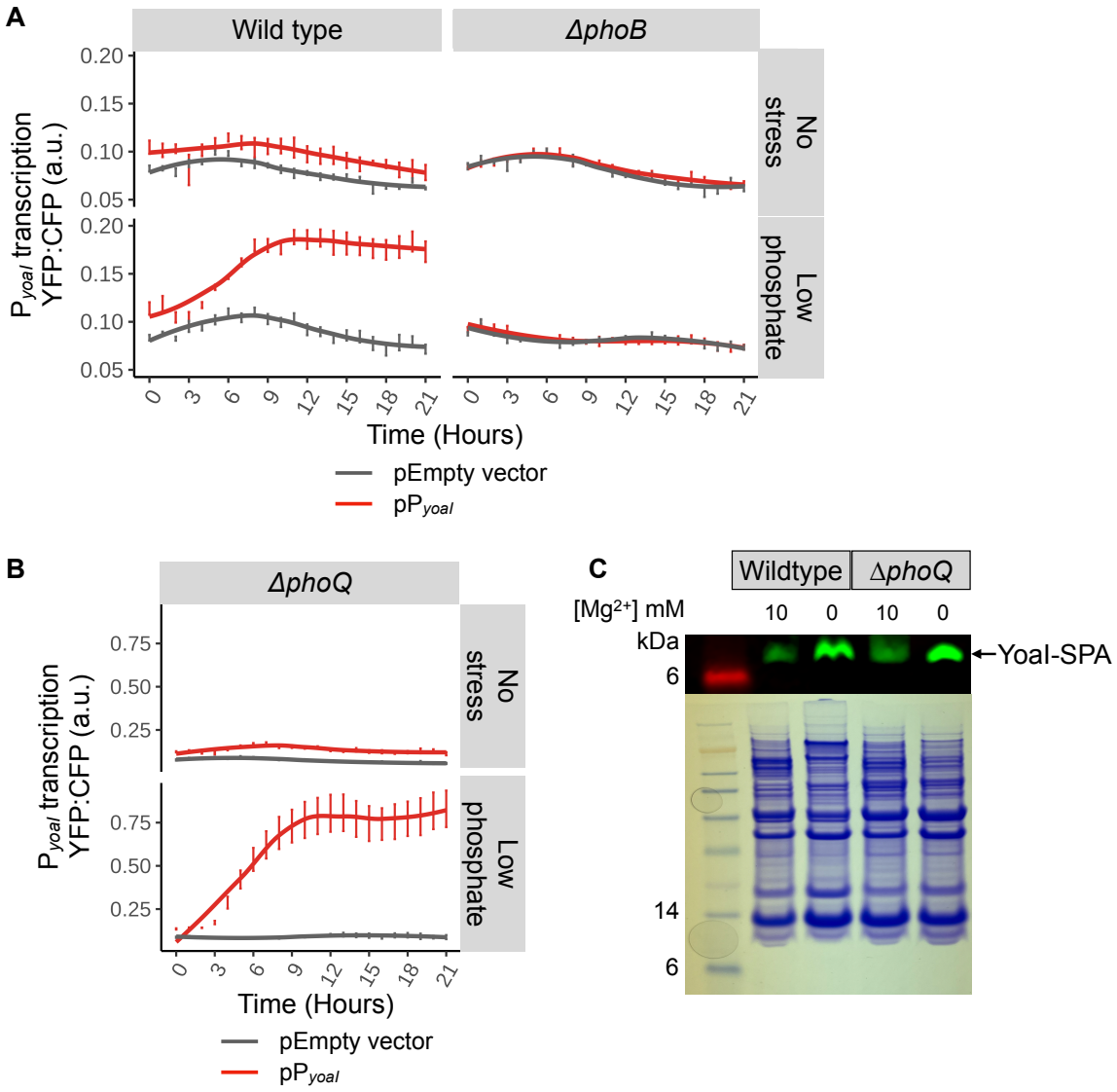

Figure 4. Regulation of YoaI expression during magnesium limitation. (A-B) Transcriptional activity of *yoaI* was measured as a function of YFP reporter fluorescence in *E. coli* MG1655, Δ*phoB* (SV48), and Δ*phoQ* (TIM100) strains under phosphate stress as indicated. The red and gray lines represent cells carrying plasmid-encoded P_{yoaI}-*yfp* transcriptional reporter (pPJ18) and *yfp*-only control vector (pMR120), respectively. The cultures were grown in a supplemented MOPS minimal medium with 6 μg ml^{-1} chloramphenicol with either 1 mM K_2HPO_4 for no stress condition, or no added K_2HPO_4 for phosphate stress. The data illustrate average YFP:CFP fluorescence with standard error of the means, derived from four independent replicates. (C) Detection of YoaI protein in *E. coli* wild-type (GSO317) and Δ*phoQ* (SV60) strains containing *yoaI-SPA* genomic translational fusion. Cells were grown in supplemented minimal A medium, with $MgSO_4$ added at the specified concentration (10mM or no added $MgSO_4$). Membrane fractions were analyzed by western blotting using M2 anti-FLAG antibodies (top) and by Coomassie Brilliant Blue staining (bottom). The data represent results from two independent replicates.

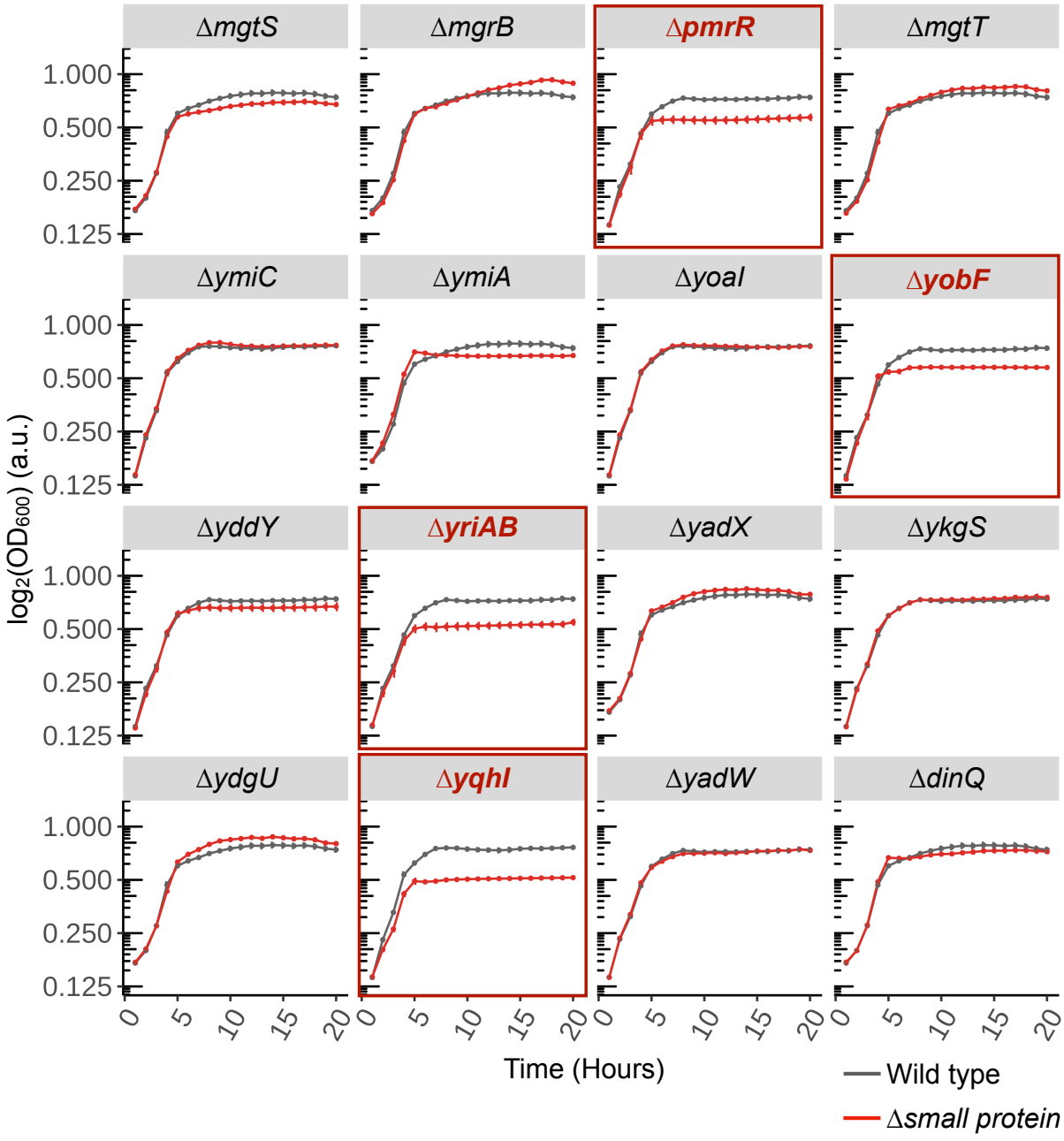

Figure 5. Effect of deleting genes encoding low Mg^{2+} stress-induced small proteins on bacterial growth. Growth curves of wild-type *E. coli* MG1655 (gray) and mutants corresponding to the deletions of small protein-encoding genes (red) (strains SV64, AML67, SV35, SV31, SV41, SV57, SV59, SV33, SV29, SV25, SV39, SV43, SV58, SV37, SV27, and SV56, please see Table S1 and methods for strain details). Deletion mutants showing reduced growth yield compared to wild-type cells are highlighted in red. The cultures were grown in supplemented minimal A medium with no added magnesium and 50 μg ml^{-1} carbenicillin. Data represent averages and standard errors of means for four independent cultures.

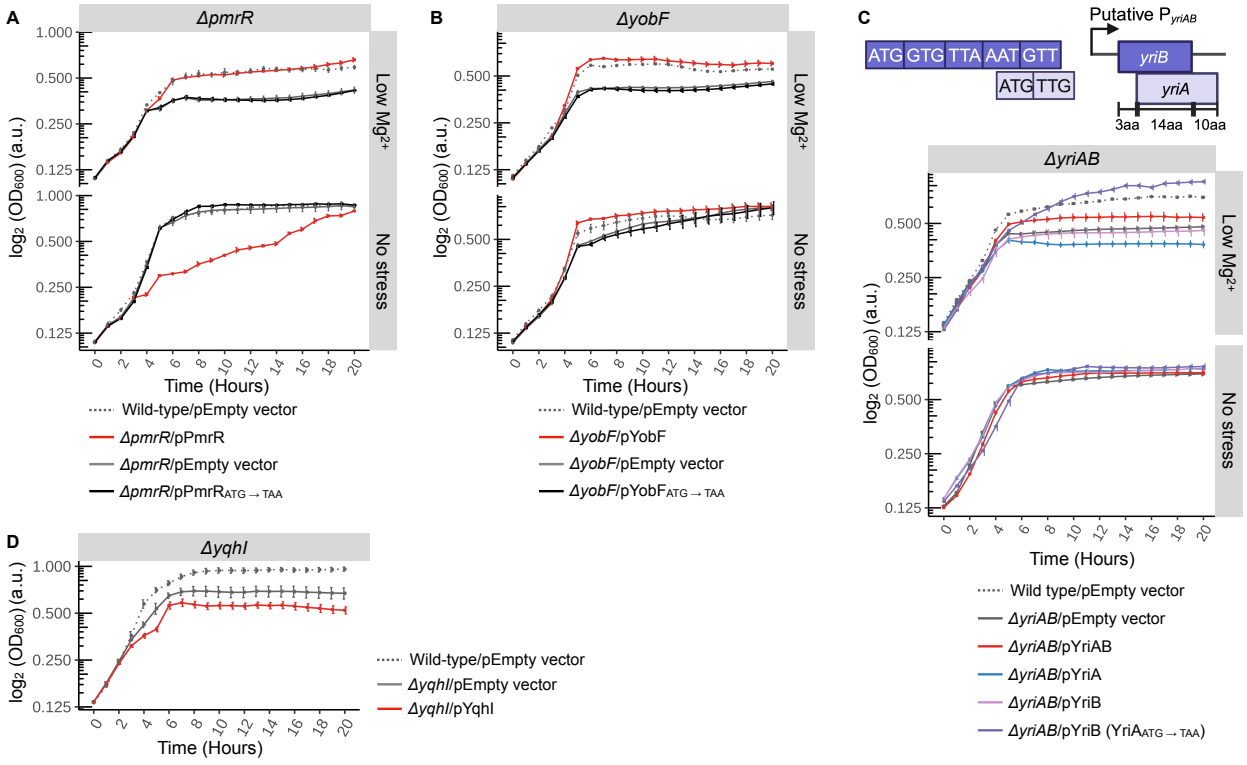

Figure 6. Complementation of growth phenotypes associated with *pmrR,* and *yobF* deletions. (A-B) Growth curves of Δ*pmrR* (SV35), and Δ*yobF* (SV34) deletion strains carrying an empty vector (pEB52, solid gray line) or complemented with plasmids encoding small proteins pPmrR (pSV35) and pYobF (pJS5) (red line) or their variants $pPmrR_{ATG→TAA}$ (pSV38), and $pYobF_{ATG→TAA}$ (pSV45) (black line), as indicated. Wild-type MG1655 cells containing the empty vector are included as a control (dashed gray line). (C) Schematic of the overlapping genes *yriAB* followed by the growth curves of gene deletion *ΔyriAB* (SV25) complemented with pYriAB (pSV58), pYriA (pJS1), pYriB (pSV37), pYriB ($YriA_{ATG→TAA}$) (pSV59), or an empty vector (pEB52, as indicated. (D) Growth curves of gene deletion *ΔyqhI* (SV37) carrying an empty vector (pEB52), or complemented with a plasmid encoding YqhI. Wild-type cells containing an empty vector (pEB52, dashed gray line) are included as a control. For panels A-D, cultures were grown in supplemented minimal A medium containing 50 μg ml^{-1} carbenicillin and either no added magnesium or 10 mM $MgSO_4$ as indicated. 500 μM IPTG was used for induction, except for PmrR derivatives (pSV35 and pSV38), where 12.5 μM IPTG was used. Data represent averages and standard errors of means for four independent cultures.

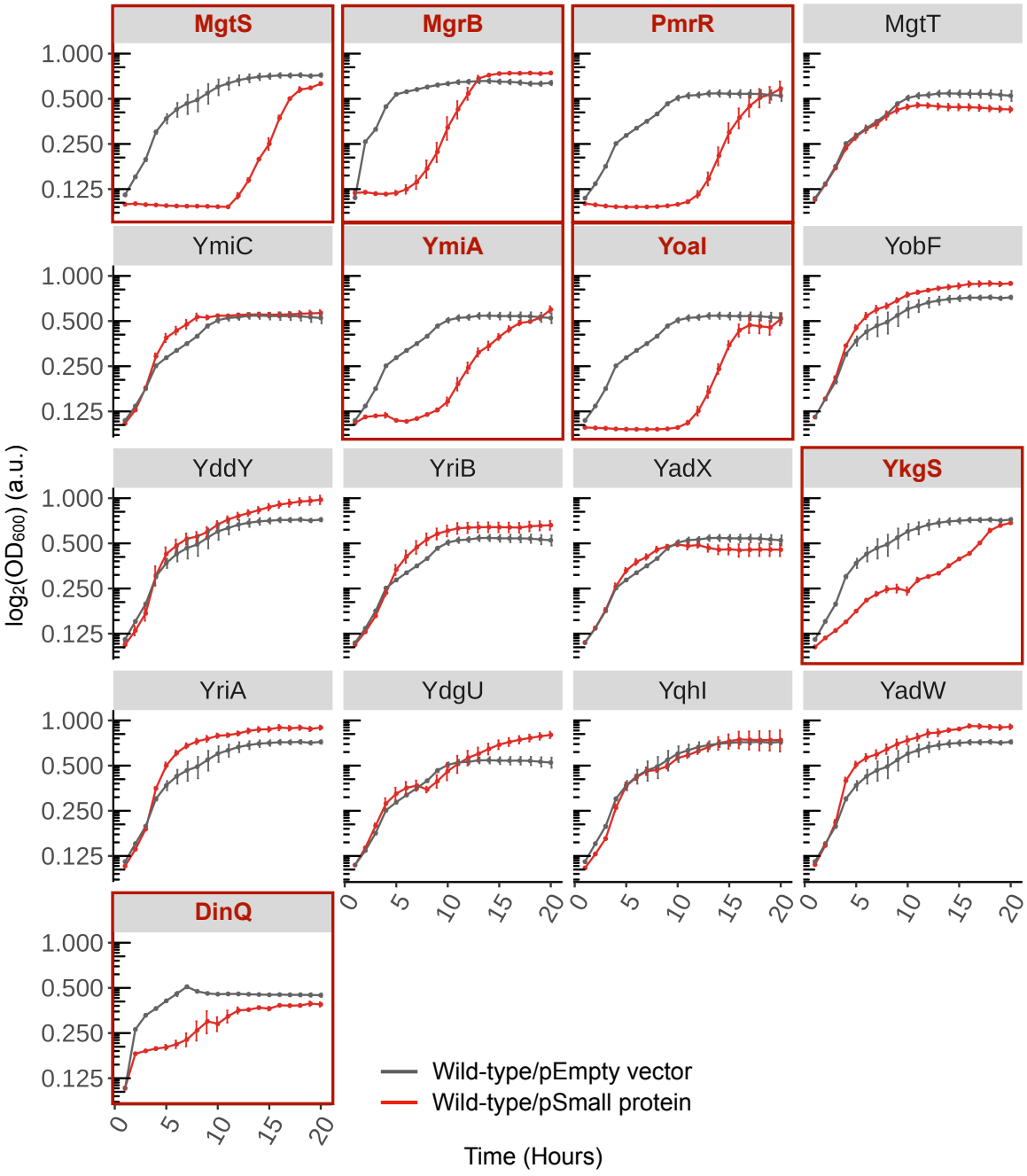

Figure 7. Effect of overexpression of low Mg^{2+} stress-induced small proteins on growth. Growth curves of *E. coli* MG1655 cells expressing each of the 17 stress-specific small proteins (encoded by plasmids pSV30-37, pSV54, pSV60, or pJS1-7; please see Table S2 for details) are represented in red, while cells carrying the empty vector (pEB52 and pBAD24) are shown in gray. The cells were grown under low Mg^{2+} stress (no added magnesium). Small proteins whose expression causes a growth defect or delay are highlighted in red. The cultures were grown in supplemented minimal A medium with 50 μg ml^{-1} carbenicillin. 500 μM IPTG was used as an inducer for all P_{trc}-based vectors, in the case of pSV54and pBAD24, 0.5% arabinose was used. Data represent averages and standard error of means for four independent cultures.

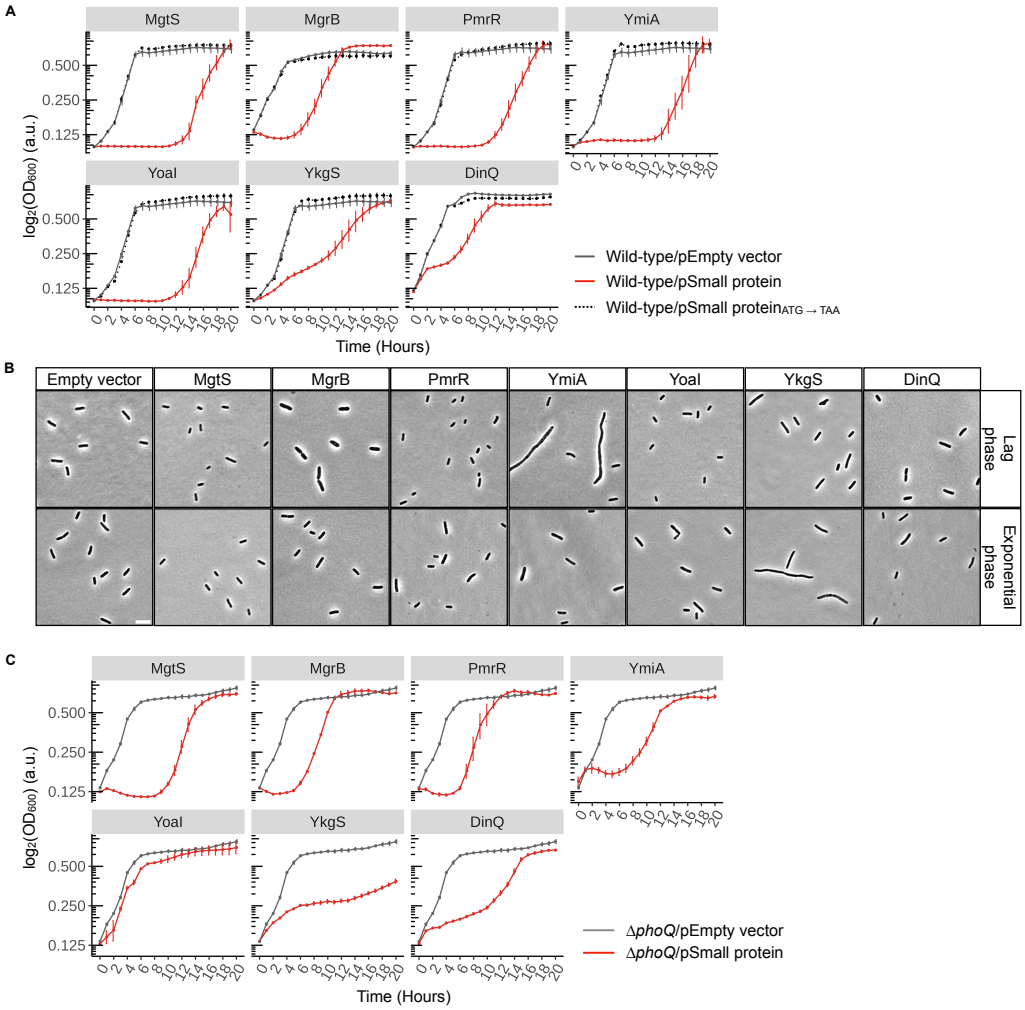

Figure 8. Analysis of growth defect and cell size changes associated with overexpression of small proteins, MgtS, MgrB, PmrR, YkgS, YoaI, YmiA and DinQ. (A) Growth curves of *E. coli* MG1655 cells expressing the indicated small proteins (red line) and empty vector control (pEB52 or pBAD24, gray line). The start codon (ATG) of each small protein is mutated to a stop codon (TAA), and the growth curves of cells expressing these constructs are depicted in dotted black. Plasmids pSV34-36, pSV38-42, pSV54-55, pSV60-61, or pJS4, pJS7 were used as applicable, please see Table S2 for details. Data represent averages and standard error of means for four independent cultures. (B) Representative phase contrast micrographs of the cells expressing small proteins during lag (top panel) and exponential phase (bottom panel) after induction, scale bar = 5 μm. Data is representative of three independent cultures. (C) Growth curves of Δ*phoQ* (TIM202) cells expressing the indicated small proteins (red line) and empty vector control (pEB52 or pBAD24, gray line). Plasmids pSV34-36, pSV54, pSV60, pJS4, and pJS7 were used as applicable, please see Table S2 for details. Data represent averages and standard error of means for four independent cultures. For panels A-C, the cultures were grown in supplemented minimal A medium containing no added magnesium, 50 μg ml^{-1} carbenicillin, and 500 μM IPTG for all P_{trc}-based vectors, except for pSV54 and pBAD24, where 0.5% arabinose was utilized instead. (Also see Figures S6 and S7)

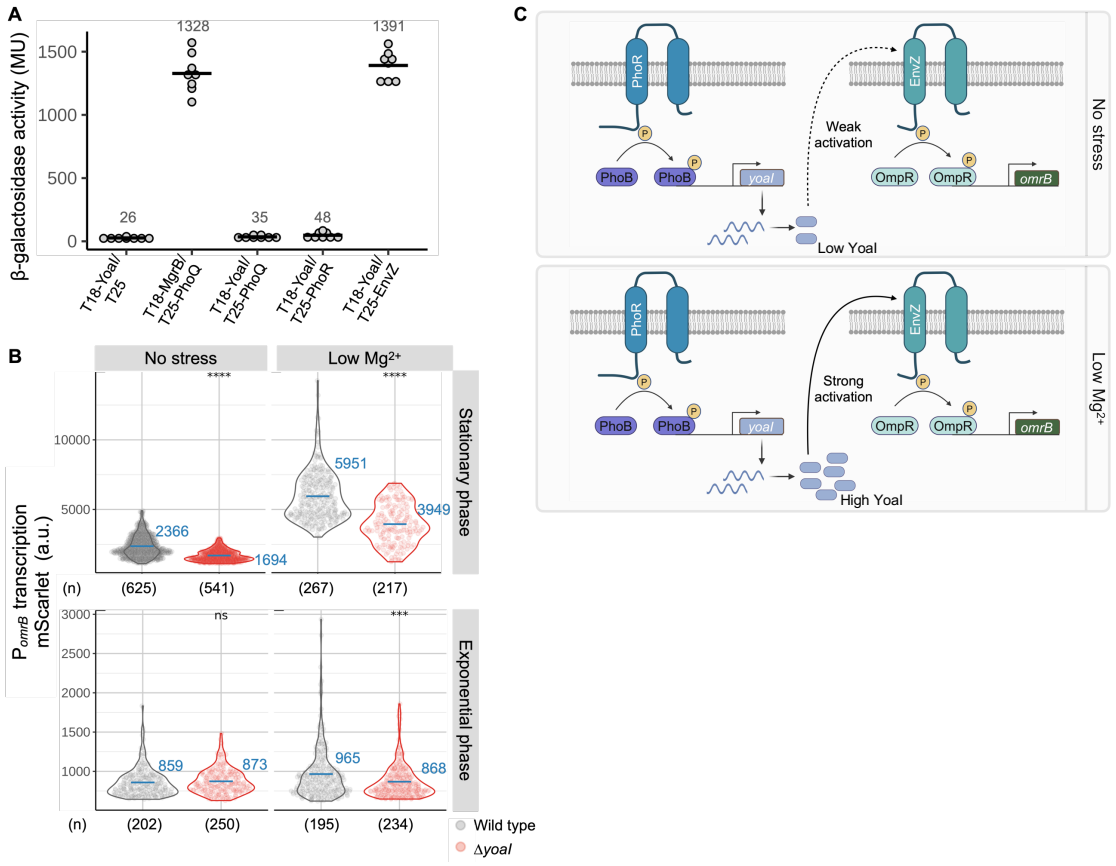

Figure 9. Effect of YoaI expression on the EnvZ-OmpR system. (A) BACTH assays were conducted using cells harboring T18 and T25 fusion proteins of *B. pertussis* adenylyl cyclase, in a *cyaA* mutant BACTH host strain, SAM85, which contains *lacI*^{q}. β-gal activity was measured to assess interactions between T18-YoaI (pSV47) and T25-linked PhoQ (pAL27), PhoR (pSY68), or EnvZ (pKK14). T25 alone was used as a negative control, and T18-MgrB (pAL33) combined with T25-PhoQ (pAL27) was used as a positive control. The cultures were grown in LB medium containing 50 µg ml^{-1} kanamycin, 100 µg ml^{-1} carbenicillin, and 500 µM IPTG. Each circle represents a biological replicate, with the mean values from two independent experiments indicated, expressed in Miller units (MU). (B) Transcriptional activity of *omrB* was measured as a function of mScarlet reporter fluorescence in *E. coli* MG1655 (SV97), and Δ*yoaI* (SV95) strains at the stationary phase (top panel) and exponential phase (bottom panel). Each circle corresponds to a single cell. Δ*yoaI* cells are depicted in red, while wild-type cells are in gray. The cultures were grown in supplemented minimal A medium containing either 10mM (no stress) or no added magnesium (Mg^{2+} stress). Data are derived from three independent replicates and the number of cells analyzed is indicated by (n). Mean fluorescence is shown with blue bars and is noted in blue text. P-values indicate the results of a t-test when Δ*yoaI* cells were compared to the wild-type cells, ****P ≤ 0.0001, ***P ≤ 0.001, and "ns" = P > 0.05. (C) Schematic representation of small membrane protein YoaI as a connector of the two-component systems, PhoR-PhoB and EnvZ-OmpR. YoaI is transcriptionally controlled by the PhoR-PhoB system, under low Mg^{2+} YoaI protein levels increase and it binds sensor kinase EnvZ and modulates signaling through the EnvZ-OmpR pathway. (Also see Figure S9)

Table 1. Summary of the 17 small proteins induced under low magnesium stress in *E. coli*. Small proteins with at least a 3-fold increase in reads mapping to the translation initiation site under low Mg^{2+} relative to no stress are indicated below. The analysis of transcriptional regulation, localization, and characterization of deletion and overexpression phenotypes is summarized.

Small protein	Transcriptional Regulation		Membrane localization	Phenotypic characterization	
				Deletion	Overexpression
MgtS	+	PhoQP-dependent, in an operon *mgtS-mgtT*	Y	No effect	Growth defect (prolonged lag phase) & decrease in cell size during lag and exponential phase
MgrB	+	PhoQP-dependent	Y	Increase in cell length, and change in colony morphology (larger, rough, translucent colonies)[28]	Growth defect (prolonged lag phase) & increase in cell size during lag phase
PmrR	+	BasSR-dependent [33,35]	Y	Growth defect (lower yield at saturation)	Growth defect (prolonged lag phase) & decrease in cell size during lag phase
MgtT	+	PhoQP-dependent, in an operon *mgtS-mgtT*	N	No effect	No effect
YmiC	+	PhoQP-dependent, in an operon *ymiA-yciX-ymiC*	Y	No effect	No effect
YmiA	+		Y	No effect	Growth defect (prolonged lag phase) & increase in cell length during lag phase
YoaI	-	PhoRB-dependent [47–49]	Y	No effect	Growth defect (prolonged lag phase) & decrease in cell size during lag phase
YobF	-		Y	Growth defect (lower yield at saturation)	No effect
YddY	+	PhoQP-dependent	N	No effect	No effect
YriB	+	PhoQP-dependent, in an operon *yriA-yriB*	N	Growth defect (lower yield at saturation)	No effect
YadX	+	PhoQP-dependent, in an operon *yadX-clcA-yadW*	N	No effect	No effect
YkgS	-		N	No effect	Growth defect (slow growth) & increase in cell length during exponential phase
YriA	+	PhoQP-dependent, in an operon *yriA-yriB*	N	No effect	No effect
YdgU	+	PhoQP-dependent, in an operon *asr-ydgU*	Y	No effect	No effect
YqhI	+		N	No effect	No effect
YadW	+	PhoQP-dependent, in an operon *yadX-clcA-yadW*	N	No effect	No effect
DinQ	-		Y	No effect	Growth defect (slow growth)

+ indicates transcriptional upregulation under magnesium stress vs. no stress; - indicates no change in transcriptional activity under magnesium stress vs. no stress; 'Y' indicates proteins predicted to contain membrane helices using TMHMM [51] and Phobius [53] and shown to localize to the membrane; 'N' indicates a lack of membrane helices based on bioinformatic prediction

Table 2. Analysis of transcriptional regulation of low magnesium stress-induced small proteins. Putative regulatory regions corresponding to the stress-induced small proteins and their dependence on PhoQ-PhoP signaling system.

Small protein	Putative region(s) of interest	Length of region (bp)	Genomic location in *E. coli* MG1655	PhoQP-dependence	Low Mg^{2+} stress-specific expression reported in
MgrB	P_{mgrB}	500	1908767 - 1909266	Yes	[27]
MgtS, MgtT	$P_{mgtS\text{-}mgtT}$	405	1622241 - 1622645	Yes	[31], This study
ProP, PmrR	$P_{proP\text{-}pmrR}$	500	4330002 - 4330501	No	This study
PmrR	P_{pmrR}	500	4331616 - 4332115	No	This study
YmiA, YmiC	$P_{ymiA\text{-}yciX\text{-}ymiC}$	500	1334648 - 1335147	Yes	This study
YmiC	P_{ymiC}	272	1335300 - 1335571	No	This study
YoaI	P_{yoaI}	500	1874183 - 1874682	No	This study
YobF	P_{yobF}	500	1907592 - 1908091	No	This study
YddY	P_{yddY}	500	1567220 - 1567719	Yes	This study
YriA	$P_{yriA\text{-}yriB}$	500	3640697 - 3641196	Yes	This study
YriB					
YadX, YadW	$P_{yadX\text{-}clcA\text{-}yadW}$	500	174548 - 175047	Yes	This study
YadW	P_{yadW}	500	176052 - 176551	No	This study
YkgS	P_{ykgS}	230	290280 - 290509	No	This study
YdgU	$P_{asr\text{-}ydgU}$	400	1670976 - 1671375	Yes	This study
	P_{ydgU}	500	1671277 - 1671776	No	This study
YqhI	P_{yqhI}	500	3147741 - 3148240	No	This study
DinQ	P_{dinQ}	272	3647789- 3648060	No	This study

Supporting Information (Vellappan *et al.*, 2024)

Table S1. List of strains used in the study

Strain	Genotype	Source or Reference
AML67	MG1655 *ΔmgrB*::(FRT-kan-FRT) *ΔlacZ* λ_{att}::(P_{mgtA}-*lacZ cat*)	[1]
E. cloni	F^- *mcrA Δ(mrr-hsdRMS-mcrBC) endA1 recA1 φ80lacZΔM15 ΔlacX74 araD139 Δ(ara-leu)7697 galU galK rpsL nupG tonA (attL araC-PBAD-trfA250 bla attR) λ−*	Lucigen Corporation
E. coli K-12 MG1655	F- λ- ilvG- rfb-50 rph-1	*E. coli* Genetic Stock Center, CGSC# 7740
GSO195	MG1655 *ΔdinQ*::(FRT-kan-FRT)	[2]
GSO219	MG1655 *ΔydgU*::(FRT-kan-FRT)	[2]
GSO225	MG1655 *ΔymiA*::(FRT-kan-FRT)	[2]
GSO232	MG1655 Δ*yoaI*::(FRT-kan-FRT)	[2]
GSO317	MG1655 *yoaI*-SPA::kan	[3]
JM2110	MG1508 *mhpR*-$P_{LtetO\text{-}1\text{-}omrB\text{-}104+8}$-$lacZ_{+28}$ *Δmini-λ-Tet*	Guillier lab stock (unpublished)
JM2113	OK510 *argG*-[TT1-$P_{LtetO\text{-}1\text{-}omrB\text{-}104+8}$-$mScarlet_{+4}$-FRT-*nptII*-FRT-TT2]-*yhbX*, *Δmini-λ-Tet*	Guillier lab stock (unpublished)
JW2162	BW25113 Δ*lpxT*::(FRT-kan-FRT)	[4]
MDG147	MG1655 (seq) Φ($ompF^+$-yfp^+)30 Φ($ompC^+$-cfp^+)31	[5]
MG1508	MG1655 *mal::lacI*^{q}, *mini- λ-Tet*, *mhpR*-$P_{LtetO\text{-}1}$-*cat-sacB-lacZ*	[6]
OK510	MG1432 *argG*-[TT1-$P_{LtetO\text{-}}$1(no -10)-*sacB-cat*-mScarlet(no ATG)- FRT-*nptII*-FRT-TT2]-*yhbX*	[7]
SAM85	F+ *lacI*^{q}*ZΔM15* Tn*10*(Tet^R), *cya-99 araD139 galE15 galK16 rpsL1* (Str^R) *hsdR2 mcrA1 mcrB1*. Strain prepared by conjugation: BTH101 (F-) x XL1-Blue (F+).	[8]
SV25	MG1655 *ΔyriAB*::(FRT-kan-FRT), coordinates deleted: 3,640,612 - 3,640,699	This study
SV27	MG1655 *ΔyadW*::(FRT-kan-FRT), coordinates deleted: 176,552 - 176,594	This study
SV29	MG1655 *ΔyddY*::(FRT-kan-FRT), coordinates deleted: 1,567,219 - 1,567,178	This study
SV31	MG1655 *ΔmgtT*::(FRT-kan-FRT), coordinates deleted: 1,622,742 - 1,622,816	This study

SV33	MG1655 *ΔyobF*::(FRT-kan-FRT), coordinates deleted: 1,907,451 - 1,907,573	This study
SV35	MG1655 *ΔpmrR*::(FRT-kan-FRT), coordinates deleted: 4,332,116 - 4,332,178	This study
SV37	MG1655 *ΔyqhI*::(FRT-kan-FRT), coordinates deleted: 3,147,597 - 3,147,740	This study
SV39	MG1655 *ΔyadX*::(FRT-kan-FRT), coordinates deleted: 175,048 - 175,077	This study
SV41	MG1655 *ΔymiC*::(FRT-kan-FRT), coordinates deleted: 1,335,572 - 1,335,667	This study
SV43	MG1655 *ΔykgS*::(FRT-kan-FRT), coordinates deleted: 290,510 - 290,641	This study
SV47	MG1655 Δ*lpxT*::(FRT-kan-FRT)	This study
SV50	MG1655 *ΔpmrR*	This study
SV54	MG1655 *ΔlpxT*::(FRT-kan-FRT) *ΔpmrR*	This study
SV56	MG1655 *ΔdinQ*::(FRT-kan-FRT)	This study
SV57	MG1655 *ΔymiA*::(FRT-kan-FRT)	This study
SV58	MG1655 *ΔydgU*::(FRT-kan-FRT)	This study
SV59	MG1655 *ΔyoaI*::(FRT-kan-FRT)	This study
SV60	MG1655 *yoaI*-SPA-kan *ΔlacZ ΔphoQ*	This study
SV64	MG1655 *ΔmgtS*::(FRT-kan-FRT), coordinates deleted: 1,622,646 - 1,622,735	This study
SV91	MG1655 Δ*yoaI*	This study
SV95	MG1655 *argG*-[TT1-$P_{LtetO\text{-}1\text{-}o}$*mrB*$_{\text{-}104+8}$-mScarlet$_{+4}$-FRT-*nptII*-FRT-TT2]-*yhbX*, *Δmini-λ-Tet*	This study
SV97	MG1655 *argG*-[TT1-$P_{LtetO\text{-}1\text{-}o}$*mrB*$_{\text{-}104+8}$-mScarlet$_{+4}$-FRT-*nptII*-FRT-TT2]-*yhbX*, *Δmini-λ-Tet* Δ*yoaI*	This study
TIM92	MG1655 λ_{att}::($P_{mgrB\text{-}yfp}$) HK_{att}::($P_{tetA\text{-}cfp}$)	[9]
TIM100	MG1655 *ΔphoQ* λ_{att}::($P_{mgrB\text{-}yfp}$) HK_{att}::($P_{tetA\text{-}cfp}$)	[9]
TIM202	MG1655 Δ*lacZ*::FRT Δ*phoQ*::FRT	[10]
TOP10	*F– mcrA Δ(mrr-hsdRMS-mcrBC) φ80lacZΔM15 ΔlacX74 recA1 araD139 Δ(ara-leu)7697 galU galK λ– rpsL(StrR) endA1 nupG*	Invitrogen
XL1-Blue	*recA1 endA1 gyrA96 thi-1 hsdR17 supE44 relA1 lac [F´ proAB lacIqZΔM15 Tn10 (Tetr)]*	[11]

Φ and Ψ denote transcriptional and translational fusions, respectively

Table S2. List of plasmids used in the study

Plasmid	Relevant genotype	Source or reference
pAL27	pKT25 P_{lac}-*cyaA*$_{T25}$-*phoQ*, Kan^R	[1]
pAL33	pUT18C P_{lac}-*cyaA*$_{T18}$-*mgrB*, Amp^R	[1]
pAL38	pEB52 P_{trc}-*gfpA206K-mgrB*, Amp^R	[1]
pAL39	pEB52 P_{trc}-*gfpA206K*, Amp^R	[1]
pBAD24	pMB1-derived plasmid, *araBAD,* Amp^R	[12]
pCP20	ori(pSC101) *rep101(ts) bla* λP_R-FLP λcI(ts) cat. Amp^R, Cam^R	[13]
pEB52	pTrc99a with the NcoI site removed, Amp^R	Goulian lab collection
pJS1	pEB52 P_{trc}-*yriA*. Amp^R	This study
pJS2	pEB52 P_{trc}-*yadW*. Amp^R	This study
pJS3	pEB52 P_{trc}-*yqhI*. Amp^R	This study
pJS4	pEB52 P_{trc}-*ykgS*. Amp^R	This study
pJS5	pEB52 P_{trc}-*yobF*. Amp^R	This study
pJS6	pEB52 P_{trc}-*yddY*. Amp^R	This study
pJS7	pEB52 P_{trc}-*mgtS*. Amp^R	This study
pKD13	ori(R6K) FRT-kan-FRT, Amp^R	[14]
pKD46	ori(pSC101) *rep101*(*ts*) P_{araB}-*gam-betexo araC*, Amp^R	[14]
pKK14	pKT25 P_{lac}-*cyaA*$_{T25}$-EnvZ, Kan^R	Goulian lab collection
pKT25	*ori*$_{p15A}$ P_{lac}-*cyaA*$_{T25}$-MCS, Kan^R	Euromedex
pMR120	A derivative of pSMART VC (Lucigen) containing two copies of the *rrnB* transcription terminator, $P_{putative\ promoter}$-*yfpA206K*-P_{tetA}-*cfp*, Cam^R	Goulian lab collection
pPJ1	pEB52 P_{trc}-*gfpA206K-mgtT*, Amp^R	This study
pPJ2	pEB52 P_{trc}-*gfpA206K-pmrR*, Amp^R	This study
pPJ3	pEB52 P_{trc}-*gfpA206K-ydgU*, Amp^R	This study
pPJ4	pEB52 P_{trc}-*yoaI-gfpA206K*, Amp^R	This study
pPJ5	pEB52 P_{trc}-*gfpA206K-yqhI*, Amp^R	This study
pPJ6	pEB52 P_{trc}-*gfpA206K-yobF*, Amp^R	This study
pPJ7	pEB52 P_{trc}-*gfpA206K-yriA*, Amp^R	This study
pPJ8	pEB52 P_{trc}-*gfpA206K-yddY*, Amp^R	This study

pPJ9	pEB52 P_{trc}-*gfpA206K-yadW*, Amp^R	This study
pPJ10	pEB52 P_{trc}-*gfpA206K-yadX*, Amp^R	This study
pPJ11	pEB52 P_{trc}-*gfpA206K-yriB*, Amp^R	This study
pPJ12	pEB52 P_{trc}-*gfpA206K-ymiA*, Amp^R	This study
pPJ13	pEB52 P_{trc}-*gfpA206K-ymiC*, Amp^R	This study
pPJ14	pMR120 putative P_{pmrR}-*yfp*, Cam^R	This study
pPJ16	pMR120 putative $P_{asr\text{-}ydgU}$-*yfp*, Cam^R	This study
pPJ17	pMR120 putative P_{ydgU}-*yfp*, Cam^R	This study
pPJ18	pMR120 putative P_{yoaI}-*yfp*, Cam^R	This study
pPJ19	pMR120 putative P_{yqhI}-*yfp*, Cam^R	This study
pPJ20	pMR120 putative $P_{yriA\text{-}yriB}$-*yfp*, Cam^R	This study
pPJ23	pMR120 putative $P_{yadX\text{-}clcA\text{-}yadW}$-*yfp,* Cam^R	This study
pSMART	pSMART VC *BamHI* (BAC) with single-copy replication origin *ori2 repE IncC parABC*, *oriV cat* Cam^R	Lucigen Corporation
pSV14	pEB52 P_{trc}-*yobF*-GGSG-6XHis, Amp^R	This study
pSV16	pMR120 putative P_{ykgS}-*yfp*, Cam^R	This study
pSV17	pMR120 putative $P_{proP\text{-}pmrR}$-*yfp*, Cam^R	This study
pSV18	pMR120 putative P_{yadW}-*yfp*, Cam^R	This study
pSV19	pMR120 putative P_{ymiC}-*yfp*, Cam^R	This study
pSV20	pMR120 putative $P_{ymiA\text{-}yciX\text{-}ymiC}$-*yfp*, Cam^R	This study
pSV21	pMR120 putative P_{dinQ}-*yfp*, Cam^R	This study
pSV24	pMR120 putative P_{yobF}-*yfp*, Cam^R	This study
pSV25	pEB52 P_{trc}-*gfpA206K-ykgS*, Amp^R	This study
pSV26	pEB52 P_{trc}-*pmrR*-GGSG-6XHis, Amp^R	This study
pSV28	pMR120 putative P_{yddY}-*yfp*, Cam^R	This study
pSV29	pMR120 putative $P_{mgtS\text{-}mgtT}$-*yfp*, Cam^R	This study
pSV30	pEB52 P_{trc}-*mgtT*. Amp^R	This study
pSV31	pEB52 P_{trc}-*ydgU*. Amp^R	This study
pSV32	pEB52 P_{trc}-*yadX*. Amp^R	This study
pSV33	pEB52 P_{trc}-*ymiC*. Amp^R	This study
pSV34	pEB52 P_{trc}-*yoaI*. Amp^R	This study
pSV35	pEB52 P_{trc}-*pmrR*. Amp^R	This study
pSV36	pEB52 P_{trc}-*ymiA*. Amp^R	This study

pSV37	pEB52 P_{trc}-*yriB*. Amp^R	This study
pSV38	pEB52 P_{trc}-$pmrR_{ATG->TAA}$ where the start codon ATG is substituted with a stop TAA, Amp^R	This study
pSV39	pEB52 P_{trc}-$yoaI_{ATG->TAA}$ where the start codon ATG is substituted with a stop TAA, Amp^R	This study
pSV40	pEB52 P_{trc}-$mgtS_{ATG->TAA}$ where the start codon ATG is substituted with a stop TAA, Amp^R	This study
pSV41	pEB52 P_{trc}-$ykgS_{ATG->TAA}$ where the start codon ATG is substituted with a stop TAA, Amp^R	This study
pSV42	pEB52 P_{trc}-$ymiA_{ATG->TAA}$ where the start codon ATG is substituted with a stop TAA, Amp^R	This study
pSV45	pEB52 P_{trc}-$yobF_{ATG->TAA}$ where the start codon ATG is substituted with a stop TAA, Amp^R	This study
pSV47	pUT18C P_{lac}-$cyaA_{T18}$-*yoaI*, Amp^R	This study
pSV54	pBAD24 P_{araBAD}-*dinQ,* Amp^R	This study
pSV55	pBAD24 P_{araBAD}-$dinQ_{ATG->TAA}$ where the start codon ATG is substituted with a stop TAA, Amp^R	This study
pSV58	pEB52 P_{trc}-*yriAB,* Amp^R	This study
pSV59	pEB52 P_{trc}-$yriB_{ATG->TAA}$ where the start codon ATG is substituted with a stop TAA, Amp^R	This study
pSV60	pEB52 P_{trc}-*mgrB,* Amp^R	This study
pSV61	pEB52 P_{trc}-$mgrB_{ATG->TAA}$ where the start codon ATG is substituted with a stop TAA, Amp^R	This study
pSY68	pKT25 P_{lac}-$cyaA_{T25}$-*phoR*, Kan^R	8
pTrc99a	$lacI^q$, P_{trc}-MCS, Amp^R	15
pUT18C	pUC19 P_{lac}-$cyaA_{T18}$-MCS, Amp^R	Euromedex

Amp^R = carries a carbenicillin/ampicillin-resistance marker; Cam^R = carries a chloramphenicol-resistance marker; Kan^R = carries a kanamycin-resistance marker

Table S3. List of primers used in the study

Primer	Sequence (5'-> 3')	Use
C-term-pmrR-F1	AGCTTTCTTTATATCTGGTTTGCCACGTACGGCGGCAGCGGCCACCATCACCATCACCATTAAGCTTAATTAGCTGACCTACTAGAGTCG	Cloning of pSV26
C-term-pmrR-R1	GCTGACCACCAGCACGCTGAACACGGTAGTTAAACTTTCATAAACACGGTTTTTCATGCTTAATTTCTCCTCTTTAATTCTAGGTACCCG	Cloning of pSV26
dinQ_del_screen_1	aagatgggggcaaccaaaaaag	Validation of GSO195
dinQ_del_screen_2	ttcactctggcaatgcgcata	Validation of GSO195
dinQ_F1	ATATGAATTCCATCAATGCTAATACCATACTGAAACTATTGCA	Cloning of pSV21
dinQ_R1	ATATGGATCCCCGTTTTCTCCATGCGATGGAG	Cloning of pSV21
dinQ_pBAD_R	CAGCGCAATTAACGCCCCTAGAACGATGATTGCTTTATCAATcatTGAATTCCTCCTGCTAGCCCAAA	Cloning of pSV54
dinQ_pBAD_F	CTGGAACTGATCCGCTTTCTGCTTCAGCTTCTGAACTAAGGTACCCGGGGATCCTCTAG	Cloning of pSV54
dinQ_stop_F	TAAATTGATAAAGCAATCATCGTTCTAGGGG	Cloning of pSV55
dinQ_stop_R	TGAATTCCTCCTGCTAGCCCA	Cloning of pSV55
F_yoaI_BATCH	ACTGTCTAGAGatgAACGATCAAATGTTTGTCGAGACAC	Cloning of pSV47
Fp_Inv_PCR_yobF	TAAGCTTAATTAGCTGACCTACTAGAGTCGAC	Cloning of pSV14
JA1	GCGTACGCAATCAAAATCCCCAGCCAATACAAcatTTAACACCATgcttaatttctcctctttaattctaggtacccg	Cloning of pSV58
JA2	AGACCGTAGGCCAGATAAGGTGTTTACGCTGATCAGGtaaGCTTAATTAGCTGACCTactagagtcgac	Cloning of pSV58
JS4	taaTTGTATTGGCTGGGGATTTTGATTGC	Cloning of pSV59
lpxT_del_F	gacagccgtattgagctgatttcc	Validation of JW2162
lpxT_del_R	aaagtgatacagaaagttaataagcgggg	Validation of JW2162
mgrB_forward	atgaaaaagtttcgatgggtcgttct	Cloning of pSV60
mgrB_stop3	TAAaaaaagtttcgatgggtcgttctg	Cloning of pSV61

MgtS_del_F	AAAATTAAGGTAAGCGAGGAAACACACCACACCATAAACGGAGGCAAATAattccggggatccgtcgacctgcagttcgaagttcctatt	Construction of SV64
MgtS_del_R	AACTGTAACAAGGGGCCGGTTAGGTGAGGGATTATCTCCGTTcatTAGTCtgtaggctggagctgcttcgaagttcctatact	Construction of SV64
mgtS_del_screen_1	cccgcgctttgttgatttaagtc	Validation of SV64 together with primer mgtT_del_screen2
mgtS_forward_2_correct	TCTGGTTTTCTGGCCGCGTATTTCAGCCACAAATGGGATGACtaaTAAGCTTAATTAGCTGACCTactagagtcgac	Cloning of pJS7
mgtS_reverse	AAATAAAATTATTCCCAGTACGGCCATAAAAACATTCATATTACCCAGcatgcttaatttctcctctttaattctaggtacccg	Cloning of pJS7
mgtS_stop	TAACTGGGTAATTAAAATGTTTTTATGGCCGTACTGGGAATAATTTTATTTTCTGG	Cloning of pSV40
mgtT_del_F	TATTTTCTGGTTTTCTGGCCGCGTATTTCAGCCACAAATGGGATGACTAAattccggggatccgtcgacc	Construction of SV31
mgtT_del_R	CAAATCTATCCATGCAAGCATtcaCCGCCGGTTTACTGGCGGTTTTTTTTtgtaggctggagctgcttcg	Construction of SV31
mgtT_del_screen1	CACACCACACCATAAACGGAGG	Validation of SV31
mgtT_del_screen2	ACCGGAAGAAATCGCTGCATG	Validation of SV31
mgtT_F	GAGAATTCTCAGCTGCGGTATTTACTGTCGG	Cloning of pSV29
mgtT_R	GGGGATCCTAGTCATCCCATTTGTGGCTGAAATACG	Cloning of pPJ1
mgtT_R1	ATATGGATCCTATTTGCCTCCGTTTATGGTGTGGTG	Cloning of putative pSV29
mgtT-forward	ATGAACGGAGATAATCCCTCACCTAAC	Cloning of pSV30
N_term_pmrR_forward	ATGAAAAACCGTGTTTATGAAAGTTTAACTACCG	Cloning of pSV35
pEB52-rev	GCTTAATTTCTCCTCTTTAATTCTAGGTACCCG	When targeting N-terminal-tagged small proteins, this primer, along with a small protein-specific forward primer, removes the tags by binding to the pEB52 backbone

phoB_del_F	cgaaaaagcatgggcgcgatta	Validation of JW0389
phoB_del_R	agggcaggtaaccaaaaaatgcac	Validation of JW0389
pmrR Primer 1	CTGGTGGTCAGCAGCTTTCTTTATATCTGGTTTGCCACGTACTGATAAGCTTAATTAGCTGACCTactagagt	Cloning of pPJ2
pmrR Primer 2	CACGCTGAACACGGTAGTTAAACTTTCATAAACACGGTTTTTCATtttgtatagttcatccatgccatgtg	Cloning of pPJ2
pmrR_del_F	CTTAATCTCTGACGCGCATACTCTCCTCCAGGTTAACGGAGGAGAGTGCAattccggggatccgtcgacc	Construction of SV35
pmrR_del_R	GCCTGGGTACGGCTGAAGAAAGAtcaGTACGTGGCAAACCAGATATAAGtgtaggctggagctgcttcg	Construction of SV35
pmrR_del_screen1	GCGAATTGATGAATAAGCTGAAACGG	Validation of SV35
pmrR_del_screen2	CGTTTGTACGTATGGACAGCCG	Validation of SV35
pmrR_stop	TAaAAAAACCGTGTTTATGAAAGTTTAACTACCG	Cloning of pSV38
pmrR1_F	GAGAATTCTGGCTTCTACCTTGCCAGCG	Cloning of pPJ14
pmrR1_R	GGGGATCCTGCACTCTCCTCCGTTAACCTG	Cloning of pPJ14
pmrR2_F	GAGAATTCCCGACCACGCGTCACTATTACC	Cloning of pSV17
pmrR2_R	GGGGATCCAGCTTTCCTCGCAGAGTTGG	Cloning of pSV17
pSMART SV_19	GACCATAACCGAAAGTAGTGAC	Sequencing primer for pMR120 based vectors
R_yoaI_BATCH	TACTGAATTCctaGCCGGTCCGTTCGATAAGAAG	Cloning of pSV47
Rp_Inv_PCR_yobF	ATGGTGATGGTGATGGTGGCCGCTGCCGCCGATTGTTTTCTTCGCCCGCAGG	Cloning of pSV14
SA26R	CATCCGCCAAAACAGCCAAG	Sequencing primer for pEB52 based vectors
yadW Primer 1	TGCCGATGTCGTTTGGAGCAAAATATGAGTGATAAGCTTAATTAGCTGACCTactagagt	Cloning of pPJ9
yadW Primer 2	ATTGGGCAAATTCTAACCCAATAATAATCGCCATtttgtatagttcatccatgccatgtg	Cloning of pPJ9
yadW_del_F	GCCGCATCAGCCAGCGAGAATACTTGAACGAAATACCAGGGTATTAGATAattccggggatccgtcgacc	Construction of SV27
yadW_del_R	TCGGTAAACTCCAGCGGCAGTGCTACGTCAtcaCTCATATTTTGCTCCAAACGtgtaggctggagctgcttcg	Construction of SV27

yadW_del_screen1	CGGGAAACCGCTATACTCGG	Validation of SV27
yadW_del_screen2	GGTGAAACCATACTGGAAGCCG	Validation of SV27
yadW_forward	atgGCGATTATTATTGGGTTAGAATTTGCC	Cloning of pJS2
yadW1_F	GAGAATTCTTCCATTTCGGTTGGTGCACCAA	Cloning of pSV18
yadW1_R	GGGGATCCCCAATGATCACTTATTGGTCATACAAATAAGATGAC	Cloning of pSV18
yadW2_F	GAGAATTCACCATGCGCACCATATCCATGG	Cloning of pPJ23
yadW2_R	GGGGATCCGAAAATCCTTTGCAAAGCGTAATGTTTCAAAT	Cloning of pPJ23
yadX Primer 1	TCATCTTATTTGTATGACCAATAATAAGCTTAATTAGCTGACCTactagagt	Cloning of pPJ10
yadX Primer 2	CGGCATTTTACTCGCACGTTCCATtttgtatagttcatccatgccatgtg	Cloning of pPJ10
yadX_del_F	AGTATAAAAGTTTTGTGCATTTGAAACATTACGCTTTGCAAAGGATTTTCattccggggatccgtcgacc	Construction of SV39
yadX_del_R	AGAGGGAGTATCAGTTTTCATCCAATGATCACttaTTGGTCATACAAATAtgtaggctggagctgcttcg	Construction of SV39
yadX_del_screen1	CATGGAGGGTTCCTGATTCGTAG	Validation of SV39
yadX_del_screen2	GCCATAAACAAAATGGCTAACGGG	Validation of SV39
yadX-forward	ATGGAACGTGCGAGTAAAATGC	Cloning of pSV32
yddY Primer 1	GCACGTTGCGTTTCATTTTGATAAGCTTAATTAGCTGACCTactagagt	Cloning of pPJ8
yddY Primer 2	GAGATCGACTAACTGCACCATtttgtatagttcatccatgccatgtg	Cloning of pPJ8
yddY_del_F	GTCCTAAATCGCTTATTTCTTTTCAGTATATCTTCATATTTCAGGAGAATattccggggatccgtcgacc	Construction of SV29
yddY_del_R	AATACATCTCCATAATTCACACCCTTATAAGGCTGGGAAATCAGACGGAAtgtaggctggagctgcttcg	Construction of SV29
yddY_del_screen1	CATACGATATTCGCTGTCACCG	Validation of SV29
yddY_del_screen2	CCGCGGCTTTAGCACGAAT	Validation of SV29
yddY_F	GAGAATTCCTGTATATCGGTATCGCCTTCTATAAAGTGG	Cloning of pSV28

yddY_forward	ATGGTGCAGTTAGTCGATCTCG	Cloning of pJS6
yddY_R	GGGGATCCATTCTCCTGAAATATGAAGATATACTGAAAAG	Cloning of pSV28
ydgU Primer 1	ATTTTATGCGCACTGATTACCGCCCGTTTTTATCTTTCCTGATAAGCTTAATTAGCTGACCTactagagt	Cloning of pPJ3
ydgU Primer 2	AAGGATGATCAGAATGAACTCAAAGCGATAACGGCCCACCATtttgtatagttcatccatgccatgtg	Cloning of pPJ3
ydgU_del_screen_1	gcagcgaagaaacacgccaa	Validation of GSO219
ydgU_del_screen_2	caaaagcagacgtcaaactaattgca	Validation of GSO219
ydgU-forward	ATGGTGGGCCGTTATCGCTT	Cloning of pSV31
ydgU1_F	ACTCGAGAATTCGAAACCAACCACTCACGGAAGTCTG	Cloning of pPJ17
ydgU1_R	CCGGGGATCCACTACCCTCCGCTAAAGGCG	Cloning of pPJ17
ydgU2_F	ACTCGAGAATTCATACCCGTCCGGACTTATTGCC	Cloning of pPJ16
ydgU2_R	GGGGATCCTGTCATACCCTCAATTTGTTTTTTCATTTAACCC	Cloning of pPJ16
ykgS_del_F2	CAGAAGCAGAAAGACATTGGATCGAATTCTACAACCAGGTCGAGTCAGAaattccggggatccgtcgacctgcagttcgaagttcctatt	Construction of SV43
ykgS_del_R2	CAAAGTCATCGGGCATTATCTGAACATAAAACACTATCAATAAGTTGGAGtgtaggctggagctgcttcgaagttcctatact	Construction of SV43
ykgS_del_screen1	GGCAAACCCGTCCGTGTG	Validation of SV43
ykgS_del_screen2	AAGTCGCTGTCGTTCTCAAA	Validation of SV43
ykgS_F	ATATCTCGAGAAGTGTTTTTTGTATAAATCGGACATTTTATCCTCG	Cloning of pSV25
ykgS_F1	ATATCTCGAGAAGTGTTTTTTGTATAAATCGGACATTTTATCCTCG	Cloning of pSV16
ykgS_forward	ATGAGAATGATTGGCCTTCTTTATGATTTTAAGG	Cloning of pJS4
ykgS_R	ATATGGATCCTTCTGACTCGACCTGGTTGTAGAATTCG	Cloning of pSV25
ykgS_R1	ATATGGATCCTTCTGACTCGACCTGGTTGTAGAATTCG	Cloning of pSV16
ykgS_stop	TAAAGATAAATTGGCCTTCTTTATGATTTTAAGGATTATGCT	Cloning of pSV41

ymiA Primer 1	TGGCGGTTTTTCTTGGTTCTGCACTTTTCTGGGTGGTTGTCGCACTGCTGATTTGGAAAGTGTGGGGATAATAAGCTTAATTAGCTGACCTactagagt	Cloning of pPJ12
ymiA Primer 2	GCCAGGCTTTACGTTTTAATTCAGGATCGCGGCGGGGTTCCTGATTTCCAGAAGGCATTGCTAACCTCATtttgtatagttcatccatgccatgtg	Cloning of pPJ12
ymiA_del_screen_1	gattgaattattcactggagacgattcg	Validation of GSO225
ymiA_del_screen_2	tcatcttcagcaaacagttctataaaggc	Validation of GSO225
ymiA_F1	ATATGAATTCTCAGCCACAGTACAACCAAAATTGG	Cloning of pSV20
ymiA_R1	ATATGATCCATAATCGCCATCACTTATCAGCAAGAC	Cloning of pSV20
ymiA_stop	TAAAGGTTAGCATAACCTTCTGGAAATCAGGAACCCC	Cloning of pSV42
ymiA-forward	ATGAGGTTAGCAATGCCTTCTGGA	Cloning of pSV36
ymiC Primer 1	CTGTCGATGCTCTTCTGGGCCGAACTCCTCTGGATCATTACTCACTGATAAGCTTAATTAGCTGACCTactagagt	Cloning of pPJ13
ymiC Primer 2	AGAAAACGCGCCCATCCAGGACCAATATTTCATATTTGTGTTGATCATtttgtatagttcatccatgccatgtg	Cloning of pPJ13
ymiC_del_F	ACAGCTTGAGTTATCTCAACACAAAATAATAACCGTTAAGGGTGTAGCCTattccggggatccgtcgacc	Construction of SV41
ymiC_del_R	GAAACCTTGTGGCAAAGCAAATGACAACCCCGCCGCAGCGGGGTCAAGGAtgtaggctggagctgcttcg	Construction of SV41
ymiC_del_screen1	GATGATCAGCCGAAACAATAATTATCATCATTC	Validation of SV41
ymiC_del_screen2	AAGCCCTGATTCTCTTCAGGGT	Validation of SV41
ymiC_F1	ATATGAATTCCAGGAGCAACTGGAGTCGTC	Cloning of pSV19
ymiC_R1	ATATGGATCCAGGCTACACCCTTAACGGTTATTATTTTG	Cloning of pSV19
ymiC-forward	ATGATCAACACAAATATGAAATATTGGTCCTGGA	Cloning of pSV33
yoaI Primer 1	ATTGCTGTTGTACTGGTTTTGTCCGTTCTTCTTATCGAACGGACCGGCcgtaaaggagaagaacttttcactgg	Cloning pPJ4
yoaI Primer 2	GGCAAAAAACGATGACGTGATAATCAGTGTCTCGACAAACATTTGATCGTTcatgcttaatttctcctctttaattctaggtac	Cloning pPJ4
yoaI_del_screen_1	tggttgccgaccctctactc	Validation of GSO232

yoaI_del_screen_2	agcctgcttactttacgcttgc	Validation of GSO232
yoaI_F	GAGAATTCGCGGCTGGCTGCCCATTAA	Cloning of pPJ18
yoaI_R	GGGGATCCAGCATGCCCCCGGGAGATA	Cloning pPJ18
yoaI_stop	taAAACGATCAATAATTTGTCGAGACACTGATTATCACGTCATCG	Cloning of pSV39
yoaI-forward	TAAGCTTAATTAGCTGACCTACTAGAGTCGAC	Cloning of pSV34
yoaI-rev	GCCGGTCCGTTCGATAAGAAGA	Cloning of pSV34
yobF Primer 1	CCTTATATTGGTGCCTCATGCAGTAATGTGTCAGTTTTATCTATGTTATGCCTGCGGGCGAAGAAAACAATCcgtaaaggagaagaacttttcactgg	Cloning of pPJ6
yobF Primer 2	CTCGGCAGAGAAGCGGTATTCAACGTCAACGTGTTTACTCAGGACTTCTTTACTGAAAATGCCACAcatgcttaatttctcctctttaattctaggtac	Cloning of pPJ6
yobF_del_F	AAAGAAGTCCTGAGTAAACACGTTGACGTTGAATACCGCTTCTCTGCCGAattccggggatccgtcgacc	Construction of SV33
yobF_del_R	TTGAACCACTTAACCTGACCTTTAATCTTTGCCATTTGAAAAATTCCttatgtaggctggagctgcttcg	Construction of SV33
yobF_del_screen1	GTGTGCAAAAAAAGTGGAAGACGT	Validation of SV33
yobF_del_screen2	CCATTACCCTGGATAGCGGAG	Validation of SV33
yobF_F1	ATATGAATTCTAATTTATTAGGATGTTTACATCGGATTTGTGATTAAGCG	Cloning of pSV24
yobF_R1	ATATGGATCCAAACAGAACTGTACCTCGTTTAACCC	Cloning of pSV24
yobF_reverse	GATTGTTTTCTTCGCCCGCAGG	Cloning of pJS5
yobF_stop	taaTGTGGCATTTTCAGTAAAGAAGTCCTG	Cloning of pSV45
yqhI Primer 1	ATCTCGAAACGTGAGTTCCTCAACCTTGCGGCGAAGTGCGGTAGGCGGGATGACGGCATTAGCGTTGTTTGATAAGCTTAATTAGCTGACCTactagagt	Cloning of pPJ15
yqhI Primer 2	TTTCCCGTGAGCGTAATAGTCATAGTAATCCAGCAACTCTTGTGGGAAATCTTTGGCGGTTAAACGCGGCATtttgtatagttcatccatgccatgtg	Cloning of pPJ15
yqhI_del_F2	AATACGTGCTTATGCTTTGCTTAAAAAAACACCAACTGAGGAGTGCAACGaattccggggatccgtcgacctgcagttcgaagttcctatt	Construction of SV37
yqhI_del_R2	GGTCGGTAAACTCTACCTGAGTCGCCAGCGCATAATTTGGCTTGAGCAAAtgtaggctggagctgcttcgaagttcctatact	Construction of SV37

yqhI_del_screen 1	TGTTTCTAGTTTAGCGATTCGCCAG	Validation of SV37
yqhI_del_screen 2	GGGCTTCACCAGATAACCCC	Validation of SV37
yqhI_F	GAGAATTCTATTTACGTGAACCGCCAGAGCC	Cloning of pPJ19
yqhI_forward	ATGCCGCGTTTAACCGCC	Cloning of pJS3
yqhI_R	GGGGATCCCGTTGCACTCCTCAGTTGGTG	Cloning of pPJ19
yriA Primer 1	GCAGACCGTAGGCCAGATAAGGTGTTTACGCTGAT CAGGTAATAAGCTTAATTAGCTGACCTactagagt	Cloning of pPJ7
yriA Primer 2	GTACGCAATCAAAATCCCCAGCCAATACAACATtttgta tagttcatccatgccatgtg	Cloning of pPJ7
yriA_F	TCGAGAATTCAAATCAGGTCAGGCTTAAGTAGCGAC	Cloning of pPJ20
yriA_forward	ATGTTGTATTGGCTGGGGATTTTGAT	Cloning of pJS1
yriA_R	GGGGATCCTTAACACCATCATATTTTCCATCATTAG TGTGATC	Cloning of pPJ20
yriAB_del_F	ACACTATTACAACAGAAAATAACCAGATGATCACAC TAATGATGGAAAATattccggggatccgtcgacc	Construction of SV25
yriAB_del_R	TGTTCCTGAACGCCCGCATATGCGGGCGTTTTGCT TTTTGGCGCGCCTTGgtgtaggctggagctgcttc	Construction of SV25
yriAB_del_scree n1	GAACGCGTAAGGGATAACGC	Validation of SV25
yriAB_del_scree n2	CTGATCAACACCGTTCACGTTG	Validation of SV25
yriB Primer 1	GATTTTGATTGCGTACGCAGACCGtagTAAGCTTAAT TAGCTGACCTactagagt	Cloning of pPJ11
yriB primer 2	CCCAGCCAATACAACATTTAACACcattttgtatagttcatcca tgccatgtg	Cloning of pPJ11
yriB-forward	atgGTGTTAAATGTTGTATTGGCTGGG	Cloning of pSV37

Table S4. List of all proteins with ≥3-fold increase in read counts from Ribo-RET and differentially expressed transcripts from RNA-Seq.

Ribo-RET					RNA-Seq Differential Expression					
gene	size	no_ stress	low_ mg	fold_ change	gene	base_ Mean	log2Fold Change	lfcSE	pvalue	padj
phnC	standard	0.68	79.66	117.25	*mgtS*	14972.46	7.82	0.31	2.11E-140	6.60E-137
iraM	standard	3.4	247.31	72.8	*ymgL*	17.66	7.53	2.75	2.84E-06	2.56E-05
phoR	standard	0.68	44.65	65.71	*mgtA*	3789.38	7.13	0.39	9.56E-75	9.97E-72
ptrA	standard	1.36	72.66	53.47	*ymgK*	236.85	6.93	0.62	6.26E-29	5.02E-27
phoE	standard	5.44	242.93	44.69	*iraM*	205.15	6.71	0.63	4.09E-27	2.78E-25
eptA	standard	5.44	232.43	42.76	*mgtL*	11342.3	6.61	0.43	1.18E-54	5.27E-52
ydeT	standard	4.76	148.38	31.2	*ydeT*	28.94	6.33	1.43	6.39E-06	5.33E-05
arnC	standard	0.68	20.13	29.64	*ydeS*	9.66	6.26	2.76	1.15E-04	7.48E-04
yciX	standard	1.36	38.96	28.67	*asr*	332.57	5.91	0.48	3.80E-35	4.96E-33
waaH	standard	2.04	58.22	28.56	*ybjG*	1315.13	5.78	0.35	4.37E-63	3.42E-60
rstB	standard	0.68	18.82	27.7	*mgrB*	6552.83	5.68	0.31	4.00E-76	6.25E-73
phoQ	standard	2.04	54.71	26.84	*phnD*	25.86	5.34	1.17	1.71E-06	1.61E-05
ugpB	standard	10.87	288.45	26.53	*yebO*	1871.52	5.1	0.33	1.23E-55	6.42E-53
phoB	standard	29.21	711.72	24.36	*yriB*	18.19	4.72	1.24	3.12E-05	2.30E-04
appC	standard	6.79	162.39	23.9	*phnC*	17.35	4.63	1.25	4.47E-05	3.18E-04
otsB	standard	0.68	14.88	21.9	*pstS*	274.79	4.41	0.41	1.93E-28	1.48E-26
argD	standard	10.87	199.6	18.36	*yfeO*	91.2	4.31	0.56	1.21E-15	2.81E-14
cysD	standard	20.38	358.92	17.61	*ydgU*	24.42	4.31	0.99	2.00E-06	1.85E-05
cbl	standard	2.04	35.02	17.18	*dgcZ*	61.86	4.29	0.64	3.40E-12	6.33E-11
ynaL	standard	1.36	21.01	15.46	*pgpC*	397.23	4.24	0.37	2.38E-31	2.26E-29
asr	standard	51.64	796.2	15.42	*ygdR*	155.39	4.19	0.46	9.92E-21	3.34E-19
yriA	small	2.72	40.71	14.98	*alaV*	973.94	4.18	0.36	2.73E-32	2.85E-30
glsA	standard	0.68	10.07	14.82	*alaU*	973.94	4.18	0.36	2.73E-32	2.85E-30
yciW	standard	8.15	119.06	14.6	*alaT*	973.94	4.18	0.36	2.73E-32	2.85E-30
yohC	standard	8.15	118.18	14.5	*metZ*	673.96	4.12	0.43	6.41E-23	2.87E-21
yeeE	standard	4.08	58.65	14.39	*metW*	673.96	4.12	0.43	6.41E-23	2.87E-21
sbp	standard	6.79	96.3	14.17	*metV*	673.96	4.12	0.43	6.41E-23	2.87E-21
ydgU	small	2.04	27.14	13.31	*glyW*	9479.84	4.06	0.33	1.60E-35	2.27E-33
narU	standard	1.36	17.95	13.21	*glyV*	9479.84	4.06	0.33	1.60E-35	2.27E-33
arnB	standard	11.55	151.45	13.11	*glyX*	9479.84	4.06	0.33	1.60E-35	2.27E-33
argA	standard	16.31	212.29	13.02	*glyY*	9479.84	4.06	0.33	1.60E-35	2.27E-33
ais	standard	9.51	123	12.93	*ais*	16.7	4.03	1.15	6.60E-05	4.54E-04
ycaP	standard	1.36	17.51	12.88	*arnB*	38.15	3.91	0.76	2.56E-08	3.31E-07
phoA	standard	12.23	156.26	12.78	*ugpB*	80.2	3.83	0.57	1.18E-12	2.26E-11
ydeQ	standard	1.36	17.07	12.56	*alaX*	648.46	3.79	0.38	2.29E-24	1.21E-22
yncG	standard	2.04	25.39	12.46	*alaW*	648.46	3.79	0.38	2.29E-24	1.21E-22

ilvB	standard	1.36	16.2	11.92	*rttR*	21.62	3.74	1.06	4.26E-05	3.06E-04
yoaI	small	13.59	161.95	11.92	*metY*	276.5	3.73	0.43	6.96E-19	2.05E-17
cysP	standard	63.87	758.56	11.88	*leuW*	4113.99	3.68	0.35	1.34E-27	9.30E-26
yfcG	standard	4.08	48.15	11.81	*arnC*	29.57	3.66	0.82	9.33E-07	9.24E-06
lysA	standard	2.04	23.64	11.6	*rstA*	323.01	3.65	0.38	8.71E-23	3.84E-21
artP	standard	43.48	491.11	11.29	*msrQ*	38.7	3.63	0.72	5.34E-08	6.58E-07
yhbW	standard	1.36	15.32	11.27	*arnF*	56.91	3.62	0.61	3.42E-10	5.22E-09
dacD	standard	0.68	7.44	10.95	*phoA*	78.32	3.62	0.55	3.42E-12	6.33E-11
ruvC	standard	0.68	7.44	10.95	*ymcF*	40.82	3.61	0.71	3.74E-08	4.73E-07
ydbL	standard	1.36	14.88	10.95	*dacC*	178.45	3.59	0.42	1.11E-18	3.21E-17
argG	standard	20.38	217.98	10.69	*ileV*	995.19	3.57	0.34	3.75E-26	2.35E-24
argC	standard	6.11	64.78	10.59	*ileU*	995.19	3.57	0.34	3.75E-26	2.35E-24
ybhP	standard	0.68	7	10.31	*ileT*	995.19	3.57	0.34	3.75E-26	2.35E-24
yobF	small	12.91	132.63	10.27	*phoQ*	258.31	3.57	0.38	1.64E-21	6.11E-20
pstS	standard	48.92	490.68	10.03	*phoB*	66.9	3.56	0.57	4.75E-11	7.87E-10
nadD	standard	1.36	13.57	9.99	*eptA*	15.82	3.5	1.11	1.72E-04	0.001078186
gadE	standard	2.72	26.7	9.82	*arnA*	35.6	3.49	0.74	2.45E-07	2.70E-06
ydeS	standard	2.72	26.7	9.82	*ydhI*	62.43	3.45	0.58	3.12E-10	4.78E-09
bcsB	standard	0.68	6.57	9.66	*pdeR*	34.61	3.44	0.74	3.72E-07	3.97E-06
pcm	standard	0.68	6.57	9.66	*pstC*	127.36	3.42	0.46	7.14E-15	1.56E-13
yadW	small	1.36	13.13	9.66	*secG*	2556.53	3.41	0.38	2.56E-20	8.08E-19
pagP	standard	8.15	75.29	9.23	*phoP*	729.83	3.38	0.33	5.44E-25	3.27E-23
pstA	standard	2.04	18.82	9.23	*slyB*	3744.69	3.34	0.3	7.35E-30	6.39E-28
waaQ	standard	2.04	18.82	9.23	*hokD*	178.33	3.31	0.42	3.78E-16	8.96E-15
aroE	standard	0.68	6.13	9.02	*pagP*	21.67	3.28	0.91	3.55E-05	2.57E-04
mgrB	small	250.71	2248.97	8.97	*yliM*	5741.91	3.21	0.32	5.03E-24	2.58E-22
dtpD	standard	2.72	24.07	8.86	*yjcB*	202.42	3.2	0.4	7.82E-17	1.93E-15
tatD	standard	8.15	71.78	8.8	*relE*	150.84	3.19	0.44	6.33E-14	1.28E-12
bcr	standard	2.04	17.51	8.59	*rstB*	99.93	3.16	0.49	8.30E-12	1.48E-10
pstC	standard	44.16	377.31	8.54	*ynfB*	711.59	3.09	0.34	1.32E-20	4.34E-19
blc	standard	2.72	23.2	8.54	*ybfA*	383.07	3.09	0.38	3.59E-17	9.13E-16
nudL	standard	2.72	23.2	8.54	*deoR*	205.33	3.08	0.4	6.56E-16	1.54E-14
insQ	standard	6.79	56.9	8.38	*sraG*	43.7	3.08	0.65	2.09E-07	2.33E-06
cysJ	standard	60.47	504.25	8.34	*valT*	8108.95	3.08	0.33	7.92E-22	3.02E-20
pdeR	standard	8.15	67.41	8.27	*valZ*	8108.95	3.08	0.33	7.92E-22	3.02E-20
iaaA	standard	30.57	251.69	8.23	*valU*	8108.95	3.08	0.33	7.92E-22	3.02E-20
yhdN	standard	4.08	32.83	8.05	*valX*	8108.95	3.08	0.33	7.92E-22	3.02E-20
chaC	standard	5.44	43.33	7.97	*valY*	8108.95	3.08	0.33	7.92E-22	3.02E-20
mgtT	small	1082.31	8622.95	7.97	*tqsA*	29.99	3.05	0.76	6.71E-06	5.58E-05
gadX	standard	4.08	31.95	7.84	*lysT*	11718.26	3.05	0.33	3.00E-21	1.04E-19
rssB	standard	4.08	31.95	7.84	*lysW*	11718.26	3.05	0.33	3.00E-21	1.04E-19
hisG	standard	13.59	105.93	7.8	*lysY*	11718.26	3.05	0.33	3.00E-21	1.04E-19

cysW	standard	0.68	5.25	7.73	*lysZ*	11718.26	3.05	0.33	3.00E-21	1.04E-19
glaR	standard	0.68	5.25	7.73	*lysQ*	11718.26	3.05	0.33	3.00E-21	1.04E-19
ibsD	small	0.68	5.25	7.73	*lysV*	11718.26	3.05	0.33	3.00E-21	1.04E-19
ibsE	small	0.68	5.25	7.73	*appC*	46.53	3.02	0.63	1.57E-07	1.80E-06
ybdR	standard	0.68	5.25	7.73	*fabR*	293.94	3.02	0.37	4.17E-17	1.05E-15
hisD	standard	9.51	73.1	7.68	*csrC*	1142.49	3	0.32	6.80E-22	2.80E-20
tqsA	standard	8.15	61.28	7.52	*phoR*	33.35	2.98	0.72	3.93E-06	3.47E-05
purF	standard	15.63	117.31	7.51	*ygcN*	30.28	2.95	0.75	1.01E-05	8.10E-05
glcD	standard	8.15	60.84	7.46	*yfiS*	34.41	2.94	0.74	7.12E-06	5.88E-05
speG	standard	26.5	196.53	7.42	*queE*	213.58	2.94	0.39	5.47E-15	1.21E-13
ftsQ	standard	1.36	10.07	7.41	*yodB*	20	2.9	0.92	1.76E-04	0.001100074
ygbE	standard	3.4	24.95	7.34	*tadA*	238.08	2.89	0.38	6.15E-15	1.36E-13
yqhI	small	2.04	14.88	7.3	*arnD*	13.79	2.89	1.12	0.001001481	0.005046111
miaA	standard	13.59	96.73	7.12	*ybgS*	71.99	2.87	0.54	1.44E-08	1.91E-07
speC	standard	19.7	140.07	7.11	*metU*	243.67	2.87	0.42	6.17E-13	1.21E-11
appB	standard	0.68	4.81	7.09	*metT*	243.67	2.87	0.42	6.17E-13	1.21E-11
argH	standard	2.72	19.26	7.09	*serV*	8051.92	2.86	0.35	2.19E-17	5.70E-16
artJ	standard	13.59	96.3	7.09	*cspG*	125.16	2.85	0.44	1.28E-11	2.26E-10
cobC	standard	2.72	19.26	7.09	*ugpA*	23.5	2.84	0.85	9.04E-05	6.07E-04
rcdA	standard	2.72	19.26	7.09	*gltW*	2671.27	2.83	0.34	1.73E-17	4.54E-16
ydgD	standard	4.76	33.7	7.09	*gltU*	2671.27	2.83	0.34	1.73E-17	4.54E-16
hrpB	standard	4.08	28.89	7.09	*gltT*	2671.27	2.83	0.34	1.73E-17	4.54E-16
ydgI	standard	29.21	204.85	7.01	*gltV*	2671.27	2.83	0.34	1.73E-17	4.54E-16
yodB	standard	5.44	37.64	6.93	*speG*	402.93	2.82	0.35	2.21E-16	5.39E-15
phoH	standard	16.99	116.87	6.88	*glnW*	5581.76	2.79	0.34	2.38E-17	6.10E-16
ydhJ	standard	23.78	163.27	6.87	*glnU*	5581.76	2.79	0.34	2.38E-17	6.10E-16
yebW	standard	7.47	50.77	6.79	*phnF*	9.4	2.78	1.4	0.004516358	0.018545518
dinQ	small	1.36	9.19	6.76	*ydhJ*	35.29	2.76	0.7	8.20E-06	6.70E-05
yfbP	standard	0.68	4.38	6.44	*appB*	29.37	2.76	0.75	2.63E-05	1.97E-04
insD2	standard	0.68	4.38	6.44	*pstA*	84.17	2.76	0.5	3.89E-09	5.37E-08
lhr	standard	0.68	4.38	6.44	*phoH*	157.53	2.74	0.55	6.19E-08	7.50E-07
nhoA	standard	0.68	4.38	6.44	*glsA*	31.04	2.74	0.74	2.48E-05	1.86E-04
recX	standard	0.68	4.38	6.44	*ycgX*	11.14	2.72	1.26	0.002969559	0.012959207
ugpA	standard	0.68	4.38	6.44	*clcA*	33.59	2.7	0.71	1.68E-05	1.29E-04
yacH	standard	0.68	4.38	6.44	*relB*	212.04	2.68	0.39	9.27E-13	1.79E-11
ycaC	standard	2.04	13.13	6.44	*mlaF*	310.63	2.64	0.36	2.15E-14	4.54E-13
yidD	standard	0.68	4.38	6.44	*rhsC*	20.37	2.59	0.88	3.93E-04	0.002230904
patA	standard	3.4	21.01	6.18	*pmrD*	10.57	2.59	1.28	0.004234691	0.017596745
yncJ	standard	50.28	310.34	6.17	*ymdF*	73.54	2.57	0.52	9.59E-08	1.12E-06
rseA	standard	205.86	1264.99	6.14	*mlrA*	23.28	2.55	0.82	2.35E-04	0.001436063
opgG	standard	13.59	83.17	6.12	*mqsA*	81.15	2.54	0.5	5.50E-08	6.75E-07
ybiO	standard	1.36	8.32	6.12	*zntA*	87.62	2.54	0.48	1.74E-08	2.26E-07

yfeO	standard	1.36	8.32	6.12	*mdfA*	45.72	2.54	0.62	5.74E-06	4.90E-05
hemD	standard	2.04	12.26	6.01	*mqsR*	84.83	2.51	0.49	4.53E-08	5.69E-07
iscX	standard	12.23	73.54	6.01	*thrV*	83.75	2.47	0.53	4.55E-07	4.79E-06
mdlA	standard	2.04	12.26	6.01	*slp*	50.9	2.47	0.6	6.20E-06	5.20E-05
argR	standard	27.18	163.27	6.01	*ycfJ*	63.77	2.46	0.55	1.07E-06	1.04E-05
pmrR	small	32.61	193.91	5.95	*thrU*	145.51	2.43	0.42	6.65E-10	9.68E-09
yddY	small	22.42	130.88	5.84	*ytjA*	131.58	2.42	0.44	4.71E-09	6.41E-08
yeeD	standard	108.03	627.68	5.81	*folA*	228.35	2.4	0.38	5.26E-11	8.65E-10
apaH	standard	2.72	15.76	5.8	*mlaE*	239.82	2.4	0.37	1.49E-11	2.60E-10
folM	standard	3.4	19.7	5.8	*yddY*	25.91	2.4	0.79	3.10E-04	0.001817096
ibsA	small	0.68	3.94	5.8	*ycaC*	70.21	2.39	0.53	9.42E-07	9.30E-06
insD3	standard	0.68	3.94	5.8	*appA*	25.61	2.37	0.77	2.88E-04	0.001708407
insD4	standard	0.68	3.94	5.8	*yadE*	24.1	2.37	0.8	3.94E-04	0.002230904
insD5	standard	0.68	3.94	5.8	*ykfI*	55.47	2.37	0.56	3.18E-06	2.85E-05
insD6	standard	0.68	3.94	5.8	*arfA*	24.15	2.36	0.8	4.15E-04	0.002324926
mhpF	standard	0.68	3.94	5.8	*ychS*	106.85	2.34	0.47	9.09E-08	1.08E-06
xylB	standard	0.68	3.94	5.8	*yohC*	26.27	2.32	0.77	3.43E-04	0.00200324
ydcK	standard	1.36	7.88	5.8	*yjbJ*	153.23	2.32	0.42	4.38E-09	5.98E-08
btuE	standard	19.7	113.81	5.78	*paoD*	10.75	2.3	1.23	0.00655796	0.025024217
yjdC	standard	8.83	48.59	5.5	*yiaG*	86.74	2.3	0.5	6.84E-07	6.95E-06
glsB	standard	10.19	56.03	5.5	*rmf*	1448.26	2.29	0.32	2.75E-13	5.45E-12
recJ	standard	6.79	37.21	5.48	*ycaP*	13.38	2.27	1.07	0.004022703	0.01682759
dosC	standard	16.31	87.54	5.37	*yjdN*	14.7	2.25	1.02	0.003375377	0.01444809
yecE	standard	2.04	10.94	5.37	*symR*	13.43	2.24	1.08	0.004360634	0.01804818
cpxP	standard	86.29	461.35	5.35	*hemL*	436.05	2.23	0.35	1.79E-11	3.08E-10
ampH	standard	38.05	202.22	5.32	*glk*	152.05	2.22	0.42	1.62E-08	2.12E-07
ycgV	standard	13.59	71.78	5.28	*arrS*	71.94	2.22	0.54	5.76E-06	4.90E-05
ymgE	standard	19.02	100.24	5.27	*ybjX*	352.08	2.22	0.38	9.80E-10	1.41E-08
bepA	standard	20.38	105.49	5.18	*yagP*	15.62	2.21	0.99	0.003308268	0.014180234
ecpA	standard	1.36	7	5.15	*yijD*	302.74	2.19	0.35	8.95E-11	1.45E-09
rzoQ	standard	0.68	3.5	5.15	*gadW*	98.62	2.19	0.49	1.11E-06	1.08E-05
tfaP	standard	0.68	3.5	5.15	*zraR*	36.16	2.19	0.66	1.39E-04	8.84E-04
thiQ	standard	0.68	3.5	5.15	*psiF*	55.56	2.17	0.56	1.53E-05	1.19E-04
ybbA	standard	2.04	10.51	5.15	*mgrR*	14.06	2.17	1.04	0.004721938	0.019238208
ydbH	standard	0.68	3.5	5.15	*ydgV*	108.03	2.14	0.46	5.08E-07	5.30E-06
pgpC	standard	21.74	108.99	5.01	*yohP*	29.27	2.14	0.72	4.45E-04	0.002479686
yqgF	standard	2.72	13.57	4.99	*ygiW*	67.93	2.13	0.52	7.97E-06	6.53E-05
yeaY	standard	63.19	314.72	4.98	*pgaD*	9.14	2.13	1.38	0.012332021	0.042160671
waaO	standard	7.47	37.21	4.98	*ytfK*	199.14	2.12	0.38	4.18E-09	5.74E-08
ydcL	standard	16.99	84.04	4.95	*sixA*	116.56	2.12	0.44	3.09E-07	3.35E-06

csdE	standard	6.11	30.2	4.94	*yafW*	13.72	2.1	1.05	0.005813937	0.022796754
yeeY	standard	2.04	10.07	4.94	*yqhI*	17.34	2.1	0.92	0.003119101	0.013443068
yggC	standard	4.08	20.13	4.94	*ybaT*	19.7	2.09	0.86	0.002281827	0.010453641
waaG	standard	2.04	10.07	4.94	*opgB*	81.48	2.08	0.49	3.69E-06	3.28E-05
rseB	standard	163.74	808.02	4.93	*glnX*	1680.13	2.07	0.34	1.46E-10	2.27E-09
ykgS	small	11.55	56.9	4.93	*glnV*	1680.13	2.07	0.34	1.46E-10	2.27E-09
yfhH	standard	16.31	80.1	4.91	*holE*	345.7	2.07	0.35	5.26E-10	7.79E-09
yodE	small	40.77	200.03	4.91	*yhcN*	112.26	2.07	0.44	5.33E-07	5.52E-06
artQ	standard	1.36	6.57	4.83	*glcD*	12.51	2.07	1.11	0.007735031	0.028847334
xynR	standard	1.36	6.57	4.83	*yeeW*	19.64	2.06	0.86	0.002416881	0.010944167
yfjF	standard	5.44	26.26	4.83	*yciY*	33.11	2.06	0.68	3.66E-04	0.002099702
waaP	standard	10.19	49.02	4.81	*gadA*	55	2.06	0.6	1.09E-04	7.20E-04
opgB	standard	25.14	119.5	4.75	*kefB*	29.32	2.06	0.71	6.02E-04	0.003210015
rmf	standard	499.37	2361.46	4.73	*sibC*	62.55	2.06	0.53	1.98E-05	1.51E-04
yafS	standard	4.08	19.26	4.72	*corA*	126.56	2.03	0.44	7.50E-07	7.55E-06
yegS	standard	8.15	38.52	4.72	*ynfC*	26.23	2.02	0.74	0.001064516	0.005332848
clcB	standard	4.76	22.32	4.69	*yoaC*	21.34	2.01	0.82	0.002245505	0.010302324
yhdV	standard	25.82	120.81	4.68	*leuP*	370.92	1.99	0.44	1.03E-06	1.01E-05
yriB	small	18.34	85.79	4.68	*proP*	542.82	1.97	0.33	3.48E-10	5.29E-09
tcyJ	standard	86.97	399.19	4.59	*ecpA*	34.9	1.97	0.66	4.90E-04	0.002672328
gsiA	standard	7.47	34.14	4.57	*arnE*	10.7	1.97	1.18	0.012091365	0.04162143
amyA	standard	15.63	71.35	4.57	*hscA*	342.73	1.96	0.4	1.70E-07	1.92E-06
hscA	standard	41.44	187.78	4.53	*rpoE*	319.84	1.95	0.35	5.02E-09	6.80E-08
cysI	standard	21.74	98.05	4.51	*amiC*	208.92	1.95	0.38	5.25E-08	6.52E-07
fepE	standard	0.68	3.06	4.51	*ugpE*	16.7	1.94	0.94	0.005879849	0.023026342
folK	standard	0.68	3.06	4.51	*ymiA*	23.96	1.91	0.78	0.002399407	0.010880791
hisA	standard	0.68	3.06	4.51	*yahO*	74.6	1.91	0.51	3.29E-05	2.40E-04
hisM	standard	0.68	3.06	4.51	*phoU*	114.77	1.91	0.44	2.77E-06	2.50E-05
hyaF	standard	0.68	3.06	4.51	*ykfG*	11.5	1.9	1.13	0.012368798	0.042181183
insD1	standard	0.68	3.06	4.51	*pstB*	120.34	1.9	0.43	2.03E-06	1.86E-05
moaE	standard	0.68	3.06	4.51	*basS*	32.19	1.89	0.68	9.49E-04	0.004844557
pdxI	standard	3.4	15.32	4.51	*slyA*	260.77	1.89	0.36	3.52E-08	4.47E-07
sapF	standard	0.68	3.06	4.51	*yhiD*	15.9	1.89	0.94	0.007083942	0.026705609
waaF	standard	1.36	6.13	4.51	*kefG*	73.43	1.87	0.51	4.47E-05	3.18E-04
yafL	standard	0.68	3.06	4.51	*yobH*	41.89	1.86	0.61	4.13E-04	0.002321485
ycbV	standard	0.68	3.06	4.51	*selC*	48.44	1.85	0.58	2.89E-04	0.001710781
ydaG	small	1.36	6.13	4.51	*fdx*	172.13	1.85	0.44	5.09E-06	4.40E-05
yfdX	standard	1.36	6.13	4.51	*kbp*	41.95	1.84	0.61	4.87E-04	0.002664475
aat	standard	61.83	278.82	4.51	*gadF*	49.84	1.84	0.63	6.72E-04	0.003539518
livJ	standard	2.04	9.19	4.51	*bglA*	277.97	1.84	0.38	2.40E-07	2.66E-06
paaK	standard	2.04	9.19	4.51	*yodD*	16.48	1.83	0.92	0.007466941	0.027947439
trmD	standard	148.11	664.89	4.49	*hdeB*	216.8	1.83	0.43	3.89E-06	3.44E-05

mgtS	small	2234.61	9955.35	4.46	*osmC*	176.67	1.83	0.41	1.61E-06	1.52E-05
bfr	standard	13.59	60.4	4.45	*yhbE*	148.23	1.81	0.43	5.00E-06	4.33E-05
osmF	standard	4.76	21.01	4.42	*mlaD*	217.43	1.8	0.37	2.49E-07	2.73E-06
tomB	standard	27.86	122.12	4.38	*cspB*	69.69	1.79	0.51	9.40E-05	6.26E-04
dkgB	standard	11.55	50.34	4.36	*serW*	53.51	1.79	0.58	3.98E-04	0.002250482
bcsG	standard	2.72	11.82	4.35	*serX*	53.51	1.79	0.58	3.98E-04	0.002250482
ydeP	standard	2.72	11.82	4.35	*ortT*	31.77	1.79	0.74	0.002848726	0.012607727
ycgZ	standard	20.38	88.42	4.34	*yfeK*	18.38	1.78	0.86	0.006865127	0.025974585
glk	standard	43.48	188.22	4.33	*yafX*	24.7	1.78	0.76	0.00357779	0.015231165
cynR	standard	22.42	96.73	4.31	*basR*	41.62	1.76	0.61	7.62E-04	0.003938452
fxsA	standard	8.83	38.08	4.31	*yabI*	44.88	1.76	0.58	5.35E-04	0.002873773
yhfG	standard	12.91	55.15	4.27	*gadE*	27.23	1.76	0.76	0.004028227	0.0168282
amiB	standard	9.51	40.27	4.23	*azuC*	71.86	1.76	0.62	9.66E-04	0.004912092
ldtC	standard	16.99	71.35	4.2	*mdaB*	102.97	1.75	0.45	2.21E-05	1.67E-04
rstA	standard	64.54	270.51	4.19	*ynfS*	90.26	1.75	0.46	3.43E-05	2.50E-04
ahr	standard	9.51	39.83	4.19	*ydhR*	93	1.73	0.46	4.57E-05	3.23E-04
fbaB	standard	9.51	39.83	4.19	*rcnA*	13.84	1.73	0.99	0.01356292	0.045147211
bcsF	standard	1.36	5.69	4.19	*ysgD*	402.58	1.72	0.35	2.73E-07	2.98E-06
chbG	standard	5.44	22.76	4.19	*shoB*	19.74	1.72	0.83	0.007317217	0.027419846
fadE	standard	2.72	11.38	4.19	*ygdI*	40.7	1.71	0.6	9.86E-04	0.004994682
ycgB	standard	7.47	31.08	4.16	*mlaB*	155.62	1.71	0.4	4.03E-06	3.53E-05
gsiB	standard	3.4	14.01	4.12	*rem*	13.58	1.7	1	0.01516317	0.049319708
pxpA	standard	3.4	14.01	4.12	*ybaP*	80.94	1.7	0.47	8.16E-05	5.53E-04
wecB	standard	2.04	8.32	4.08	*mltF*	22.43	1.68	0.78	0.006371506	0.02459144
ydeM	standard	2.04	8.32	4.08	*yciX*	63.21	1.67	0.51	2.67E-04	0.001591423
nimR	standard	10.87	44.21	4.07	*leuT*	333.1	1.66	0.42	1.71E-05	1.31E-04
psiF	standard	8.83	35.89	4.06	*leuV*	333.1	1.66	0.42	1.71E-05	1.31E-04
ynjB	standard	9.51	38.08	4	*leuQ*	333.1	1.66	0.42	1.71E-05	1.31E-04
yiaG	standard	10.19	40.71	3.99	*trpT*	53.05	1.66	0.55	6.59E-04	0.0034826
uhpB	standard	12.91	51.21	3.97	*hdeA*	666.9	1.65	0.37	2.31E-06	2.11E-05
ecpR	standard	5.44	21.45	3.95	*elaB*	154.33	1.65	0.4	1.08E-05	8.61E-05
mntP	standard	23.1	91.04	3.94	*letA*	25.84	1.64	0.73	0.005293456	0.021180592
msyB	standard	78.13	307.71	3.94	*mltD*	413.19	1.64	0.34	4.54E-07	4.79E-06
dgcQ	standard	6.11	24.07	3.94	*glmY*	73.6	1.61	0.49	2.56E-04	0.001541773
ydbJ	standard	99.87	392.19	3.93	*maeA*	355.15	1.61	0.37	3.00E-06	2.70E-05
alx	standard	7.47	29.33	3.92	*ykfF*	34.95	1.6	0.64	0.002915101	0.012813055
yraQ	standard	38.05	148.82	3.91	*tatD*	80.68	1.6	0.48	2.05E-04	0.001258503
ldtA	standard	29.89	116.87	3.91	*ynaI*	32.23	1.6	0.67	0.003919051	0.016504319
rhoL	small	10.87	42.46	3.91	*rseA*	791.21	1.59	0.33	2.88E-07	3.13E-06
ygiW	standard	6.79	26.26	3.87	*glgS*	35.1	1.59	0.66	0.003814277	0.016106441
gudX	standard	0.68	2.63	3.87	*gcvB*	3584.49	1.59	0.32	1.68E-07	1.91E-06
ibsB	small	2.72	10.51	3.87	*msyB*	63.26	1.58	0.52	6.14E-04	0.003265833

malX	standard	0.68	2.63	3.87	*valW*	46.96	1.58	0.59	0.001741963	0.008208737
mdtD	standard	0.68	2.63	3.87	*aspU*	650.02	1.58	0.34	1.23E-06	1.18E-05
moaD	standard	1.36	5.25	3.87	*aspV*	650.02	1.58	0.34	1.23E-06	1.18E-05
msrP	standard	1.36	5.25	3.87	*aspT*	650.02	1.58	0.34	1.23E-06	1.18E-05
phnN	standard	0.68	2.63	3.87	*ompX*	4546.19	1.57	0.32	2.02E-07	2.27E-06
pphA	standard	1.36	5.25	3.87	*pmrR*	156.83	1.57	0.39	1.97E-05	1.50E-04
recO	standard	1.36	5.25	3.87	*tyrV*	115.05	1.56	0.44	1.12E-04	7.33E-04
rseC	standard	0.68	2.63	3.87	*tyrT*	115.05	1.56	0.44	1.12E-04	7.33E-04
sxy	standard	1.36	5.25	3.87	*mlaC*	223.38	1.56	0.37	6.04E-06	5.08E-05
trmO	standard	2.72	10.51	3.87	*emrD*	40.84	1.55	0.6	0.0025991	0.011651268
ydhP	standard	18.34	70.91	3.87	*ydhP*	31.46	1.54	0.67	0.005090086	0.020524328
yfbN	standard	0.68	2.63	3.87	*dinJ*	131.95	1.54	0.41	5.98E-05	4.14E-04
yjcO	standard	0.68	2.63	3.87	*iscR*	308.39	1.54	0.51	7.04E-04	0.003669559
pyrR	standard	2.04	7.88	3.87	*sra*	525.89	1.53	0.34	1.75E-06	1.64E-05
ybjC	standard	8.15	31.52	3.87	*yoeB*	53.81	1.52	0.54	0.001361759	0.006609666
paaJ	standard	2.04	7.88	3.87	*gltS*	37.19	1.5	0.62	0.004079394	0.017019232
tmcA	standard	2.04	7.88	3.87	*osmY*	248.23	1.5	0.4	4.80E-05	3.38E-04
yceM	standard	2.04	7.88	3.87	*ugpC*	28.39	1.46	0.69	0.009072358	0.032932027
ydeI	standard	2.04	7.88	3.87	*soxS*	136.64	1.45	0.42	1.65E-04	0.001041569
yghB	standard	42.8	164.58	3.85	*yejG*	207.82	1.45	0.4	8.98E-05	6.04E-04
ymiA	small	138.6	530.51	3.83	*ykiD*	30.44	1.44	0.66	0.008017026	0.029651623
yibF	standard	7.47	28.45	3.81	*cof*	36.87	1.43	0.61	0.005648098	0.022314267
yphH	standard	11.55	43.77	3.79	*rcnR*	28.58	1.43	0.68	0.00981519	0.035219873
curA	standard	22.42	84.92	3.79	*rpoS*	518.95	1.41	0.33	5.85E-06	4.95E-05
npr	standard	15.63	59.09	3.78	*ryfA*	56.68	1.41	0.52	0.002227727	0.010235766
ytfF	standard	9.51	35.89	3.77	*yqhA*	154.26	1.39	0.39	1.37E-04	8.75E-04
cysE	standard	47.56	178.59	3.76	*psiE*	28.88	1.39	0.68	0.011626599	0.040374065
yedA	standard	7.47	28.01	3.75	*glyU*	39.24	1.38	0.6	0.006460553	0.024823494
osmY	standard	40.09	150.14	3.75	*erpA*	165.91	1.35	0.47	0.001365789	0.006615408
gadW	standard	63.19	236.37	3.74	*yeaQ*	65.54	1.35	0.5	0.002133684	0.009848486
dacC	standard	55.71	208.35	3.74	*dkgB*	31.73	1.35	0.65	0.011599563	0.040332427
ytiA	standard	3.4	12.69	3.74	*yceK*	99.9	1.33	0.46	0.00134666	0.006563393
dnaC	standard	9.51	35.45	3.73	*adhP*	30.59	1.33	0.65	0.012832445	0.043221442
phoP	standard	233.04	864.48	3.71	*cspF*	36.22	1.32	0.61	0.009769932	0.035138064
hybD	standard	2.72	10.07	3.7	*cydH*	77.27	1.32	0.47	0.001728634	0.008158215
tatB	standard	2.72	10.07	3.7	*yefM*	123.88	1.32	0.41	5.11E-04	0.002764991
yebE	standard	12.91	47.27	3.66	*yedR*	30.32	1.31	0.65	0.014078261	0.046418208
nagA	standard	14.95	54.71	3.66	*degP*	308.32	1.3	0.36	9.23E-05	6.19E-04
hemF	standard	6.11	22.32	3.65	*yqeF*	37.96	1.29	0.61	0.011566698	0.040303115
dadX	standard	2.04	7.44	3.65	*yebV*	154.21	1.29	0.41	5.61E-04	0.003003626
ggt	standard	4.08	14.88	3.65	*iscS*	431.78	1.29	0.45	0.001488886	0.007167266
yoeB	standard	2.04	7.44	3.65	*zapC*	130.31	1.28	0.4	5.74E-04	0.003072022

letA	standard	52.99	193.03	3.64	*yncL*	120.28	1.28	0.42	9.49E-04	0.004844557
ytjA	standard	47.56	172.46	3.63	*ohsC*	109.96	1.27	0.42	0.001015212	0.005098873
uvrY	standard	27.18	98.05	3.61	*yrbN*	225.13	1.27	0.37	2.38E-04	0.001449485
yhjD	standard	8.15	29.33	3.6	*mdtK*	62.12	1.27	0.5	0.00443095	0.018242686
tehA	standard	18.34	65.66	3.58	*yghE*	41.85	1.27	0.58	0.010335855	0.036693964
adhP	standard	5.44	19.26	3.54	*rsxA*	53.19	1.26	0.54	0.006530064	0.024978693
cmoB	standard	1.36	4.81	3.54	*sfsA*	54.6	1.25	0.52	0.006450973	0.024823494
pncA	standard	1.36	4.81	3.54	*ytiB*	51.03	1.25	0.54	0.007595897	0.028362246
uhpC	standard	1.36	4.81	3.54	*tusA*	75.69	1.25	0.47	0.003008532	0.013056443
insA4	standard	4.08	14.44	3.54	*rplS*	741.32	1.24	0.34	1.17E-04	7.62E-04
pmrD	standard	158.3	556.33	3.51	*rnlB*	45.16	1.23	0.56	0.010036429	0.035808421
slp	standard	19.02	66.53	3.5	*blr*	68.02	1.23	0.49	0.004412675	0.018201483
yfjD	standard	4.76	16.63	3.5	*bfr*	69.08	1.23	0.49	0.004582157	0.018766453
talA	standard	13.59	47.27	3.48	*ibpA*	46.01	1.2	0.55	0.011140268	0.038903904
yhbO	standard	6.79	23.64	3.48	*tatE*	68.34	1.19	0.48	0.005545779	0.022021246
yidZ	standard	29.89	103.74	3.47	*iscX*	499.84	1.18	0.4	0.001193108	0.005907016
yecN	standard	42.8	147.95	3.46	*obgE*	194.26	1.17	0.39	9.99E-04	0.005046111
mepM	standard	15.63	53.84	3.45	*tolC*	692.49	1.17	0.33	2.01E-04	0.001238049
ecnA	small	2.04	7	3.44	*iscU*	305.42	1.16	0.43	0.002823147	0.012529967
fecC	standard	2.04	7	3.44	*frmR*	87.67	1.15	0.45	0.004308386	0.01787923
phnD	standard	4.08	14.01	3.44	*rseC*	118.42	1.15	0.41	0.002334944	0.010619245
ycgY	standard	2.04	7	3.44	*eco*	76.98	1.15	0.47	0.006182743	0.024121949
ychO	standard	4.08	14.01	3.44	*atpI*	308.54	1.14	0.35	4.75E-04	0.002606775
ynjD	standard	2.04	7	3.44	*rpoZ*	113.46	1.14	0.44	0.004444168	0.018273064
thiL	standard	8.83	30.2	3.42	*roxA*	178.9	1.14	0.38	0.001264669	0.006212163
ybiR	standard	8.83	30.2	3.42	*lpxT*	53.03	1.14	0.53	0.013268514	0.04421425
ytjB	standard	69.3	236.8	3.42	*hdeD*	64.47	1.13	0.53	0.012893055	0.043351172
metI	standard	4.76	16.2	3.41	*rcnB*	64.97	1.13	0.49	0.008988767	0.032666496
ybjS	standard	93.76	318.66	3.4	*yffB*	84.37	1.12	0.46	0.006420724	0.024741928
dnaK	standard	14.95	50.77	3.4	*cdsA*	70.95	1.1	0.49	0.011431427	0.03987618
rcsC	standard	12.91	43.77	3.39	*iscA*	310.37	1.1	0.42	0.004388433	0.018139242
phnO	standard	10.87	36.77	3.38	*osmB*	100.71	1.09	0.43	0.005613039	0.022203793
pspD	standard	40.77	137.44	3.37	*lysU*	87.48	1.08	0.46	0.008192364	0.030264355
hokD	standard	38.73	130.44	3.37	*ecnB*	69.09	1.08	0.48	0.010833276	0.038044129
inaA	standard	15.63	52.53	3.36	*pepB*	120.64	1.08	0.42	0.004873856	0.019754267
pabB	standard	39.41	131.75	3.34	*rseB*	238.27	1.07	0.36	0.001374135	0.006645545
yfdC	standard	19.7	65.66	3.33	*nadD*	71.06	1.05	0.47	0.012553295	0.042741306
fumE	standard	25.82	85.79	3.32	*ivy*	123.06	1.05	0.41	0.005102016	0.020545956
aroC	standard	4.76	15.76	3.31	*bax*	212.78	1.04	0.36	0.002015903	0.009331005
wecF	standard	16.99	56.03	3.3	*bssS*	188.72	1.03	0.37	0.002690689	0.011976054
yadX	small	23.78	78.35	3.29	*bolA*	157.88	1.02	0.4	0.00569691	0.022448028
degP	standard	21.06	69.16	3.28	*ydgK*	78.89	1.01	0.45	0.012656898	0.042898198

ydhI	standard	14.27	46.84	3.28
ymdF	standard	14.27	46.84	3.28
hisQ	standard	16.99	55.59	3.27
yodC	standard	161.7	524.82	3.25
abpA	standard	24.46	79.23	3.24
ybjG	standard	303.02	980.92	3.24
yeaG	standard	29.89	96.73	3.24
mrcB	standard	48.24	155.83	3.23
mrdB	standard	1.36	4.38	3.22
acpS	standard	0.68	2.19	3.22
arnF	standard	0.68	2.19	3.22
essQ	standard	0.68	2.19	3.22
hcr	standard	0.68	2.19	3.22
ilvH	standard	0.68	2.19	3.22
insB2	standard	0.68	2.19	3.22
insB3	standard	0.68	2.19	3.22
kduI	standard	0.68	2.19	3.22
lpxK	standard	2.04	6.57	3.22
narJ	standard	0.68	2.19	3.22
sufD	standard	0.68	2.19	3.22
treA	standard	0.68	2.19	3.22
yaaI	standard	1.36	4.38	3.22
ydhT	standard	1.36	4.38	3.22
ydhU	standard	2.04	6.57	3.22
ynaK	standard	0.68	2.19	3.22
ynbA	standard	0.68	2.19	3.22
ypdC	standard	0.68	2.19	3.22
yqeC	standard	1.36	4.38	3.22
yqiA	standard	16.99	54.28	3.2
ybgA	standard	9.51	30.2	3.18
ydgJ	standard	108.03	342.73	3.17
ynfC	standard	8.83	28.01	3.17
yhbQ	standard	74.74	236.8	3.17
metL	standard	10.87	34.14	3.14
eamA	standard	14.27	44.65	3.13
dusC	standard	9.51	29.76	3.13
relE	standard	4.76	14.88	3.13
ygdR	standard	307.1	952.03	3.1
yfeY	standard	57.07	176.84	3.1
dnaG	standard	17.66	54.71	3.1
mukE	standard	35.33	108.99	3.08
slt	standard	15.63	48.15	3.08

lpxB	94.1	1	0.44	0.011029168	0.038645314
deaD	606.52	0.99	0.33	0.001428271	0.006886069
frmA	117.64	0.96	0.41	0.009881474	0.03533615
ybiE	142.68	0.96	0.39	0.008000962	0.029627231
yrbL	258.5	0.94	0.35	0.004091926	0.017048785
pheM	167.34	0.93	0.38	0.008333725	0.030642886
ybhL	238.82	0.91	0.38	0.008835762	0.032260328
hspQ	188.37	0.87	0.38	0.012704292	0.042928435
ydiH	403.56	0.86	0.33	0.005399113	0.021548245
cpxP	205.41	0.86	0.37	0.011798686	0.040793466
thrW	199.73	0.83	0.36	0.013973818	0.046178214
nlpD	735.03	0.77	0.31	0.008684907	0.031820928
csrB	2954.91	0.68	0.29	0.014267278	0.046991908

ybiJ	standard	6.11	18.82	3.08
moaA	standard	26.5	81.41	3.07
zraR	standard	23.1	70.91	3.07
insH5	standard	32.61	99.8	3.06
cvpA	standard	17.66	53.4	3.02
tcdA	standard	30.57	91.92	3.01
ycjX	standard	8.15	24.51	3.01
yigL	standard	4.08	12.26	3.01
ymiC	small	282.63	839.53	3.00

Table S5. Verification of protein expression from the genomic locus for the 17 candidates identified in this study using Ribo-RET.

Small Protein	Small protein expression by genomic tagging first reported in	Media used
MgtS	16	LB
	17	Supplemented N-minimal medium with no added Mg^{2+}
MgrB	16	LB
PmrR	18	N-minimal medium, pH 7.7 with 10 μM Mg^{2+}
MgtT	19	LB
YmiC	20	LB
YmiA	16	LB
YoaI	[This Study]	Supplemented minimal A medium with 10 mM, 1 mM and no added Mg^{2+}
YobF	16	LB
	3	LB + heat shock (45°C)
YddY	20	LB
YriB	19	LB
YadX	19	LB
YkgS	20	LB
YriA	19	LB
YdgU	16	LB
YqhI	20	LB
YadW	20	LB
DinQ	21	LB

Table S6. Localization, Tag, and Membrane Topology Prediction of Small Proteins

Small Protein	Localization	Epitope tag	Reference	Prediction of transmembrane helix and orientation		
				TMHMM [22]	TMPred [23]	Phobius [24]
MgtS	Membrane	C-terminal/FLAG and C-terminal/GFP	[16,25]	Yes	Predicted helix: 7-25 (19aa); Inside to Outside: N-terminus facing cytoplasm	Cytoplasmic (1-6aa) / Transmembrane (7-25aa) / Non - cytoplasmic (26-31aa)
MgrB	Membrane	C-terminal/FLAG and N-terminal/GFP	[1,16]	Yes	Predicted helix: 6-24 (19aa); Inside to Outside: N-terminus facing cytoplasm	Positively charged or n-region (1-5aa) / Hydrophobic α-helical or h-region (6-17aa)/ Non cytoplasmic (22-47)
PmrR	Membrane	C-terminal/6XHis	This study	Yes	Predicted helix: 5-27 (23aa); Inside to Outside: N-terminus facing cytoplasm	Cytoplasmic (1-8aa) / transmembrane (9-26 aa) / non cytoplasmic (27-29aa)
		N-terminal/FLAG-6XHis (*S. enterica* PmrR)	[18]			
MgtT	Cytoplasm	N-terminal/GFP	This study	No	NA	Non cytoplasmic
YmiC	Membrane	N-terminal/GFP	This study	Yes	Predicted helix: 8-29 (22aa); Inside to Outside: N-terminus facing cytoplasm	Cytoplasmic (1-8aa) / Transmembrane (9-29aa) / Non - cytoplasmic (30-31aa)
YmiA	Membrane	N-terminal/GFP	This study	Yes	Predicted helix: 22-42 (21aa); Inside to Outside: N-terminus facing cytoplasm	Cytoplasmic (1-20aa) / Transmembrane (21-42aa) / Non - cytoplasmic (43-46aa)

YoaI	Membrane	C-terminal/GFP	This study	Yes	Predicted helix: 10-20 (21aa); Outside to Inside: N-terminus facing periplasm	Non - cytoplasmic (1-5aa) / Transmembrane (6-30aa) / Cytoplasmic (31-34aa)
YobF	Membrane	C-terminal/6XHis	This study	Yes	Predicted helix: 25-41 (17aa); Outside to Inside: N-terminus facing periplasm	Non cytoplasmic
YddY	Cytoplasm	N-terminal/GFP	This study	No	NA	Non cytoplasmic
YriB	Cytoplasm	N-terminal/GFP	This study	No	NA	Non cytoplasmic
YadX	Cytoplasm	N-terminal/GFP	This study	No	NA	Cytoplasmic
YkgS	Cytoplasm	N-terminal/GFP	This study	No	NA	Cytoplasmic
YriA	Cytoplasm	N-terminal/GFP	This study	No	NA	Non cytoplasmic
YdgU	Membrane	N-terminal/GFP	This study	Yes	Predicted helix: 7-26 (20aa); Inside to Outside: N-terminus facing cytoplasm	Cytoplasmic (1-6aa) / Transmembrane (7-26aa) / Non - cytoplasmic (27aa)
YqhI	Cytoplasm	N-terminal/GFP	This study	No	NA	Non cytoplasmic
YadW	Cytoplasm	C-terminal/GFP	This study	No	NA	Non cytoplasmic
DinQ	Membrane	N-terminal FLAG	[21]	Yes	Predicted helix: 1-22 (22aa); Outside to Inside: N-terminal facing periplasm	Non - cytoplasmic (1-5aa) / Transmembrane (6-23aa) / Cytoplasmic (24-27aa)

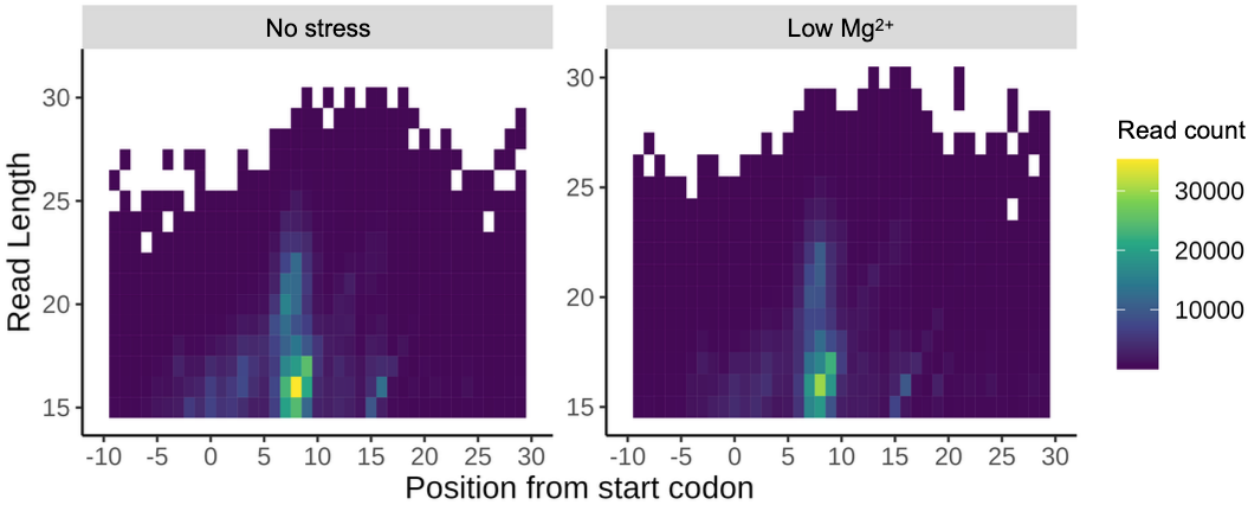

Figure S1. A Ribogrid analysis representing Ribo-RET reads aligned to the genome. The rows represent reads of varying lengths, and the columns indicate the position of the 3'-end of a footprint.

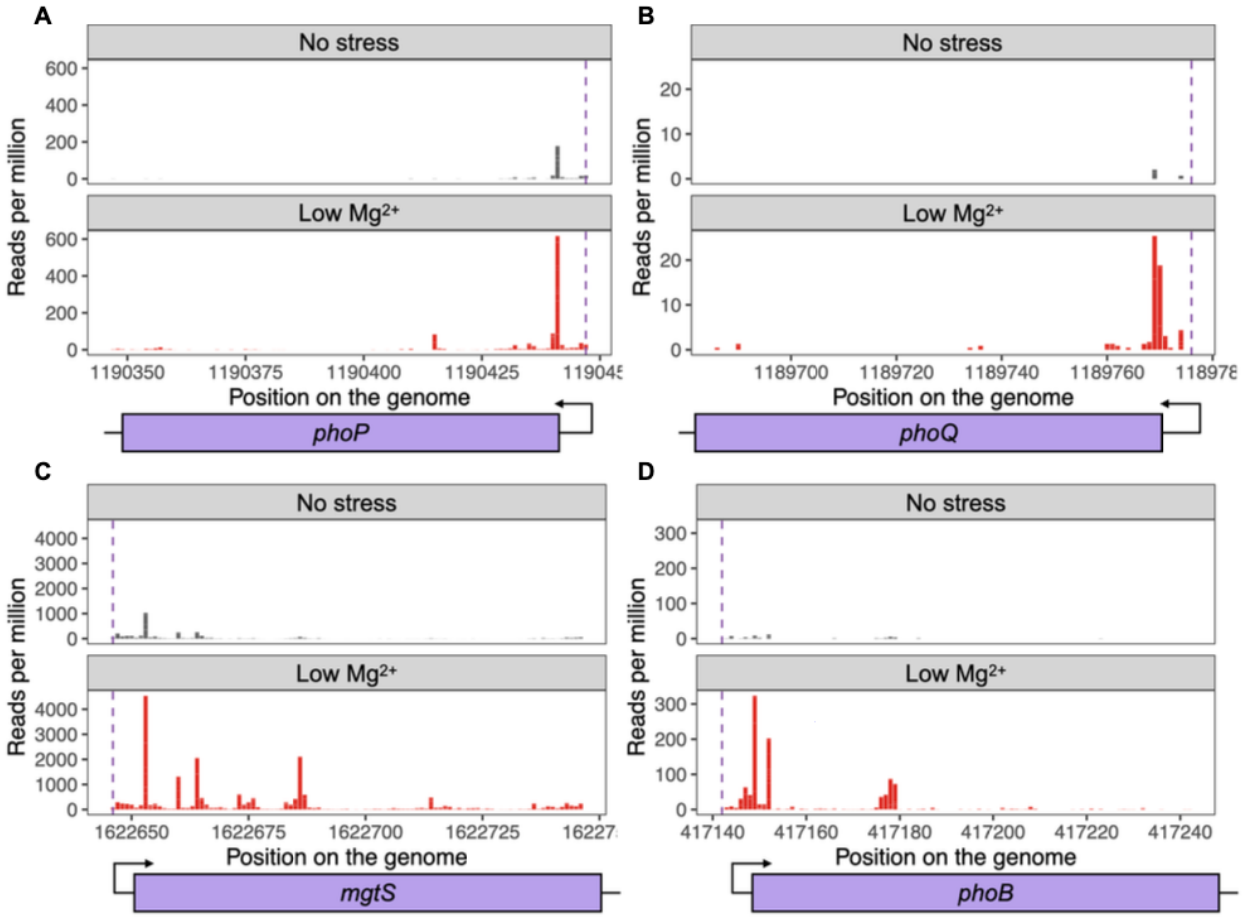

Figure S2. Validation of Ribo-RET in detecting ribosome occupancy on annotated start site of proteins known to be induced under low Mg^{2+} stress.
(A-D) Ribo-RET reads mapping to the translation start site of proteins (A) PhoP, (B) PhoQ, (C) MgtS, and (D) PhoB at no stress condition (10 mM Mg^{2+}) and low Mg^{2+} stress. A purple dashed line indicates the translation start site.

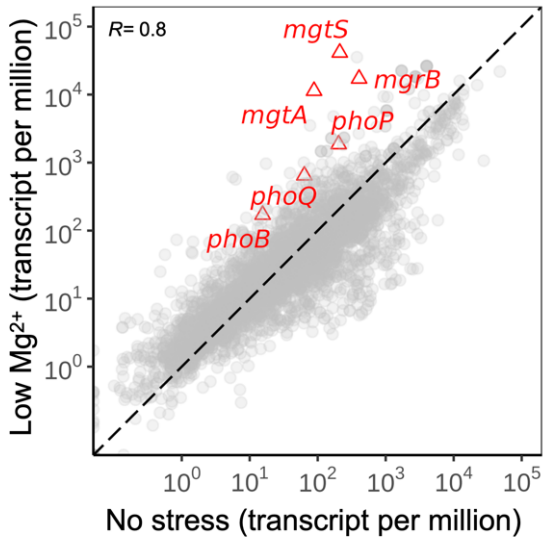

Figure S3. Validation of RNA-Seq in detecting transcripts known to be induced under low Mg^{2+} stress. Scatterplot showing the correlation between the normalized RNA-Seq reads mapping to all the annotated genes under low Mg^{2+} stress and no stress. *mgtS, mgrB, phoP, phoQ*, *mgtA,* and *phoB,* known to be induced under magnesium starvation, are highlighted in red triangle, while the rest of the transcripts are highlighted in gray circles. Pearson's coefficient, r= 0.8. The data is derived from the average of two biological replicates.

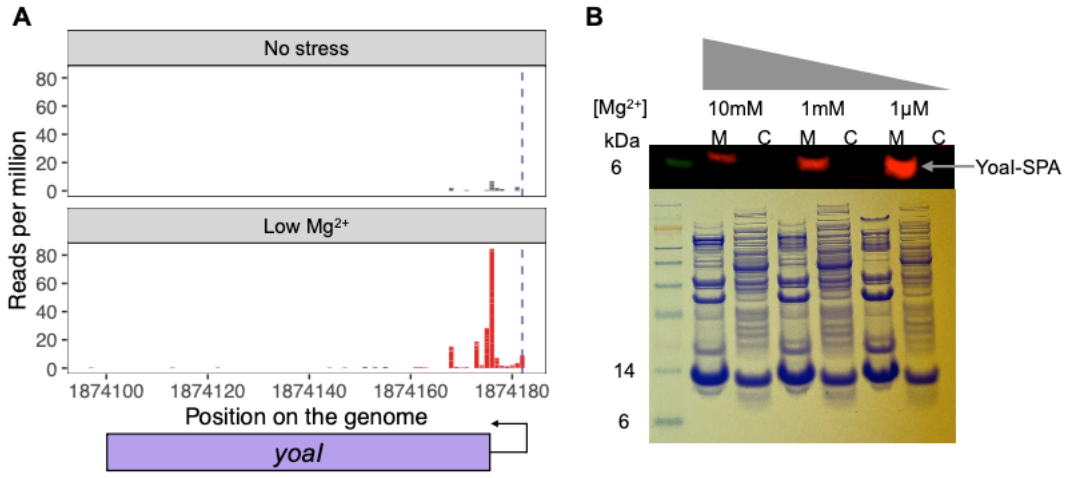

Figure S4. Validation of low magnesium-dependent expression of a small protein, YoaI in the cell. (A) Ribo-RET data for small protein YoaI induced under low Mg^{2+} stress. The translation start site is indicated by a purple dashed line. (B) Validation of YoaI expression using a strain containing *yoaI-SPA* genomic fusion (GSO317). Cells were grown in supplemented minimal A medium containing $MgSO_4$ at the indicated concentration. Membrane (M) and cytoplasmic (C) fractions were analyzed by western blotting using M2 anti-FLAG antibodies (top) and by Coomassie Brilliant Blue staining (bottom). The data represents results from two independent replicates.

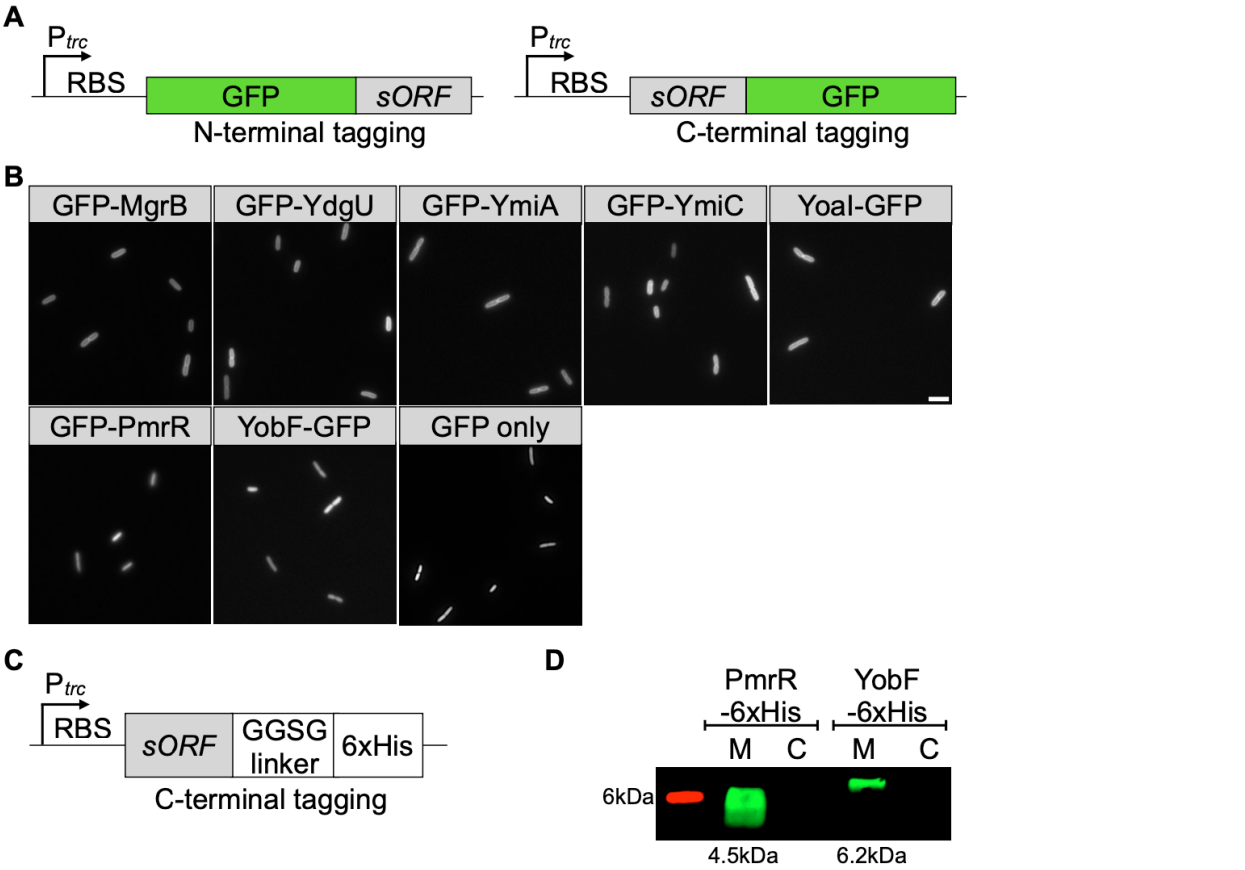

Figure S5. Membrane localization of small proteins identified by epitope tagging. (A) Schematic representation of GFP-tagged small protein constructs. (B) Fluorescence micrographs of *E. coli* K-12 MG1655 cells expressing GFP-MgrB (pAL38), GFP-YdgU (pPJ3), GFP-YmiA (pPJ12), GFP-YmiC (pPJ13), YoaI-GFP (pPJ4), GFP-PmrR (pPJ2), YobF-GFP (pPJ6), and GFP only (pAL39). (C) Schematic representation of 6XHis-tagged small protein constructs. (D) Western blot analysis of *E. coli* K-12 MG1655 cells expressing PmrR-6XHis (pSV14) and YobF-6XHis (pSV26), probed with anti-His antibodies. Membrane (M) and cytoplasm (C) fractions are indicated. In Panel B, cells were cultured in supplemented minimal A medium containing 1 mM Mg^{2+} and 50 µg ml^{-1} carbenicillin. In Panel D, the cells were grown in LB containing 100 µg ml^{-1} carbenicillin. After four hours of growth, cells were induced with 500 µM IPTG and harvested two hours post-induction. The data represents results from two independent replicates. Scale bar = 5 µm. (Also see Table S6)

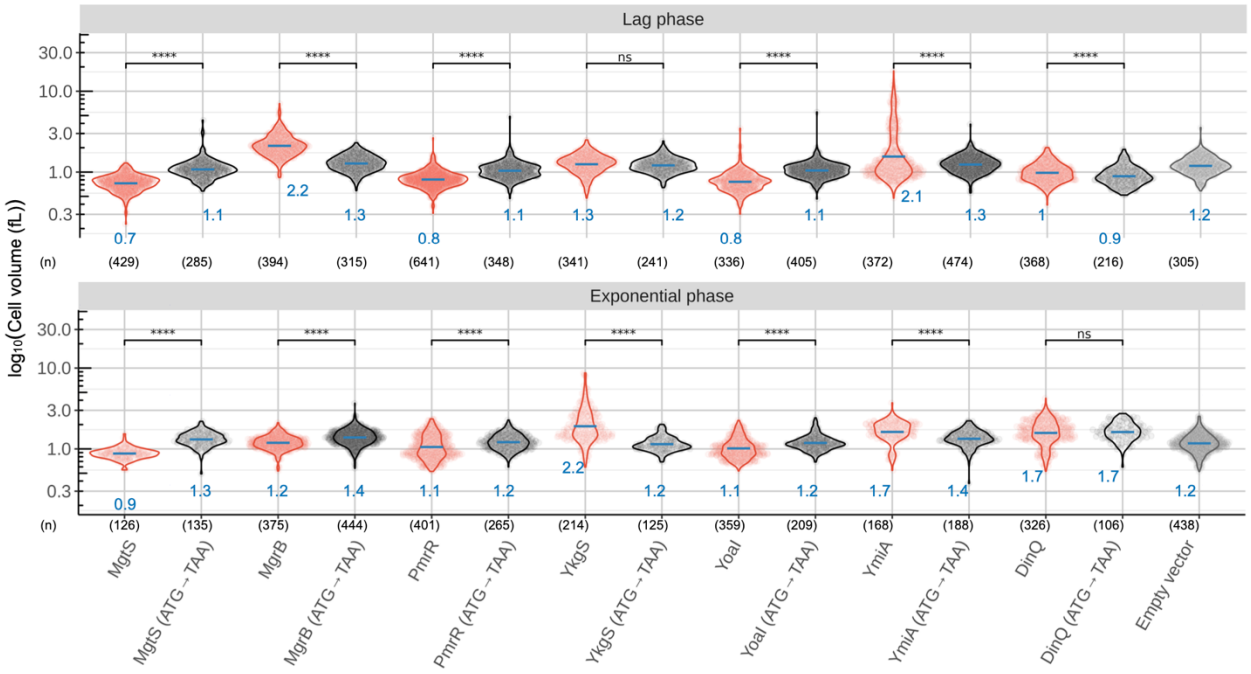

Figure S6. Quantification of cell size changes associated with overexpression of small proteins, MgtS, MgrB, PmrR, YkgS, YoaI, YmiA and DinQ. Cell volume quantification (representative micrograph images are shown in Figure 8B) for the cells expressing small proteins during lag (top panel) and exponential phase (bottom panel) after induction are shown. Each circle corresponds to a single cell. Cells expressing small proteins are shown in red, cells expressing the start codon mutants are depicted in black, and the empty vector (pEB52) control is shown in gray. The cultures were grown in supplemented minimal A medium with no added magnesium. For pSV34-36, pSV38-42, pSV60-61, pJS4, and pJS7, the medium contained 50 μg ml^{-1} carbenicillin and 500 μM IPTG, while for pSV54-55, 0.5% arabinose was utilized. Data are derived from two independent replicates and the number of cells analyzed is indicated by (n). Mean cell volumes are shown with blue bars and are noted in blue text. P-values indicate the results of a t-test when the strains expressing small protein were compared to their variant with the translation start codon mutated, ****P ≤ 0.001, and “ns” = P > 0.05.

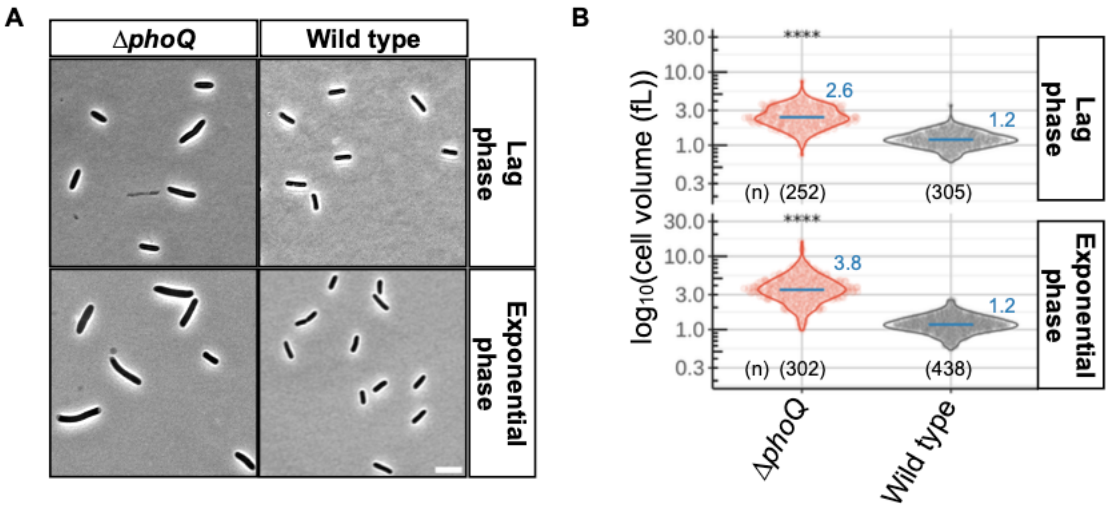

Figure S7. Cell size changes associated with Δ*phoQ* under magnesium starvation. (A) Representative phase contrast micrographs of Δ*phoQ* (TIM202), and wild type (MG1655) cells expressing an empty vector control (pEB52) during lag and exponential phase, scale bar = 5 μm. Cells were grown in supplemented minimal A medium with no added magnesium, and 50 μg ml^{-1} carbenicillin. (B) Quantification of cell volume for the cells depicted in panel A. Each circle corresponds to a single cell. Cells expressing Δ*phoQ* are shown in red and wild type cells are shown in gray. Data are derived from three independent replicates and the number of cells analyzed is indicated by (n). Mean cell volumes are shown with blue bars and are noted in blue text. P-values indicate the results of a t-test when Δ*phoQ* cells were compared to the wild-type cells, ****P ≤ 0.0001.

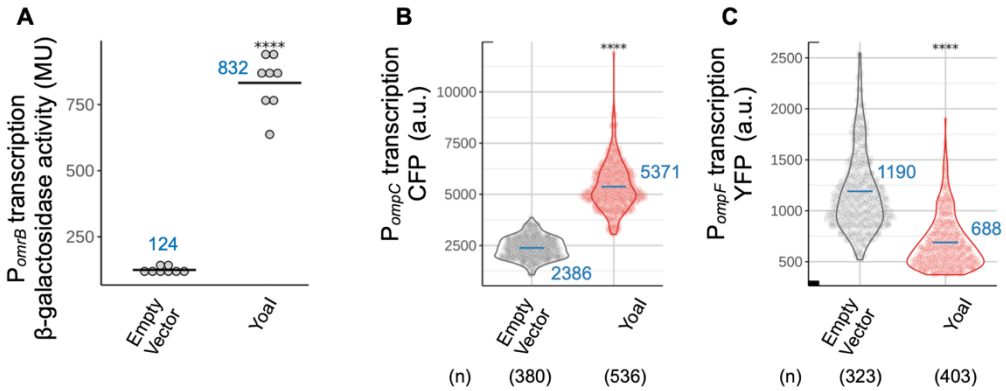

Figure S8. Effect of YoaI overexpression on the EnvZ-OmpR system. (A) Transcriptional activity of *omrB* was measured as a function of *lacZ* expression in wild-type (JM2110) strain during the exponential growth phase upon YoaI (pSV34) and empty vector (pEB52) overexpression. Each circle represents a biological replicate, with the mean values from two independent experiments indicated, expressed in Miller units (MU). The cells were grown in LB containing 100 µg ml^{-1} carbenicillin. After three hours of growth, cells were induced with 500 µM IPTG, and β-gal activity was measured two hours post-induction. (B-C) Porin expression was measured using CFP fluorescence (corresponding to *ompC*) and YFP fluorescence (corresponding to *ompF*) in wild-type (MDG147) strain during the exponential growth phase upon YoaI (pSV34) and empty vector (pEB52) overexpression. Each circle corresponds to a single cell. Cells overexpressing YoaI are depicted in red, while those with the empty vector are in gray. The cultures were grown in supplemented minimal A medium containing 10mM $MgSO_4$ (no stress), 50 µg ml^{-1} carbenicillin, and 500 µM IPTG. Data are derived from three independent replicates and the number of cells analyzed is indicated by (n). Mean fluorescence is shown with blue bars and is noted in blue text. P-values indicate the results of a t-test when cells overexpressing YoaI were compared to the empty vector control, ****P ≤ 0.0001.

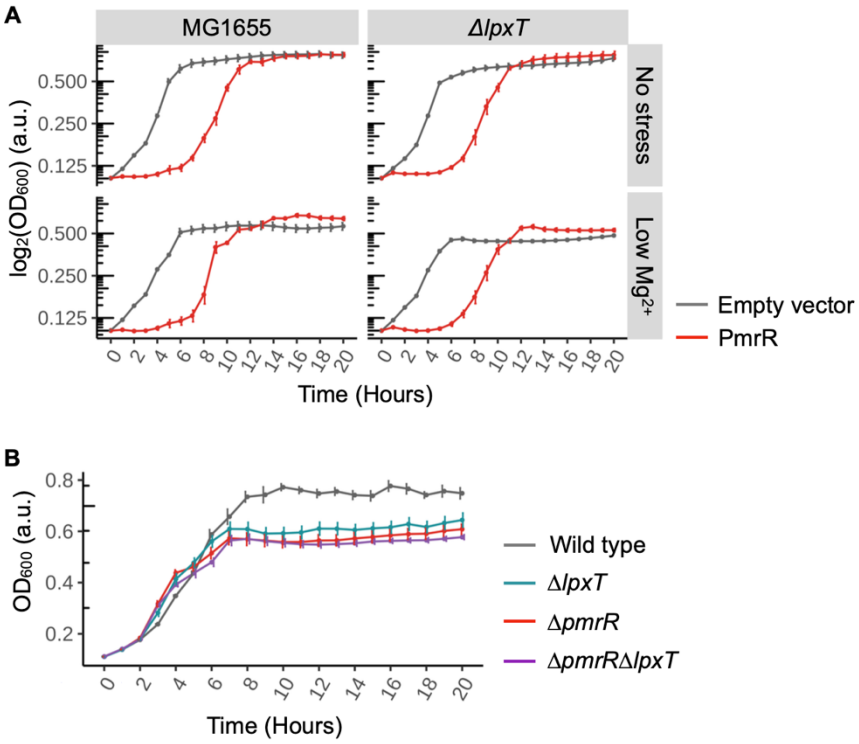

Figure S9. The phenotypes associated with PmrR are LpxT independent. (A) Growth comparison of *E. coli* K-12 MG1655 wild-type and Δ*lpxT* strain (SV47) carrying a plasmid encoding the small protein PmrR (pSV35, red line), or an empty vector (pEB52, gray line). The cultures were grown in supplemented minimal A medium containing 50 μg ml^{-1} carbenicillin, 500 μM IPTG, and either 10 mM $MgSO_4$ (no stress) or no added magnesium (low Mg^{2+}). (B) The plot represents growth curves of wild-type *E. coli* MG1655 (gray) and mutants corresponding to gene deletions Δ*pmrR* (SV35, red line), Δ*lpxT* (SV47, green line), and Δ*pmrR* Δ*lpxT* (SV54, purple line). Please see Table S1 for details. The cultures were grown in supplemented minimal A medium with no added magnesium. Data represent averages and standard errors of means for four independent cultures.

References

1. Lippa, A.M., and Goulian, M. (2009). Feedback inhibition in the PhoQ/PhoP signaling system by a membrane peptide. PLoS Genet. *5*, e1000788.

2. Hobbs, E.C., Astarita, J.L., and Storz, G. (2010). Small RNAs and small proteins involved in resistance to cell envelope stress and acid shock in Escherichia coli: analysis of a bar-coded mutant collection. J. Bacteriol. *192*, 59–67.

3. Hemm, M.R., Paul, B.J., Miranda-Ríos, J., Zhang, A., Soltanzad, N., and Storz, G. (2010). Small stress response proteins in Escherichia coli: proteins missed by classical proteomic studies. J. Bacteriol. *192*, 46–58.

4. Baba, T., Ara, T., Hasegawa, M., Takai, Y., Okumura, Y., Baba, M., Datsenko, K.A., Tomita, M., Wanner, B.L., and Mori, H. (2006). Construction of Escherichia coli K-12 in-frame, single-gene knockout mutants: the Keio collection. Mol. Syst. Biol. *2*, 2006.0008.

5. Batchelor, E., Silhavy, T.J., and Goulian, M. (2004). Continuous control in bacterial regulatory circuits. J. Bacteriol. *186*, 7618–7625.

6. Coornaert, A., Chiaruttini, C., Springer, M., and Guillier, M. (2013). Post-transcriptional control of the Escherichia coli PhoQ-PhoP two-component system by multiple sRNAs involves a novel pairing region of GcvB. PLoS Genet. *9*, e1003156.

7. Bastet, L., Korepanov, A.P., Jagodnik, J., Grondin, J.P., Lamontagne, A.-M., Guillier, M., and Lafontaine, D.A. (2024). Riboswitch and small RNAs modulate btuB translation initiation in Escherichia coli and trigger distinct mRNA regulatory mechanisms. Nucleic Acids Res. *52*, 5852–5865.

8. Yadavalli Srujana S., Goh Ted, Carey Jeffrey N., Malengo Gabriele, Vellappan Sangeevan, Nickels Bryce E., Sourjik Victor, Goulian Mark, Yuan Jing, and Silhavy Thomas J. (2020). Functional Determinants of a Small Protein Controlling a Broadly Conserved Bacterial Sensor Kinase. J. Bacteriol. *202*, e00305-20.

9. Miyashiro, T., and Goulian, M. (2007). Stimulus-dependent differential regulation in the Escherichia coli PhoQ PhoP system. Proc. Natl. Acad. Sci. U. S. A. *104*, 16305–16310.

10. Goldberg, S.D., Clinthorne, G.D., Goulian, M., and DeGrado, W.F. (2010). Transmembrane polar interactions are required for signaling in the *Escherichia coli* sensor kinase PhoQ. Proc. Natl. Acad. Sci. U. S. A. *107*, 8141–8146.

11. Bullock, W.O. (1987). XL1-blue : a high efficiency plasmid transforming recA Escherichia coli strain with beta-ga-lactosidase selection. Biotechniques *5*, 376.

12. Guzman, L.M., Belin, D., Carson, M.J., and Beckwith, J. (1995). Tight regulation, modulation, and high-level expression by vectors containing the arabinose PBAD promoter. J. Bacteriol. *177*, 4121–4130.

13. Cherepanov, P.P., and Wackernagel, W. (1995). Gene disruption in Escherichia coli: TcR and KmR cassettes with the option of Flp-catalyzed excision of the antibiotic-resistance determinant. Gene *158*, 9–14.

14. Datsenko, K.A., and Wanner, B.L. (2000). One-step inactivation of chromosomal genes in Escherichia coli K-12 using PCR products. Proc. Natl. Acad. Sci. U. S. A. *97*, 6640–6645.

15. Amann, E., Ochs, B., and Abel, K.J. (1988). Tightly regulated tac promoter vectors useful for the expression of unfused and fused proteins in Escherichia coli. Gene *69*, 301–315.

16. Hemm, M.R., Paul, B.J., Schneider, T.D., Storz, G., and Rudd, K.E. (2008). Small membrane proteins found by comparative genomics and ribosome binding site models. Mol. Microbiol. *70*, 1487–1501.

17. Wang, H., Yin, X., Wu Orr, M., Dambach, M., Curtis, R., and Storz, G. (2017). Increasing intracellular magnesium levels with the 31-amino acid MgtS protein. Proc. Natl. Acad. Sci. U. S. A. *114*, 5689–5694.

18. Kato, A., Chen, H.D., Latifi, T., and Groisman, E.A. (2012). Reciprocal control between a bacterium's regulatory system and the modification status of its lipopolysaccharide. Mol. Cell *47*, 897–908.

19. Weaver, J., Mohammad, F., Buskirk, A.R., and Storz, G. (2019). Identifying Small Proteins by Ribosome Profiling with Stalled Initiation Complexes. MBio *10*. https://doi.org/10.1128/mBio.02819-18.

20. VanOrsdel, C.E., Kelly, J.P., Burke, B.N., Lein, C.D., Oufiero, C.E., Sanchez, J.F., Wimmers, L.E., Hearn, D.J., Abuikhdair, F.J., Barnhart, K.R., et al. (2018). Identifying New Small Proteins in Escherichia coli. Proteomics *18*, e1700064.

21. Weel-Sneve, R., Kristiansen, K.I., Odsbu, I., Dalhus, B., Booth, J., Rognes, T., Skarstad, K., and Bjørås, M. (2013). Single transmembrane peptide DinQ modulates membrane-dependent activities. PLoS Genet. *9*, e1003260.

22. Möller, S., Croning, M.D., and Apweiler, R. (2001). Evaluation of methods for the prediction of membrane spanning regions. Bioinformatics *17*, 646–653.

23. Ikeda, M., Arai, M., Okuno, T., and Shimizu, T. (2003). TMPDB: a database of experimentally-characterized transmembrane topologies. Nucleic Acids Res. *31*, 406–409.

24. Käll, L., Krogh, A., and Sonnhammer, E.L.L. (2004). A combined transmembrane topology and signal peptide prediction method. J. Mol. Biol. *338*, 1027–1036.

25. Fontaine, F., Fuchs, R.T., and Storz, G. (2011). Membrane localization of small proteins in Escherichia coli. J. Biol. Chem. *286*, 32464–32474.